IMC-BASED PID CONTROLLER DESIGN FOR A TWO-LINK SCARA ROBOT

SIPASEUTH SUVILATH

A THESIS SUBMITTED IN PARTIAL FULFILLMENT

OF THE REQUIREMENT FOR THE DEGREE OF

MASTER OF ENGINEERING IN COMPUTER ENGINEERING

INTERNATIONAL COLLEGE

KING MONGKUT'S INSTITUTE OF TECHNOLOGY LADKRABANG

2012

KMITL-2012-IC-M-006-004

Thesis Certification

International College

King Mongkut's Institute of Technology Ladkrabang

Thesis Title	IMC-Based PID Controller Design for a Two-link SCARA Robot
Student	Mr. Sipaseuth Suvilath
Student ID.	53601153
Degree	Master of Engineering
Program	Computer Engineering
Thesis Advisor	Assoc. Prof. Dr. Taworn Benjanarasuth
Thesis Co-Advisor	Assoc. Prof. Noriyuki Komine
Thesis Reference Number	KMITL-2012-IC-M-006-004

EXAMINERS	SIGNATURES
Assoc. Prof. Dr. Vanchai Riewruja	
Assoc. Prof. Dr. Taworn Benjanarasuth	
Assoc. Prof. Dr. Jongkol Ngamwiwit	
Assoc. Prof. Dr. Worapong Tangsirat	
Dr. Don Isarakorn	

Date 3 October 2012 **Time** 13.00 - 15.00

Place Room IC 02, International College, 8th floor, 55th Anniversary Chalermprakiat Building

สถาบันเทคโนโลยีพระจอมเกล้าเจ้าคุณทหารลาดกระบัง

KING MONGKUT'S INSTITUTE OF TECHNOLOGY LADKRABANG

(Assoc. Prof. Dr. Anantawat Kunakorn)

Dean

3 October 2012

Thesis	IMC-Based PID Controller Design for a Two-link SCARA Robot
Student	Mr. Sipaseuth SUVILATH
Student ID.	53601153
Degree	Master of Engineering
Program	Computer Engineering
Year	2012
Thesis Advisor	Assoc.Prof.Dr.Taworn Benjanarasuth
Thesis Co-Advisor	Assoc. Prof. Dr. Noroyuki Komine

ABSTRACT

In this thesis, Internal Model Control (IMC) technique is applied to design a PID controller for a two-link SCARA robot, of which the model contains an integral term. In IMC controller design, a filter structure must be selected suitably because it directly affects the performance of the system. In order to derive the PID controller, the IMC controller using a proposed low-pass filter is approximated by Maclaurin series expansion. The investigations of the proposed IMC low-pass filter parameters are also presented by variation. The effectiveness of the IMC-based PID controller is verified by both simulations and experiments.

Acknowledgement

I would like to express the deepest appreciation to my supervisor, Assoc. Dr. Taworn Benjanarasuth who convincingly conveyed a spirit of teaching and advising the master dissertation. This dissertation would not have been possible without his guidance and help.

I gratefully acknowledge the ASEAN University Network/Southeast Asia Engineering Education Development Network (AUN/SEED-Net) in supporting my study at KMITL for two years. I also extend my sincere appreciation to NUOL for giving me the opportunity to do my research so that I can conduct my research at KMITL in a warm environment.

I would like to thank my co-supervisor, Assoc. Dr. Nuriyuki Komine for valuable discussion during my studying at KMITL.

Thanks to Assoc. Dr. Jongkol Ngamwiwit for her advice and support through two years of my research.

Finally, my deepest gratitude goes to my beloved family for their encouragement and persistent supports. It is their tolerance and loves that carrying me to achieve the success of my life.

Contents

List of Tables

List of Figures

Nomenclatures

a_1	Distance between gravity center position rotational positions of the first link
a_2	Distance between gravity center position rotational positions of the second link
A	State variable matrix
B	Input variable matrix
B_M	Rotor damping constant matrix
C	Output variable matrix
$C(s)$	IMC controller
$D_i(s)$	Input disturbance
$D_o(s)$	Output disturbance
$D'(s)$	Estimated disturbance
$E(s)$	Error of the system
$E_a(s)$	Current command voltage vector
$E_{a1}(s)$	Current command voltage of first link
$E_{a2}(s)$	Current command voltage of second link
$f(s)$	Low-pass filter of IMC controller
$f(x,u)$	Nonlinear state variable vector
$G(s)$	Process
$\hat{G}(s)$	Process model
$\hat{G}_+(s)$	Process model contains all the time delays and right-half-plane zeros
$\hat{G}_-(s)$	Transfer function with minimum phase characteristic and contains no predictive item
$h(x)$	Nonlinear output variable
J_{M1}	Moment of inertia of motor of first link
J_{M2}	Moment of inertia of motor of second link
J_M	Moment of inertia matrix of motor

Chapter 1

Introduction

1.1 Background and Significance of the Problem

A robot manipulator composes of number of links attached serially to each other with joints, where each joint can be moved by some types of actuators. The end effector of the robot manipulator can be moved to any desired location within its workspace by moving its joint. As the robot is capable of performing many different tasks, is able to control to any desired position within its workspace precisely and is able to operate with routine tasks without boredom and tiredness, it is widely used as one of powerful elements in industrial automation, which is save more time, more reliable and lower manufacturing products cost [1]. In some industrial scenes with dangerous work places where human are not able to work, such as in some chemical reaction processes and in high-temperature plants, the robot is appropriate to replace human in order to raise safety standard. Among several types of the robot, a SCARA robot (Selective Compliance Assembly Robot Arm) is very common utilized in assembly operation. The SCARA robot is a horizontal multi-joint robot and will be considered as a process for designing appropriate controllers.

In order to control the motion of the robot moving to the desired position accurately and effectively, the controllers must be suitably designed. There are several control techniques such as Fuzzy Logic [2] and Neural Network techniques [3] have been presented to design the controllers for the SCARA robot. By using these methods, the angular position can track the set point satisfactorily; however, the controller design procedures and implementation are quite complicated. Among various controllers, the PID controller is the most popular controller that has been adopted in industrial scenes due to its simplicity and practical applicability. However, the parameters of PID controllers must be suitably tuned. Ziegler-Nichols [4] tuning method and Cohen-Coon tuning method [5] have been proposed tuning rules for the PID controller. The reference [4] and [5] also have been adopted as reported in [6] and [7], respectively. However, in actual implementation, PID controller gains are mostly determined by trial-and-error process by a skilled expert. For example, the PID controller with the trial-and-error gains is applied to control the SCARA robot [8]. In controlling SCARA robot, a controller designed by IMC method has been also reported in [9]. In this method, the performance of the system depends on the structure and the parameters of IMC low-pass filter. The advantage of IMC control technique is that the

desired output can be obtained by introducing the IMC low-pass filter which is equivalent to the specified reference trajectory [10]. In IMC controller design, the transfer function of IMC controller is rational form.

From the advantage of IMC control technique, it has been applied to design the popular PID controller [11]. To do so, the designed IMC controller with its transfer function in rational form is approximated by Maclaurin series expansion. By ignoring the higher order terms of the approximated IMC controller, the remaining terms are matched to the PID controller structure so that the PID controller can be obtained. In this method, several low-pass filters have been proposed for difference model structures [10, 12]. However, these structures do not match to the model of the SCARA robot. Therefore these IMC low-pass filter structures are not suitable for this model.

In this thesis, a suitable IMC low-pass filter structure is proposed for the model of the SCARA robot in order to deal with this problem. The effectiveness of the IMC-based PID controller design using the proposed low-pass filter is verified by simulations and implementations.

1.2 Research Objective

The accuracy of the two-link SCARA robot angular position control, the effect of input and output disturbances rejection, simplicity of controller design and popularity of PID controller have motivated to do the research under the topic as "IMC-based PID Controller Design for a Two-link SCARA Robot". The research objectives are as follows:

1. To derive the mathematical model of the two-link SCARA robot and to linearize the model to simplify the controller design of the system.
2. To study IMC control concept, to transform IMC control to general feedback control and to approximate the general feedback control to PID control by Maclaurin series expansion.
3. To consider the IMC low-pass filter for the model of two-link SCARA robot in order to eliminate the effect of input and output disturbances.
4. To implement the proposed controller.

1.3 Thesis Outline

This thesis is composed of five chapters which are briefly summarized as follows.

Chapter 1 introduces general background and utilities of the robot in factory automation. The controller design algorithms for the SCARA robot manipulator are given as example and explain their performance briefly; then, a proposed IMC-based PID technique is mentioned as well.

Chapter 2 describes the literature reviews the mathematical modeling of the two-link SCARA robot. The mathematical model of the system can be derived by Lagrangian equation. A completed dynamic equation of the system in nonlinear form is linearized then a linear equation is obtained. The basic theory of IMC and its transformation to general feedback control are explained in detail. The approximation of general feedback controller into PID controller is also demonstrated in this chapter.

Chapter 3 presents the application of the proposed method for the process used in the laboratory. In this chapter, the linear equation for the two-link SCARA robot derived in Chapter 2 is used in controller design. In IMC-based PID controller design method, the filter directly affects the performance of the system. Consequently, a suitable low-pass filter of IMC controller design method is selected for the model of the SCARA robot. The general feedback controller is approximated by performing Maclaurin series expansion. By ignoring higher order terms of the series, the remains of first three terms are matched to the structure of PID controller.

Chapter 4 describes the actual equipment briefly. The effectiveness of the proposed IMC low-pass filter for designing IMC-based PID controller is evaluated by simulations. The simulation results are also compared to the experimental results graphically. The characteristic of simulation results are identical to the characteristic of experiment results.

Chapter 5 concludes the research results of the thesis.

Chapter 2

Mathematical Model of the Two-link SCARA Robot

This chapter presents mathematical modeling of the two-link SCARA robot. The mathematical tools, Lagrangian equation and linearization are useful for analyzing process dynamic. Generally, Newtonian mechanics can be used to find the dynamic equation for robots. However, the actual process used in the laboratory is multiple-degree-of-freedom mechanisms. It is difficult to use Newtonian mechanics. Therefore, Lagrangian mechanics is an option to use instead. Then the dynamic equations of the system are linearized. A controller is designed from the linearized model in order to obtain the automatic control system.

2.1 The Structure of the Two-link SCARA Robot

The two-link SCARA robot shown in figure 2.1 has two revolute joints that are parallel. The robot moves in horizontal plane. SCARA robot is very common in assembly operation. Its specific characteristic is that it is more compliant in the x-y plane.

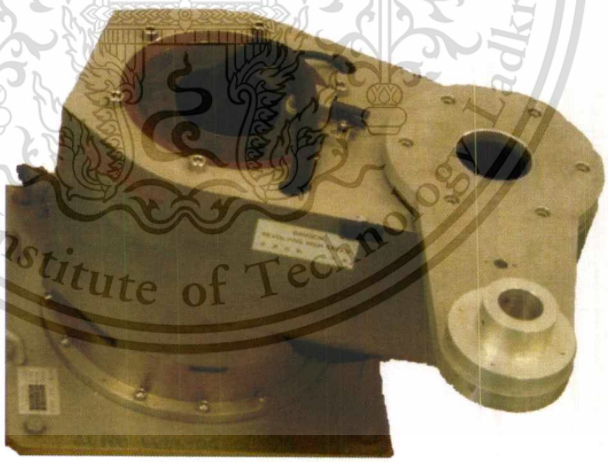

Figure 2.1 SCARA robot used in the laboratory.

SCARA robot used for experiment in the laboratory consists of two links. The first link is attached to the base and the second link is attached to the end of the first link. The end of the second link is called "end-effector" and it is the position for tool setting. Two links of the robot are directly driven by AC

servo motors without gear boxes (see in the appendix A). Therefore, the robot can be also called as Direct Drive Robot (DDR).

2.2 Mathematical Model for the Two-link SCARA Robot

The schematic diagram of the two-link robot manipulator considered in this thesis is shown in figure 2.2, where θ_1 and θ_2 are angular positions of each link, m_1 and m_2 are masses of each link, l_1 and l_2 are lengths of each link and a_1 and a_2 are distances between the gravity center positions and rotational positions of the first link and the second link respectively.

From figure 2.2, the position equations of the two-link SCARA robot can be described as (2.1) and (2.2),

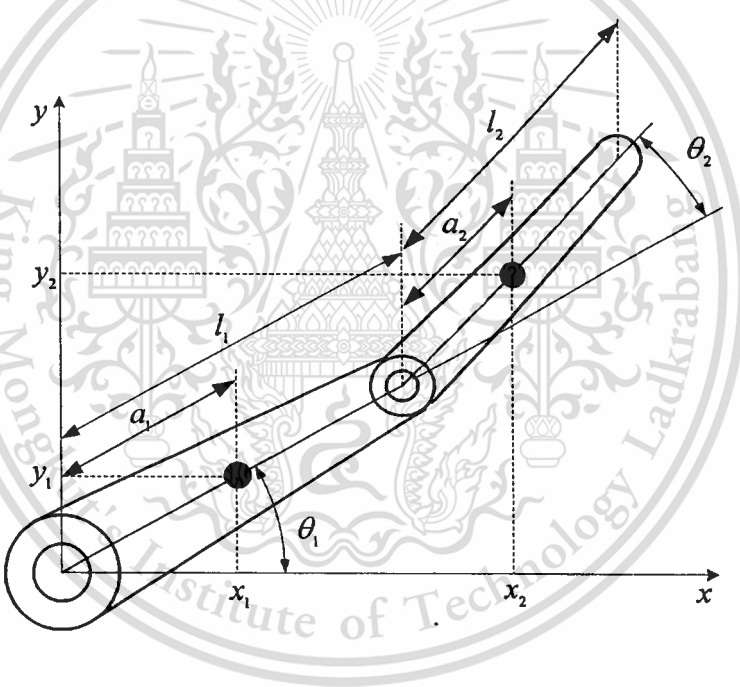

Figure 2.2 SCARA robot scheme (top plane).

$$x_1 = a_1 c_1, \qquad y_1 = a_1 s_1 \tag{2.1}$$

$$x_2 = l_1 c_1 + a_2 c_{12}, \qquad y_2 = l_1 s_1 + a_2 s_{12} \tag{2.2}$$

where $c_1 = \cos\theta_1$, $s_1 = \sin\theta_1$, $c_{12} = \cos(\theta_1 + \theta_2)$ and $s_{12} = \sin(\theta_1 + \theta_2)$ when x_1, y_1, x_2 and y_2 are the coordinates of the gravity center position of both links. The velocity of each link can be obtained by differentiating its position. Therefore, the velocity equation for each link is given as (2.3) and (2.4).

$$v_1^2 = \dot{x}_1^2 + \dot{y}_1^2 = a_1^2\dot{\theta}_1^2, \tag{2.3}$$

$$v_2^2 = \dot{x}_2^2 + \dot{y}_2^2 = l_1^2\dot{\theta}_1^2 + a_1^2(\dot{\theta}_1 + \dot{\theta}_2)^2 + 2l_1a_2c_2\theta_1(\dot{\theta}_1 + \dot{\theta}_2). \tag{2.4}$$

The dynamic energy for the multiple-degree-of-freedom robots is complicated. However, it can be categorized in to two main classes, kinetic energy and potential energy. The kinetic energy of the two-link SCARA robot for the first link and the second link can be expressed as (2.5) and (2.6), respectively

$$K_1 = \frac{m_1v_1^2}{2} = \frac{m_1a_1^2\dot{\theta}_1^2}{2}, \tag{2.5}$$

$$K_2 = \frac{m_2v_2^2}{2} = \frac{m_2\left[l_1^2\dot{\theta}_1^2 + a_2^2(\dot{\theta}_1^2 + 2\dot{\theta}_1\dot{\theta}_2 + \dot{\theta}_2^2) + 2l_1a_2c_2\dot{\theta}_1(\dot{\theta}_1 + \dot{\theta}_2)\right]}{2}. \tag{2.6}$$

The potential energy of the robot is the sum of the potential energy of the two links. Since the two-link robot manipulator is designed to move in horizontal plane, the potential energy of each link is considered to be zero.

2.2.1 Lagrangian Equation

Lagrangian mechanics is based on the differentiation of the energy terms with respect to the system's variables and time. For simple cases, it may take longer to use this technique than Newtonian mechanics. However, as the complexity of the SCARA robot system, the Lagrangian method becomes simpler method to solve with this system. This method comprise of linear motion equations and rotational motion equations which can be expressed as

$$T = \frac{d}{dt}\left(\frac{\partial L}{\partial \dot{\theta}}\right) - \frac{\partial L}{\partial \theta}, \tag{2.7}$$

where T is the summation of torques in a rotational motion and θ is angular position. Torque T and angular position are expressed as

$$T = \begin{bmatrix} T_1 & T_2 \end{bmatrix}^T \tag{2.8}$$

and

$$\theta = \begin{bmatrix} \theta_1 & \theta_2 \end{bmatrix}^T \tag{2.9}$$

Respectively, where T_1 and T_2 are torque of each link and θ_1 and θ_2 are angular position of each link.

The Lagrangian operator L in (2.7) is given as

$$L = K - P, \tag{2.10}$$

where L is the Lagrangian operator, K is summation of kinetic energies of the system and P is summation of the potential energies of the system. The kinetic energies summation of the first link and the second is given by

$$K = K_1 + K_2. \tag{2.11}$$

As the potential energies are considered to be zero, the Lagrangian operator becomes the total sum of kinetic energy which can be written as

$$L = K = \frac{1}{2} m_1 a_1^2 \dot{\theta}_1^2 + \frac{1}{2} m_2 \left[l_1^2 \dot{\theta}_1^2 + a_2^2 (\dot{\theta}_1^2 + 2\dot{\theta}_1 \dot{\theta}_2 + \dot{\theta}_2^2) + 2 l_1 a_2 c_2 \dot{\theta}_1 (\dot{\theta}_1 + \dot{\theta}_2) \right] \tag{2.12}$$

The torque equation of each link can be considered separately and can be expressed as follow

$$T_1 = \frac{d}{dt}\frac{\partial L}{\partial \dot{\theta}_1} - \frac{\partial L}{\partial \theta_1}, \tag{2.13}$$

$$T_2 = \frac{d}{dt}\frac{\partial L}{\partial \dot{\theta}_2} - \frac{\partial L}{\partial \theta_2}. \tag{2.14}$$

By substituting Lagragian operator from (2.12) into (2.13) and (2.14), two equations of torque can be obtained as

$$T_1 = (m_1 a_1^2 + m_2 l_1^2 + m_2 l_1 a_2 c_2)\ddot{\theta}_1 + (m_2 a_2^2 + m_2 l_1 a_2 c_2)\ddot{\theta}_2 - m_2 l_1 a_2 s_2 (2\dot{\theta}_1\dot{\theta}_2 + \dot{\theta}_2^2), \tag{2.15}$$

$$T_2 = (m_2 a_2^2 + m_2 l_1 a_2 c_2)\ddot{\theta}_1 + m_2 a_2^2 \ddot{\theta}_2 + m_2 l_1 a_2 s_2 \dot{\theta}_1^2. \tag{2.16}$$

By assigning $J_1 = m_1 a_1^2 + m_2 l_1^2$, $J_2 = m_2 a_2^2$ and $r = m_2 l_1 a_2$, the simple form of torque equation becomes

$$T_1 = (J_1 + J_2 + r c_2)\ddot{\theta}_1 + (J_2 + r c_2)\ddot{\theta}_2 - r s_2 (2\dot{\theta}_1\dot{\theta}_2 + \dot{\theta}_2^2), \tag{2.17}$$

$$T_2 = (J_2 + r c_2)\ddot{\theta}_1 + J_2 \ddot{\theta}_2 + r s_2 \ddot{\theta}_1^2, \tag{2.18}$$

where $\dot{\theta}_1$ and $\dot{\theta}_2$ are angular velocities of the first and second links while $\ddot{\theta}_1$ and $\ddot{\theta}_2$ are angular accelerations of the first and second links. From (2.17) and (2.18), the standard form of dynamic equation for the SCARA robot can be written as

$$T = M(\theta)\ddot{\theta} + V(\theta, \dot{\theta}), \tag{2.19}$$

where $\theta \in R^2$ is joint variable vector, $M(\theta)$ is the inertia matrix and $V(\theta, \dot{\theta})$ is the Coriolis/centripetal torque vector. The parameters in $M(\theta)$ and $V(\theta, \dot{\theta})$ are

$$M(\theta)=\begin{bmatrix} J_1+J_2+2rc_2 & J_2+2rc_2 \\ J_2+2rc_2 & J_2 \end{bmatrix} \tag{2.20}$$

$$V(\theta,\dot{\theta})=\begin{bmatrix} 2rs_2\dot{\theta}_1\dot{\theta}_2-rs_2\ddot{\theta}_2^2 \\ rs_2\dot{\theta}_1^2 \end{bmatrix} \tag{2.21}$$

2.2.2 Actuator Dynamic

As each link of the SCARA robot is moved by an actuator, the dynamic actuators are added to the dynamic equation of the SCARA robot in order to derive the completed dynamic equation. By assuming that the actuators are ideal servos motor, there is no loss in power transmission circuit and the frictions of the rotors are neglected. Then the dynamic actuator equation is given as,

$$J_M\ddot{\theta}_M+B_M\dot{\theta}_M+T=K_M E_a, \tag{2.22}$$

where $\theta_M=vec\begin{bmatrix}\theta_{M1} & \theta_{M2}\end{bmatrix}$, $\dot{\theta}_M=vec\begin{bmatrix}\dot{\theta}_{M1} & \dot{\theta}_{M2}\end{bmatrix}$ and $\ddot{\theta}_M=vec\begin{bmatrix}\ddot{\theta}_{M1} & \ddot{\theta}_{M2}\end{bmatrix}$ are the angular positions, the angular velocities and the angular accelerations, respectively. The variable θ_M, $\dot{\theta}_M$ and $\ddot{\theta}_M$ of the first and second links are expressed by the suffix $M1$ and $M2$. $E_a \in R^2$ is the current command voltage vector. The constant actuator coefficient matrices for moments of inertia, rotors damping constant and torques constant of the first and second motors are respectively written by

$$J_M=diag\begin{bmatrix}J_{M1} & J_{M2}\end{bmatrix},$$

$$B_M=diag\begin{bmatrix}B_{M1} & B_{M2}\end{bmatrix},$$

$$K_M=diag\begin{bmatrix}K_{M1} & K_{M2}\end{bmatrix}.$$

The gear coupling from the first motor to first link is assigned as R_1 and the gear coupling from the second motor to the second link is assigned as R_2. Then the relation between θ_1 and θ_{M1}, θ_2 and θ_{M2} can be written as

$$\theta_1 = R_1\theta_{M1} \tag{2.23a}$$

and

$$\theta_2 = R_2\theta_{M2}. \tag{2.23b}$$

The gear ratio matrix is given by

$$R_M = diag\begin{bmatrix} R_1 & R_2 \end{bmatrix}. \tag{2.24}$$

As the manipulator used for experiment in the laboratory is the DDR, the gear ratio of each joint is considered to be one. Consequently, equation (2.23) can be written as

$$\theta_1 = \theta_{M1} \tag{2.25a}$$

and

$$\theta_2 = \theta_{M2}. \tag{2.25b}$$

2.2.3 Completed Dynamic Equation

To obtain the completed dynamic equation, the dynamic equation of manipulator and actuator dynamic equation are combined. Then the completed dynamic equation can be obtained as

$$(J_M + M(\theta))\ddot{\theta} + (B_M\dot{\theta} + V(\theta,\dot{\theta})) = K_M E_a\,, \tag{2.26}$$

and its standard form can be written as

$$\tilde{M}(\theta)\ddot{\theta} + \tilde{V}(\theta,\dot{\theta}) = K_M E_a\,, \tag{2.27}$$

where

$$\tilde{M}(\theta) = \begin{bmatrix} J_1 + J_2 + J_{M1} + 2rc_2 & J_2 + rc_2 \\ J_2 + rc_2 & J_2 + J_{M2} \end{bmatrix}$$

$$\tilde{V}(\theta,\dot{\theta}) = \begin{bmatrix} 2rs_2\dot{\theta}_1\dot{\theta}_2 - rs_2\dot{\theta}_2^2 + B_{M1}\dot{\theta}_1 \\ rs_2\dot{\theta}_1^2 + B_{M2}\dot{\theta}_2 \end{bmatrix}.$$

By solving (2.27), $\ddot{\theta}$ can be derived as

$$\ddot{\theta} = -\tilde{M}^{-1}(\theta)\tilde{V}(\theta,\dot{\theta}) + \tilde{M}^{-1}(\theta)K_M E_a, \tag{2.28}$$

or

$$\ddot{\theta}_1 = \frac{-\Delta_1(-rs_2\dot{\theta}_1^2 - B_{M2}\dot{\theta}_2 + K_{M2}E_{a2}) + (J_2 + J_{M2})[\Delta_2 - K_{M1}E_{a1}]}{\Delta}, \tag{2.29}$$

$$\ddot{\theta}_2 = \frac{-\Delta_1[\Delta_2 + K_{M1}E_{a1}] - (J_1 + J_2 + J_{M1} + 2rc_2)(rs_2\dot{\theta}_1^2 + B_{M2}\dot{\theta}_2 + K_{M2}E_{a2})}{\Delta}, \tag{2.30}$$

where

$$\Delta = J_1J_2 + J_{M1} + J_1J_{M2} + J_{M1}J_{M2} + 2J_{M2}rc_2 - r^2c_2^2$$

$$\Delta_1 = (J_2 + rc_2)$$

$$\Delta_2 = r(2\dot{\theta}_1\dot{\theta}_2 + \dot{\theta}_2^2)s_2 - B_{M1}\dot{\theta}_1.$$

The state-space equation for the completed dynamic equation can be derived by defining angular position as the state variable which is given as

$$x = \begin{bmatrix} \theta_1 & \theta_2 & \dot{\theta}_1 & \dot{\theta}_2 \end{bmatrix}^T. \tag{2.31}$$

Then the nonlinear angular position/velocity state-space equation can be derived as

$$\dot{x} = f(x,u), \tag{2.32}$$

$$y = h(x), \tag{2.33}$$

where

$$f(x,u) = \begin{bmatrix} \dot{\theta} \\ -\tilde{M}^{-1}(\theta)\tilde{V}(\theta,\dot{\theta}) \end{bmatrix} + \begin{bmatrix} 0 \\ \tilde{M}^{-1}(\theta) \end{bmatrix} K_M E_a$$

$$h(x) = \begin{bmatrix} I & 0 \end{bmatrix} x .$$

2.2.4 Linearization

As the SCARA robot system is nonlinear system, in order to design the controller easily, it must be linearized. The linear equation of motion at the equilibrium $u_0 = 0$ and $x_0 = \begin{bmatrix} 0 & 0 & 0 & 0 \end{bmatrix}^T$ are given as

$$\dot{x} = Ax + Bu, \tag{2.34}$$

$$y = Cx, \tag{2.35}$$

where

$$A = \frac{\partial f(x,u)}{\partial x}\Big|_{x=x_0, u=u_0},$$

$$B = \frac{\partial f(x,u)}{\partial u}\Big|_{x=x_0, u=u_0},$$

$$C = \frac{\partial h(x)}{\partial x}\Big|_{x=x_0}.$$

By differentiating (2.34) and (2.35) the state matrices can be derived as following

$$A=\begin{bmatrix}0 & 0 & 1 & 0\\ 0 & 0 & 1 & 1\\ 0 & 0 & a_{33} & a_{34}\\ 0 & 0 & a_{43} & a_{44}\end{bmatrix}, B=\begin{bmatrix}0 & 0\\ 0 & 0\\ b_{31} & b_{32}\\ b_{41} & b_{42}\end{bmatrix} \text{ and } C=\begin{bmatrix}1 & 0 & 0 & 0\\ 0 & 1 & 0 & 0\end{bmatrix} \tag{2.36}$$

where the element in the matrices are

$$a_{33}=\frac{(J_{M2}+J_2)B_{M1}}{-J_{M1}J_{M2}-J_{M1}J_2-J_1J_{M2}-J_1J_2-J_2J_{M2}-2rJ_{M2}+r^2},$$

$$a_{34}=\frac{-(r+J_2)B_{M2}}{-J_{M1}J_{M2}-J_{M1}J_2-J_1J_{M2}-J_1J_2-J_2J_{M2}-2rJ_{M2}+r^2},$$

$$a_{43}=\frac{-(r+J_2)B_{M1}}{-J_{M1}J_{M2}-J_{M1}J_2-J_1J_{M2}-J_1J_2-J_2J_{M2}-2rJ_{M2}+r^2},$$

$$a_{44}=\frac{(J_{M1}+J_1+J_2)B_{M2}}{-J_{M1}J_{M2}-J_{M1}J_2-J_1J_{M2}-J_1J_2-J_2J_{M2}-2rJ_{M2}+r^2},$$

$$b_{31}=\frac{-(J_{M2}+J_2)K_{M1}}{-J_{M1}J_{M2}-J_{M1}J_2-J_1J_{M2}-J_1J_2-J_2J_{M2}-2rJ_{M2}+r^2},$$

$$b_{32}=\frac{-(r+J_2)K_{M2}}{-J_{M1}J_{M2}-J_{M1}J_2-J_1J_{M2}-J_1J_2-J_2J_{M2}-2rJ_{M2}+r^2},$$

$$b_{41}=\frac{-(r+J_2)K_{M1}}{-J_{M1}J_{M2}-J_{M1}J_2-J_1J_{M2}-J_1J_2-J_2J_{M2}-2rJ_{M2}+r^2},$$

$$b_{42} = \frac{(J_{M1} + J_1 + J_2 + 2r)K_{M2}}{-J_{M1}J_{M2} - J_{M1}J_2 - J_1J_{M2} - J_1J_2 - J_2J_{M2} - 2rJ_{M2} + r^2}.$$

Transfer matrix of robot manipulator in s domain is obtained as

$$G(s) = \frac{Y(s)}{U(s)} = C(sI - A)^{-1}B = \begin{bmatrix} G_{11}(s) & G_{12}(s) \\ G_{21}(s) & G_{22}(s) \end{bmatrix} \tag{2.37}$$

$$G(s) = \begin{bmatrix} \dfrac{(s-a_{44})b_{31} + a_{34}b_{41}}{s[s^2 - (a_{33}+a_{44})s + a_{33}a_{44} - a_{34}a_{43}]} & \dfrac{(s-a_{44})b_{32} + a_{34}b_{42}}{s[s^2 - (a_{33}+a_{44})s + a_{33}a_{44} - a_{34}a_{43}]} \\ \dfrac{(s-a_{44})b_{41} + a_{43}b_{31}}{s[s^2 - (a_{33}+a_{44})s + a_{33}a_{44} - a_{34}a_{43}]} & \dfrac{(s-a_{44})b_{42} + a_{43}b_{32}}{s[s^2 - (a_{33}+a_{44})s + a_{33}a_{44} - a_{34}a_{43}]} \end{bmatrix}$$

To control the angular position of each link, the system is requires to design the controller which is proceeded in chapter 3.

2.2.5 Parameter Identification

As the current command voltage of first link is mainly affected to first link and the command voltage of the second link is mainly affected to the second link, therefore, the coupling of each link is ignored. Then, the complete dynamics equation of first link and the second link can be rewritten as

$$(J_{M1} + J_1 + J_2 + 2rc_2)\ddot{\theta}_1 + B_{M1}\dot{\theta}_1 = K_{M1}E_{a1} \tag{2.38}$$

$$(J_{M2} + J_2)\ddot{\theta}_2 + B_{M2}\dot{\theta}_1 = K_{M2}E_{a2}.$$

To derived the linear transfer functions between the current command voltages and output angular position for the first link and the second link, take Laplace (2.38) with zero initial conditions, then

$$(J_{M1} + J_1 + J_2 + 2rc_2)s^2\theta_1(s) + B_{M1}s\theta_1(s) = K_{M1}E_{a1}(s) \tag{2.39}$$

$$(J_{M2} + J_2)s^2\theta_2(s) + B_{M2}s\theta_1(s) = K_{M2}E_{a2}(s).$$

By arranging (2.39), the transfer functions can be obtained by

$$\frac{\theta_1(s)}{E_{a1}(s)} = \frac{K_{M1}/B_{M1}}{s(H_1 s+1)} \tag{2.40}$$

$$\frac{\theta_2(s)}{E_{a2}(s)} = \frac{K_{M2}/B_{M2}}{s(H_2 s+1)}$$

where $H_1 = J_{M1} + J_1 + J_2 + 2rc_2$ and $H_2 = J_{M2} + J_2$.

The first link is study by applying a step reference input (current command voltage) $E_{a1}(s) = \frac{V_C}{s}$ to the first link without any feedback control. The output of first link can be expressed as

$$\theta_1(s) = \frac{K_{M1}}{s(M_1 s + B_{M1})} \cdot \frac{V_C}{s} \tag{2.41}$$

where V_C is the magnitude of the step input of the current command voltage and $M_1 = T_{M1}.B_{M1}$. By expanding (2.41) into partial factions, the expanded equation can be expressed as

$$\theta_1(s) = \frac{K_{M1}V_C}{B_{M1}}\left[\frac{1}{s^2} - T_C\frac{1}{s} + \frac{T_C^2}{T_C s+1}\right]. \tag{2.42}$$

Taking the inverse Laplace transform of (2.42), the time domain equation of first link can be given by

$$\theta_1(t) = \frac{K_{M1}V_C}{B_{M1}}\left[t - T_C + T_C e^{-t/T_C}\right], \text{ for } t \geq 0\ . \tag{2.43}$$

From the (2.43), the response of step input of command voltage is shown in figure 2.3. Since t approaches to infinity so that the equation for steady-state response θ_{ss} can be written by

$$\theta_{ss}(t) = \frac{K_{M1}V_C}{B_{M1}}\left[t - T_C\right]. \tag{2.44}$$

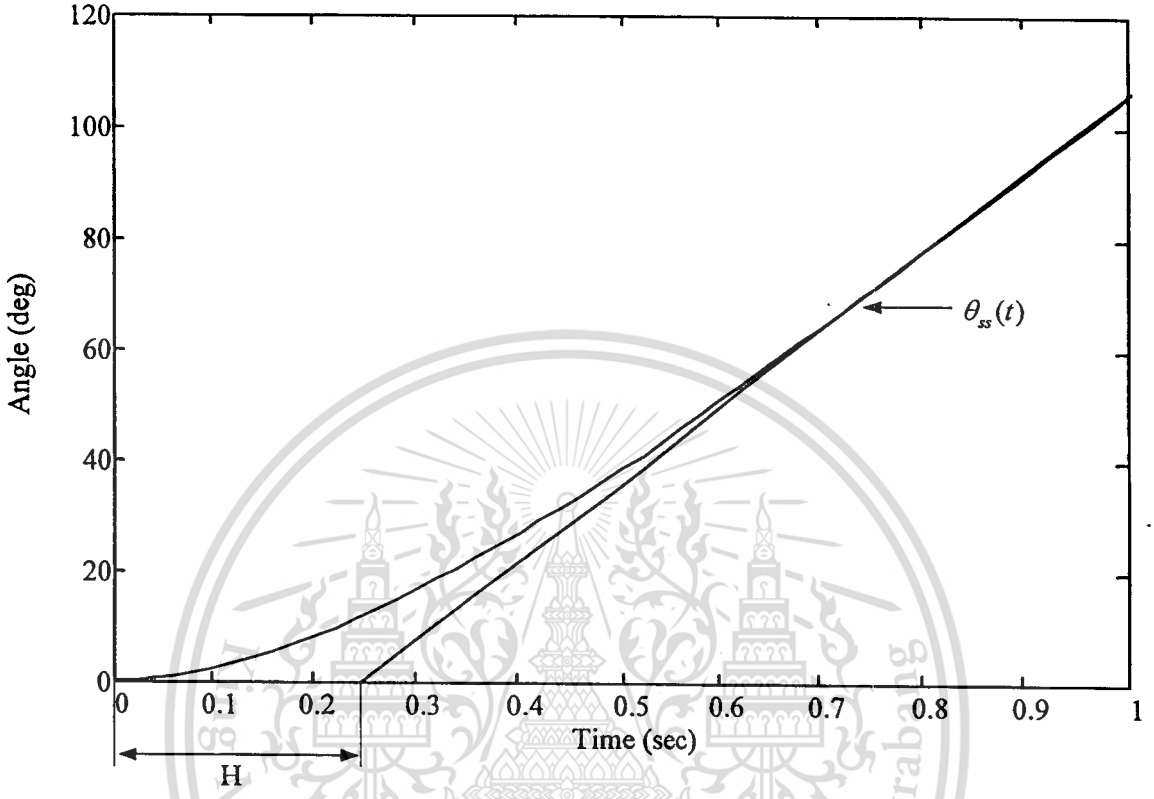

Figure 2.3 Response of step input of current command voltage (open-loop control).

From (2.44), the constant parameters can be identified as follows

- First of all, the time constant T_C can be found by extrapolating the straight line θ_{ss} back to $\theta_1 = 0$ and intersects the time axis at $t = T_C$.
- Generally, the slider mass M_1 is defined by a designer as motor mounting procedure [13]. Therefore, B_{M1} can be found from (2.44).
- $\left(\frac{K_{M1}E_{a1}}{B_{M1}}\right)$ and K_{M1} can be found from the slope of the steady-state response as well. Since the dynamic of first link is similarly to the second link, K_{M2} can be found by conducting in the same manner as stated above.

The step input of current command voltage experiment result gives the torque constants K_{M1} and K_{M2} which are used to derive the linear models of the two-link SCARA robot.

Chapter 3

IMC-Based PID Controller

The transfer matrix of the system obtained in previous chapter is required controllers in order to control moving to any desired position. In this chapter, the literature of PID controller is presented in detail in section 3.1 followed by IMC concept. After that the transformation of the IMC control to IMC-based PID controller is proposed in section 3.2 and section 3.3, respectively. In IMC controller design, IMC low-pass filter is directly affect the responses of the system. Thus it must be selected suitably. The filters that have been proposed for difference models is included in this chapter as well.

3.1 PID Controller

The PID controller is broadly used in industrial process. In this section, the PID controller consist of proportional (P), integral (I) and derivative (D) action are studied individually in continuous-time system. Since the actual controller is digital computer, the continuous-time system controller must be converted to discrete-time system which is stated along with continuous-time system.

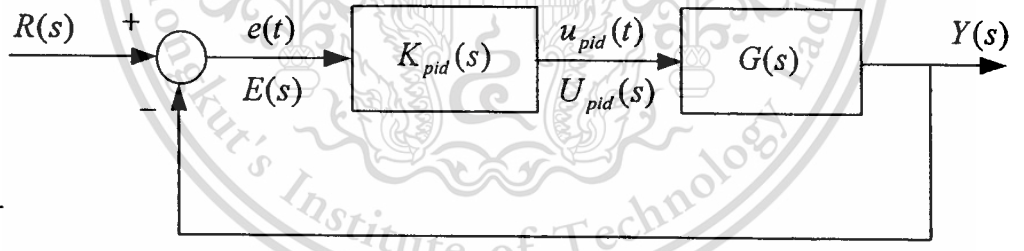

Figure 3.1 General feedback control structure.

3.1.1 Proportional Controller

For the continuous-time system, the proportional controller is described by the relation

$$u_p(t) = K_p e(t) \tag{3.1a}$$

and therefore,

$$\frac{U_p(s)}{E(s)} = K_p \tag{3.1b}$$

For the discrete-time systems, the equivalent controller is described by the relation

$$u_p(k) = K_p e(k) \tag{3.2a}$$

and therefore,

$$\frac{U_p(z)}{E(z)} = K_p \tag{3.2b}$$

3.1.2 Integral Controller

For the continuous-time systems, the integral controller is described by the relation

$$u_i(t) = K_i \int_{t_{n-1}}^{t_n} e(t)dt \ , \tag{3.3a}$$

and therefore,

$$\frac{U_i(s)}{E(s)} = \frac{K_i}{s} \ . \tag{3.3b}$$

For the discrete-time systems, the equivalent controller is described by the relation

$$u_i(k) = u_i(k-1) + \frac{K_i T_s}{2}\big(e(k-1) + e(k)\big) \ , \tag{3.4a}$$

and therefore,

$$\frac{U_i(z)}{E(z)} = \frac{K_i T_s}{2}\left(\frac{z+1}{z-1}\right), \tag{3.4b}$$

where T_s is the sampling time.

3.1.3 Derivative Controller

For continuous-time systems, the derivative controller is described by the differential equation

$$u_d(t) = K_d \frac{de(t)}{dt}, \tag{3.5a}$$

and therefore,

$$\frac{U_d(s)}{E(s)} = K_d s \tag{3.5b}$$

In the case of discrete-time systems, the differential equation (3.5a) can be approximated by difference equation

$$u_d(k) = \frac{K_d}{T_s}\big(e(k) - e(k-1)\big), \tag{3.6a}$$

when

$$\frac{U_d(z)}{E(z)} = \frac{K_d}{T_s}\left(\frac{z-1}{z}\right). \tag{3.6b}$$

3.1.4 PID Controller

Combining previous three actions P, I and D, it can be expressed in continuous-time as

$$u_{pid}(t) = K_p e(t) + K_i \int_0^t e(t)dt + K_d \frac{de(t)}{dt} \tag{3.7a}$$

when

$$\frac{U_{pid}(s)}{E(s)} = K_p + \frac{K_i}{s} + K_d s. \tag{3.7b}$$

In the case of discrete-time systems, the PID controller can be described in difference equation

$$u_{pid}(k) = u_p(k) + u_i(k) + u_d(k) \tag{3.8a}$$

where

$$u_p(k) = K_p e(k)$$

$$u_i(k) = u_i(k-1) + \frac{K_i T_s}{2}\left(e(k-1) + e(k)\right)$$

$$u_d(k) = \frac{K_d}{T_s}\left(e(k) - e(k-1)\right)$$

when

$$\frac{U_{pid}(z)}{E(z)} = K_p + \frac{K_i T_s}{2}\left(\frac{z+1}{z-1}\right) + \frac{K_d}{T_s}\left(\frac{z-1}{z}\right). \tag{3.8b}$$

Block diagrams for the case of continuous-time systems and discrete-time systems are depicted in figure 3.2 and figure 3.3.

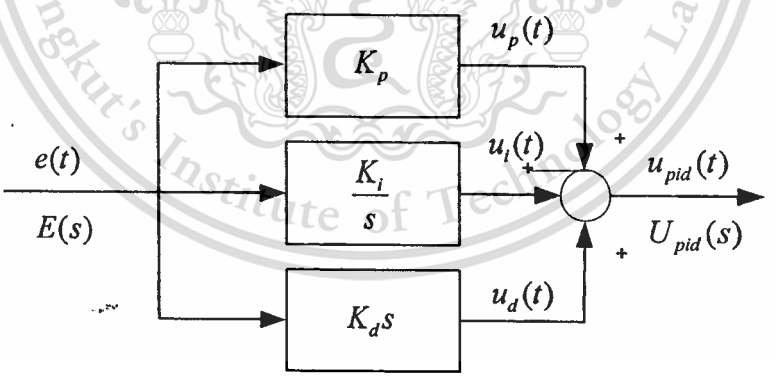

Figure 3.2 Block diagram of the continuous-time PID controller.

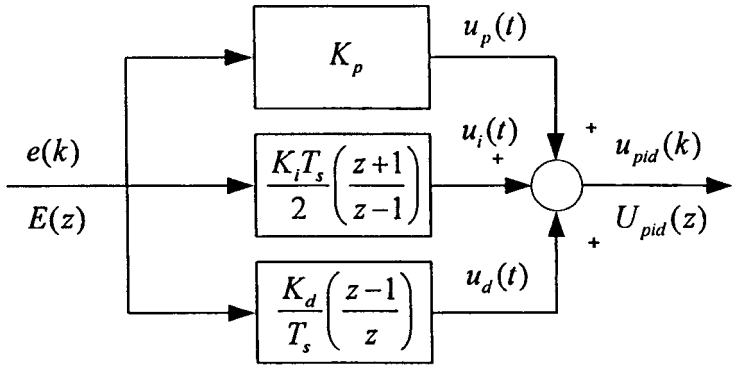

Figure 3.3 Block diagram of the discrete-time PID controller.

3.2 Internal Model Control Principle

In process control applications, model based control systems are often used to track set point and reject disturbances. The Internal Model Control (IMC) philosophy relies on the internal model principle which states that a control system can be designed if the system encapsulates and the model is exactly represented the process. Then a perfect control is easily achieved. In particular, if the control scheme is developed based on exact model of the process, then perfect control is theoretically possible.

3.2.1 Open-loop Control

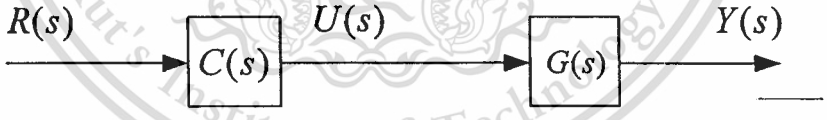

Figure 3.4 Open-loop control strategy.

From open-loop control in figure 3.3, $C(s)$ is a controller, $G(s)$ is a process, $Y(s)$ is an output of the system and $Y(s)$ is a reference input. The output can be written as

$$Y(s) = C(s)G(s)R(s). \tag{3.9}$$

Suppose $\hat{G}(s)$ is a model of the process $G(s)$. If $C(s)$ is chosen as the inverse of the model and the controller is stable and if $\hat{G}(s)$ perfectly represents the process $G(s)$ so that $\hat{G}(s)^{-1}$ and $G(s)$ can be canceled each other. Consequently, the output $Y(s)$ is obviously equal to the reference input $R(s)$.

The unknown disturbances are often entered to the system which is shown in figure 3.5.

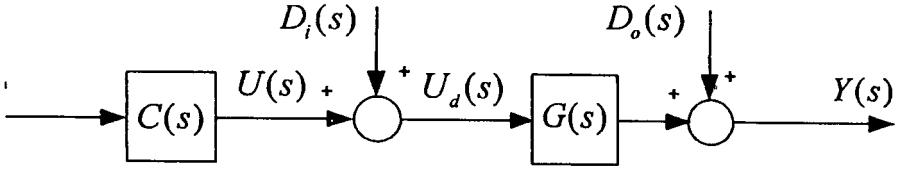

Figure 3.5 Open-loop control strategy with disturbances.

The output of the system can be rewritten as

$$Y(s) = R(s) + G(s)D_i(s) + D_o(s). \tag{3.10}$$

Even though the process model is matched, the disturbances are remaining in output of the system so the open-loop control is not achievable in implementation.

3.2.2 Structure of IMC

Practically, process model mismatch is common; the process model may not be invertible and system is often affected by unknown disturbances. Therefore, the above open-loop control arrangement is not be able to maintain output at set point. Nevertheless, it forms the basis for the development of a control strategy that has the potential to achieve perfect control. This strategy, known as IMC has the general structure depicted in figure 3.5 where $G(s)$ a controlled object is, $\hat{G}(s)$ is the model of the controlled object and $C(s)$ is the IMC controller, $R(s)$ is a reference input, $E(s)$ is an error, $U(s)$ is a command signal, $D_i(s)$ is an input disturbance, $D_o(s)$ is an output disturbance and $Y(s)$ is an output.

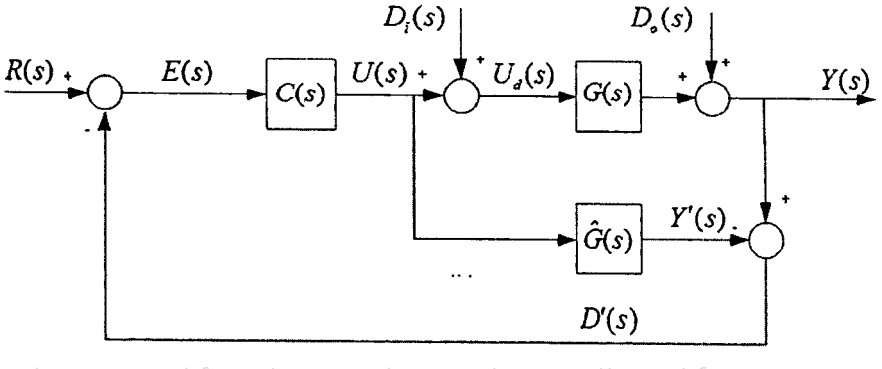

Figure 3.6 IMC structure.

In case perfect encapsulated model with no input and output disturbance, we call perfect encapsulated model if the process model equals to actual process $G(s) = \hat{G}(s)$ and without input disturbance and output disturbance, mean that $D_i(s) = 0$ and $D_o(s) = 0$. Thus, the output $Y(s)$ of IMC structure from figure 3.4 can be obtained as

$$Y(s) = C(s)G(s)R(s) \tag{3.11}$$

It can be noticed that the output in (3.11) is the same as open-loop control design mentioned in the previous section. From (3.11), if controller $C(s)$ and plant $G(s)$ are stable so that the closed-loop system is also stable.

From the figure 3.5 $D_i(s)$ and $D_o(s)$ are input disturbance entering to the system. The controller output $U(s)$ is introduced to both $G(s)$ and $\hat{G}(s)$. The output $Y(s)$ is compared with the output of the model and result a signal $D'(s)$. That is,

$$D'(s) = [G(s) - \hat{G}(s)]U(s) + G(s)D_i(s) + D_o(s) \tag{3.12}$$

If $D_i(s)$ and $D_o(s)$ are absolutely equal to zero, for example, we can also say that $D'(s)$ is measure of the difference in behavior between the process and its model and then $D'(s)$ is equal to the unknown disturbance.

Thus, $D'(s)$ may be regarded as the information that is missing in the model, $\hat{G}(s)$ and can therefore be used to improve control. This is done by sending an error $E(s)$ signal to the controller $C(s)$. The closed-loop transfer function for the IMC structure becomes

$$Y(s) = \frac{C(s)G(s)R(s) + G(s)\left[1 - C(s)G(s)\right]D_i(s) + \left[1 - C(s)G(s)\right]D_o(s)}{1 + \left[G(s) - \hat{G}(s)\right]C(s)} \tag{3.13}$$

From (3.13), we can see that if the controller is chosen as inverse of the model $C(s) = \hat{G}(s)^{-1}$ and if the model is exactly represented the process, then perfect set point tracking and the effect of disturbance rejections is completely achieved.

As mention above, the process and the process model is mismatched. To improve the robustness of the system, process mismatch should be minimized. As discrepancies between process and model

behavior usually occur at the high frequency and the controller might be improper. To deal with these problems, the low-pass filter is usually series connected to the IMC controller in order to attenuate the effects of process model mismatch and to make the controller proper. Thus, the internal model controller is usually designed as the inverse of the process model in series with a low-pass filter or

$$C(s) = \hat{G}(s)^{-1} f(s). \tag{3.14}$$

The order of the filter is usually chosen such that $C(s)$ is proper, to prevent excessive differential control action. The closed-loop transfer function then becomes

$$Y(s) = \frac{\hat{G}(s)^{-1} f(s) G(s) R(s) + \left[1 - \hat{G}(s)^{-1} f(s) \hat{G}(s)\right] D(s)}{1 + \left[G(s) - \hat{G}(s)\right] \hat{G}(s)^{-1} f(s)}. \tag{3.15}$$

In IMC controller design, to detune an uncertainties model, the IMC tuning (filter) factor is used. It should be noted that the standard IMC controller design procedure is focused on set point responses. However, the set point responses do not guarantee good disturbance rejection effect; especially for the disturbance occurred at the input of the process. The modification of the design procedure is developed in order to improve the rejection efficiency of input disturbance.

The IMC controller design procedures are:

3.2.3 Factorization

In this step, a transfer function of the process $G(s)$ is factorized into invertible and non-invertible portions. The factor containing right half plane (RHP) or positive zeros or all time delays become the poles in the inverts of the process model when designing the controller. The transfer function is mathematically given as

$$\hat{G}(s) = \hat{G}_{+}(s)\hat{G}_{-}(s), \tag{3.16}$$

Such that $\hat{G}_{+}(s)$ is non-invertible portion which is the transfer function contain all time delay and right-half-plane zero. Consequently, $\hat{G}_{-}(s)$ is the transfer function that is stable and does not involve predictors.

3.2.4 Low-pass Filter

To make the controller $C(s)$ proper, a filter is needed to series to the IMC controller of the system. If the order of the denominator is greater than the order of the numerator, the transfer function is proper. Then the controller can be physically implemented.

In order to improve the robustness of the system, the effect of the model mismatch should be minimized. Usually, different between the actual process and the model occur at high frequency response, a low-pass filter is added to attenuate the effects of the process model mismatch. Consequently, the IMC is usually designed as the inverse of the process model in series with the low pass filter which is mathematically given as

$$C(s) = \hat{G}_{-}(s)^{-1} f(s) \tag{3.17}$$

Several IMC low-pass filter for differences process also have been presented [11] which is summarized in table 3.1.

Table 3.1 General IMC low-pass filters

$G(s)$	$f(s)$	$K(s) = \dfrac{\hat{G}_{-}^{-1}(s)}{f^{-1}(s) - \hat{G}_{+}(s)}$
$\dfrac{k}{as+1}$	$\dfrac{1}{\lambda s+1}$	$\dfrac{1}{k}\dfrac{as+1}{\lambda s}$
$\dfrac{k}{(as+1)(bs+1)}$	$\dfrac{1}{\lambda s+1}$	$\dfrac{(as+1)(bs+1)}{k\lambda s}$
$\dfrac{k}{a^2s^2+2\zeta as+1}$	$\dfrac{1}{\lambda s+1}$	$\dfrac{a^2s^2+2\zeta as+1}{k\lambda s}$
$k\dfrac{-bs+1}{as+1}$	$\dfrac{1}{\lambda s+1}$	$\dfrac{as+1}{k(b+\lambda)s}$
	$\dfrac{1}{(bs+1)(\lambda s+1)}$	$\dfrac{as+1}{ks(b\lambda s+b+\lambda)}$
$k\dfrac{-bs+1}{a^2s^2+2\zeta as+1}$	$\dfrac{1}{\lambda s+1}$	$\dfrac{a^2s^2+2\zeta as+1}{k(b+\lambda)s}$
	$\dfrac{1}{(bs+1)(\lambda s+1)}$	$\dfrac{a^2s^2+2\zeta as+1}{k(b\lambda s+2b+\lambda)s}$

Table 3.1 General IMC low-pass filters (Cont.)

$\frac{k}{s}$	$\frac{1}{\lambda s+1}$	$\frac{1}{k\lambda}$
	$\frac{2\lambda+1}{(\lambda s+1)^2}$	$\frac{2\lambda s+1}{k\lambda^2 s}$
$\frac{k}{s(as+1)}$	$\frac{1}{\lambda s+1}$	$\frac{as+1}{k\lambda}$
	$\frac{2\lambda s+1}{(\lambda s+1)^2}$	$\frac{(as+1)(2\lambda s+1)}{k\lambda^2 s}$
$k\frac{-bs+1}{s}$	$\frac{1}{\lambda s+1}$	$\frac{1}{k(b+\lambda)}$
	$\frac{1}{(bs+1)(\lambda s+1)}$	$\frac{1}{k(b\lambda s+2b+\lambda)}$
	$\frac{[(b+2\lambda)s+1]}{(\lambda s+1)^2}$	$\frac{(b+2\lambda)s+1}{ks(b+\lambda)^2}$
	$\frac{[2(b+\lambda)s+1]}{(bs+1)(\lambda s+1)^2}$	$\frac{2(b+\lambda)s+1}{ks(b\lambda^2 s+\lambda^2+4b\lambda+2b^2)}$
$k\frac{-bs+1}{s(as+1)}$	$\frac{1}{\lambda s+1}$	$\frac{as+1}{k(\lambda+b)}$
	$\frac{1}{(bs+1)(\lambda s+1)}$	$\frac{as+1}{k(b\lambda s+2b+\lambda)}$
	$\frac{[2(b+2\lambda)s+1]}{(\lambda s+1)^2}$	$\frac{(as+1)[(b+2\lambda)s+1]}{ks(b+\lambda)^2}$
	$\frac{[2(b+\lambda)s+1]}{(bs+1)(\lambda s+1)^2}$	$\frac{(as+1)[2(b+\lambda)s+1]}{ks(b\lambda^2 s+\lambda^2+4\lambda b+2b^2)}$

As the general feedback control is able to transform into IMC control [9]; the transform relation between these two of controllers are discussed.

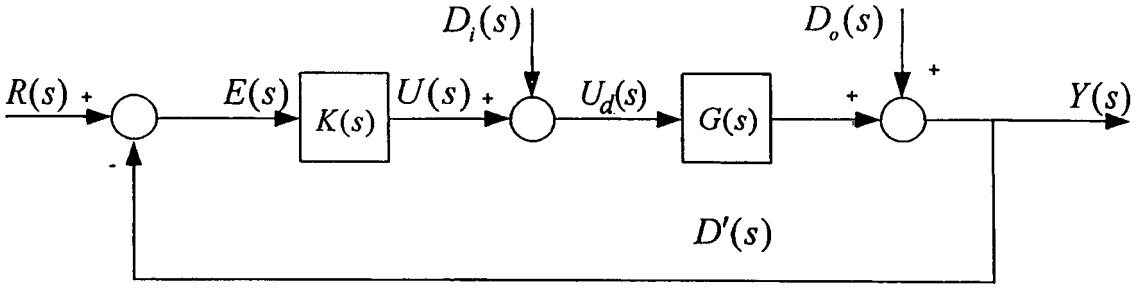

Figure 3.7 General feedback control.

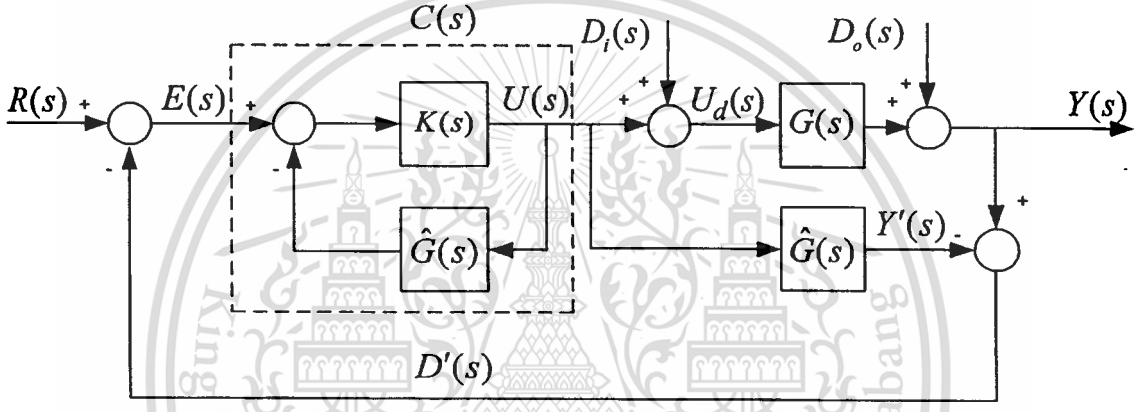

Figure 3.8 Equivalent Internal Model Control.

If controller $C(s)$ can be substituted by the part circled by the broken line in figure 3.8, the IMC structure is equivalent to control system structure as shown in figure 3.7. From the relation from input $R(s)$ to output $Y(s)$ of figure 3.8, we can found that two models $\hat{G}(s)$ can be offset. So the system shown in figure 3.8 is equivalent to general feedback control system as shown in figure 3.7. From figure 3.8, IMC controller $C(s)$ can be obtained as

$$C(s) = \frac{K(s)}{1+\hat{G}(s)K(s)} \quad , \tag{3.18}$$

and the controller $K(s)$ can be found from (3.18) as

$$K(s) = \frac{C(s)}{1-\hat{G}(s)C(s)} \quad . \tag{3.19}$$

From (3.17) and (3.18), the controller $K(s)$ for a general feedback control system can be obtained as

$$K(s) = \frac{\hat{G}_-^{-1}(s)}{f^{-1}(s) - \hat{G}_+(s)}. \tag{3.20}$$

3.3 IMC-based PID Controller Approximation

With a suitable choice of filter $f(s)$, the controller $K(s)$ can possess the integral action and appear in the following form

$$K(s) = \frac{1}{s}k(s) = \frac{1}{s}\frac{n(s)}{d(s)}, \tag{3.21}$$

Where $k(s)$ is non-integral part of controller $K(s)$, $n(s)$ is a numerator and $d(s)$ is a dominator of transfer function $k(s)$.

In order to obtain PID controller, the transfer function $k(s)$ is approximated by Maclaurin series expansion on s domain, and then it can be expressed as

$$K(s) = \frac{1}{s}\left[k(0) + \dot{k}(0)s + \frac{\ddot{k}(0)s}{2!} \cdots \right]. \tag{3.22}$$

By ignoring higher order terms and multiplying the integral term $\frac{1}{s}$ through the equation, the first three terms are matched to the PID controller

$$K(s) \approx K_{PID}(s) = K_P + \frac{K_I}{s} + K_D s, \tag{3.23}$$

where

$$K_p = \dot{k}(0),$$

$$K_i = k(0)$$

and

$$K_d = \frac{\ddot{k}(0)}{2},$$

when

$$k(0) = \frac{n(0)}{d(0)}$$

$$\dot{k}(0) = \frac{n'(0)d(0) - n(0)d'(0)}{d^2(0)}$$

$$\ddot{k}(0) = \frac{n''(0)d^3(0) - n(0)d''(0)d^2(0) - 2n'(0)d'(0)d^2(0) + 2n(0)\left[d'(0)\right]^2 d(0)}{d^4(0)}$$

Chapter 4

IMC-Based PID Controller Design for the Two-link SCARA Robot

In this chapter, the proposed control system is stated in the section 4.1. The input and output disturbance rejection is then analyzed. After that the general IMC low-pass filter and the proposed IMC low-pass filter are applied to design the controllers in order to approve input and output disturbance effect rejection.

4.1 Proposed Control System

The two-link SCARA robot is Multiple-Inputs-Multiple-Outputs (MIMO) system which the input is a current command voltage of each link. However, since the input current command voltage $E_{a1}(s)$ of the first link mainly affects the first link and the input current command voltage $E_{a2}(s)$ of the second link mainly affects the second link. Thus, two IMC-Based PID controllers are independently designed by considering the SCARA robot as two separated Single-Input-Single-Output (SISO) system. This is depicted in figure 4.1.

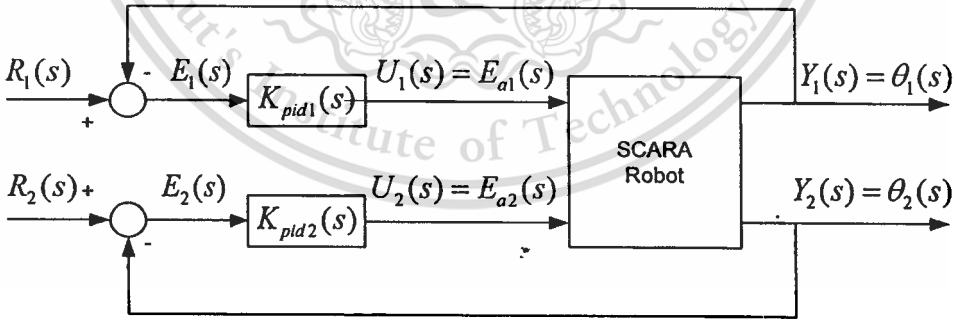

Figure 4.1 Proposed control system.

The PID controller of each link is derived by IMC-based PID design method which is presented in section 4.2.

4.2 Application of IMC-based PID Controller Design for the Two-link SCARA Robot

Two independent PID controllers in figure 4.1 are designed for simulations and experiments. To obtained PID controller for each link of the SCARA robot, IMC method mentioned in chapter 2 is applied.

The transfer function $G_{11}(s)=\frac{Y_1(s)}{U_1(s)}=\frac{\theta_1(s)}{E_{a1}(s)}$ and $G_{22}(s)=\frac{Y_2(s)}{U_2(s)}=\frac{\theta_2(s)}{E_{a2}(s)}$ obtained in chapter 2 are in the same formats. Therefore, the controller design for both links can be conducted in the same manner. The transfer function of both links are in the form as

$$\hat{G}(s)=\frac{as+b}{s(s^2+a's+b')}. \tag{4.1}$$

In implementation, the process $G(s)$ and the model mismatch is common. Consequently, the output of the system is not exactly equal to the reference input. To attenuate the effect of the process mismatch, the low-pass filter is usually multiplied to the IMC controller. Several low-pass filters have been proposed for difference models as summarized in table 3.1. Some low-pass filters in this table can be used for the proposed model. In theoretically, the responses can track the step reference input and the output disturbances effects can be eliminated completely. However, the input disturbances effect is not able eliminated which will be explained and compared by simulations in next chapter. To deal with this problem, the low-pass filter for the two-link SCARA robot is selected suitably. Consider the general feedback control for figure 3.6, the relation between the output of the system $Y(s)$ and the input disturbance $D_o(s)$ can be found as

$$\frac{Y(s)}{D_o(s)}=\frac{1}{1+K(s)G(s)}. \tag{4.2}$$

The input disturbance effect rejection of the system is achieved when the relation between output of the system $Y(s)$ and input disturbance $D_i(s)$ equals to zero. It can be noticed that the process $G(s)$ of the two-link SCARA robot is in integral form as

$$G(s)=\frac{1}{s}g(s), \tag{4.3}$$

when $g(s)$ is non-integral term of the process. And then (4.2) can be re-written as

$$\frac{Y(s)}{D_o(s)} = \frac{s}{s + K(s)g(s)}. \tag{4.4}$$

From (4.4), the relation of system output and input disturbance is equal to zero when s approaches to zero. Therefore, the output disturbance can be eliminated completely.

Consider the relation between output of the system $Y(s)$ and input disturbance $D_i(s)$

$$\frac{Y(s)}{D_i(s)} = \frac{G(s)}{1 + K(s)G(s)}. \tag{4.5}$$

Substituting (4.3) to (4.5), the following equation is obtained as

$$\frac{Y(s)}{D_i(s)} = \frac{g(s)}{s + K(s)g(s)}. \tag{4.6}$$

The relation of system output and input disturbance from (4.6) is not equal to zero when s approaches to zero. Notice that to achieve this requirement, the controller $K(s)$ must be in integral form as well,

$$K(s) = \frac{1}{s}k(s), \tag{4.7}$$

when $k(s)$ is non-integral term of the controller. Then (4.5) can be obtained as

$$\frac{Y(s)}{D_i(s)} = \frac{sg(s)}{s + k(s)g(s)}. \tag{4.8}$$

Obviously, the input disturbance is eliminated when s approaches to zero.

4.2.1 IMC-based PID Controller Design by Applying a General IMC Low-pass Filter

The general IMC low-pass filter for integral model in table 3.1 is applied to design the controller of the two-link SCARA robot which is given as

$$f(s) = \frac{1}{(\lambda s + 1)^2}, \tag{4.9}$$

From the IMC-based PID controller design steps introduced in Chapter 2, the transfer function of the system shown in (4.1) can be divided into two parts

$$\hat{G}_+(s)=1, \tag{4.10}$$

and

$$\hat{G}_-(s)=\frac{as+b}{s(s^2+a's+b')}. \tag{4.11}$$

By substituting (4.9), (4.10) and (4.11) to the general feedback controller $K(s)$ shown in (3.29), then it can be obtained as

$$K(s)=\frac{s^2+a's+b'}{a\lambda^2 s^2+(b\lambda^2+a\lambda)s+2b\lambda} \tag{4.12}$$

The controller $K(s)$ can be directly approximated as PD controller by Maclaurin series expansion due to missing of integral term. Then the controller $K(s)$ can be expanded as

$$K(s)=K(0)+K'(0)s+\frac{K''(0)s^2}{2!}.... \tag{4.13}$$

Keeping first two terms and neglecting higher order terms, the remaining terms are matched to the PD controller. Thus, the PD controller parameters can be derived as

$$K_P=K(0) \tag{4.14}$$

$$K_D=K'(0) \tag{4.15}$$

where

$$K(0)=\frac{b'}{2b\lambda} \tag{4.16}$$

$$K'(0) = \frac{2a'b - b'(a + b\lambda)}{4b^2\lambda}. \tag{4.17}$$

Theoretically, analysis above, the general feedback controller $K(s)$ from (4.12) can track the step reference input and can reject the effect of output disturbance. However, it cannot reject the effect of input disturbance. The responses of the controllers are evaluated in chapter 5 by simulations and experiments.

4.2.2 IMC-based PID Controller Design by Applying the Proposed IMC Low-pass Filter

To eliminate the effect of input disturbance and output disturbance, the controller $K(s)$ must be in integral form. According to the literature mentioned in the chapter 2, the low-pass filter is an achievable factor for this requirement. Several low-pass filters for difference processes have been proposed in [11, 12] which are re-presented in previous chapter. However, those filters are not responding the requirement of this process. Therefore, the suitable low-pass filter $f(s)$ for the SCARA robot model is selected in the form as

$$f(s) = \frac{zs + 1}{xs^3 + ys^2 + zs + 1}, \tag{4.18}$$

By substituting equation (4.10), (4.11) and (4.18) to equation (3.20) and then $K(s)$ can be expressed as

$$K(s) = \frac{zs^3 + (a'z + 1)s^2 + (b'z + a')s + b'}{s\left[axs^2 + (ay + bx)s + by\right]}. \tag{4.19}$$

To approximate $K(s)$ as PID parameters, we assign non-integral term of $K(s)$ as

$$k(s) = \frac{n(s)}{d(s)} = \frac{zs^3 + (a'z + 1)s^2 + (b'z + a')s + b'}{\left[axs^2 + (ay + bx)s + by\right]}. \tag{4.20}$$

Then $k(s)$ is performed by Maclaurin series expansion and its approximated equation is given as

$$K(s)=\frac{1}{s}\left[k(0)+\dot{k}(0)s+\frac{\ddot{k}(0)s^2}{2!}\cdots\right]. \tag{4.21}$$

By ignoring higher order terms and multiplying the integral term through (4.21), it can be noticed that the first three terms are matched to the PID controller parameters as

$$K_{pid}(s)\approx K_p+\frac{K_i}{s}+K_d s\,, \tag{4.22}$$

where

$$K_p=\dot{k}(0)\,, \tag{4.23}$$

$K_i=k(0)$ and

$$K_d=\frac{\ddot{k}(0)}{2}$$

when

$$k(0)=\frac{n(0)}{d(0)}=\frac{b'}{by} \tag{4.24}$$

$$\dot{k}(0)=\frac{n'(0)d(0)-n(0)d'(0)}{d^2(0)}=\frac{(a'+b'z)by-b'(ay+bx)}{(by)^2}$$

$$\ddot{k}(0)=\frac{n''(0)d^3(0)-n(0)d''(0)d^2(0)-2n'(0)d'(0)d^2(0)+2n(0)\left[d'(0)\right]^2 d(0)}{d^4(0)}$$

$$=\frac{1}{2}\frac{(1+a'z)(by)^2-\left[ab'x-(a+b'y)(ay+bx)\right]by+b'(ay+bx)}{(by)^3}$$

The characteristic of the parameters x , y , and z is studied in the next chapter.

Chapter 5

Simulations and Experiments

This chapter describes the effectiveness of IMC-based PID controller which is designed in chapter 4. The effectiveness of general IMC low-pass filter for the model of the SCARA robotis first presented. The input-output disturbances effect rejection is verified by simulation as well. Then, the proposed IMC low-pass filter is presented. In this case, the input and output disturbances effect rejection are evaluated by simulations and experiments. As IMC-based PID controller design is conducted in the same manner, thus, the simulations and experiments are studied mainly for the first link. Finally, the responses of both links are demonstrated. The experimental system of the two-link SCARA robot is depicted in figure 5.1.

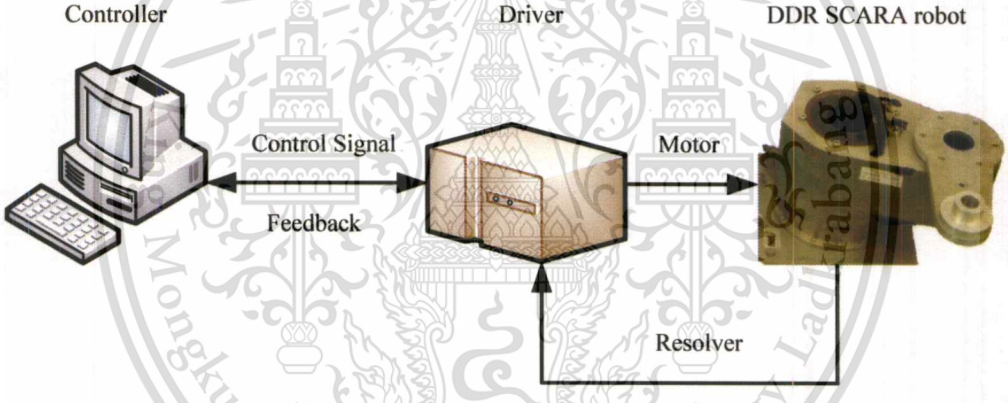

Figure 5.1 Experimental system.

The parameters of two-links SCARA robot in the laboratory are given by table 5.1. The actuators of the first link and the second link are direct driven by AC servo motor. Maximum torques of $70Nm$ for first link and of $15Nm$ for the second link are produced at $\pm 8V$ by 2 channel of 24bits DAC interface card. High speed optical encoders of first link and the second link are 614,400 pulse/rev and 507,904 pulse/rev, respectively.

Table 5.1 Parameters of the two-link SCARA robot

Parameters	Values	Unit
m_1	4.37	kg
m_2	1.24	kg
l_1	200	mm
l_2	200	mm
a_1	63	mm
a_2	80	mm
J_{M1}	0.085	$kg \cdot m$
J_{M2}	0.060	$kg \cdot m$
K_{M1}	2.7590	$N \cdot m / V$
K_{M2}	1.3281	$N \cdot m / V$
B_{M1}	0.8691	$N \cdot m/(rad/s)$
B_{M2}	0.4347	$N \cdot m/(rad/s)$

5.1 Open-loop Responses

In this section, the command voltage E_{a1} and E_{a2} at 4 volts are applied to the first link and the second link of the SCARA robot, respectively. The responses of them are shown in figure 5.2. It can be seen that the links move continuously.

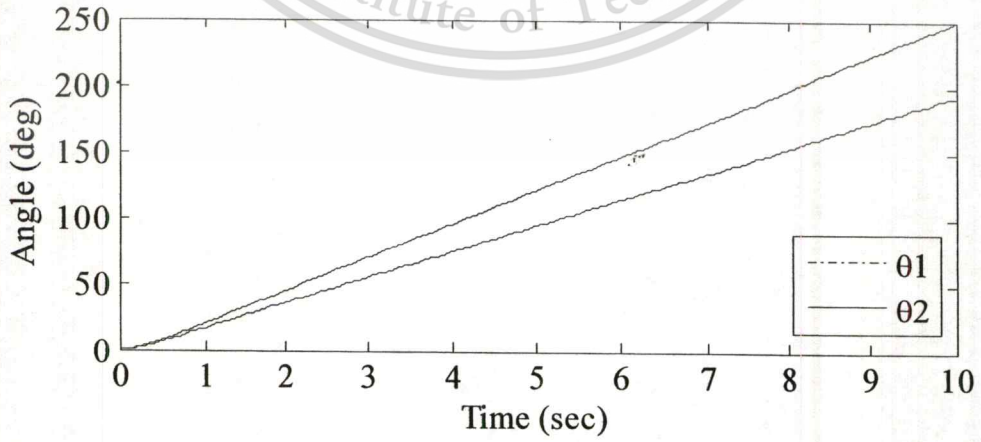

Figure 5.2 Open-loop responses.

In order to control the angular position of the two-link the SCARA robot to the desired position accurately, the designed IMC-based PID controller described in Chapter 4 is applied to control the robot system. The controller parameters are tuned to achieve the desired performances. In next section, the performances of controlled system are shown by simulations and experiments.

5.2 Investigation on Utilizing the General IMC Low-pass Filter

In this section, the parameter of a general IMC low-pass filters shown in (4.9) will be studied in order to find its effect on the SCARA robot control system. The alternative form is shown in (5.1).

$$f(s) = \frac{1}{(\lambda^2 s^2 + 2\lambda s + 1)} \tag{5.1}$$

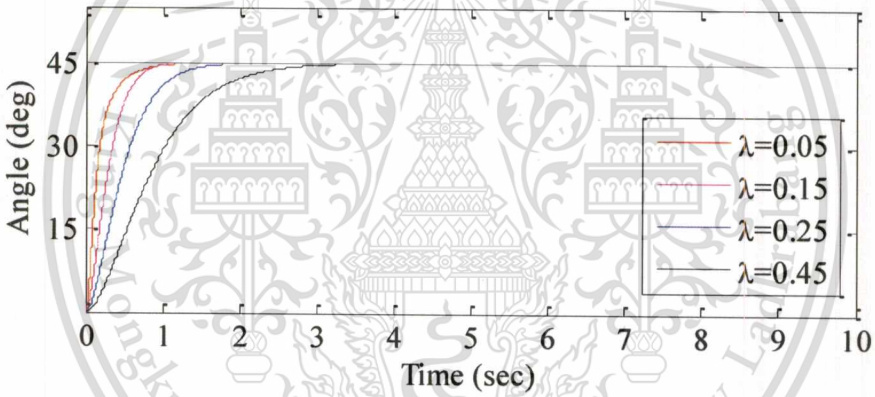

(a) Step responses for first link

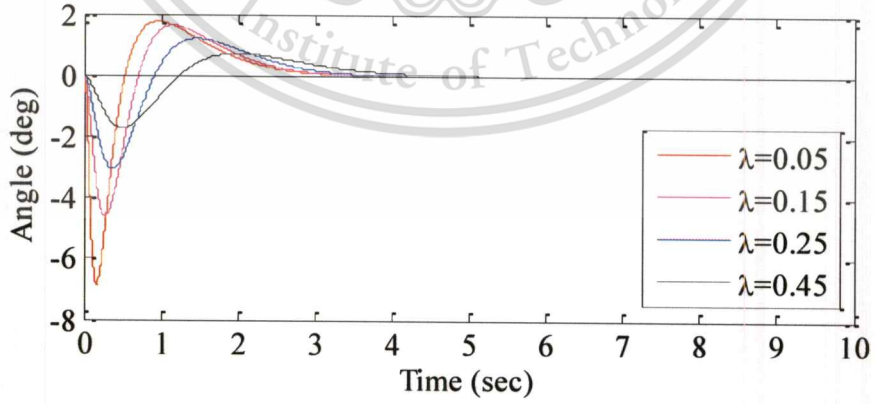

(b) Effects of the second link due to the first link

Figure 5.3 Step responses of the system applying the general IMC low-pass filter.

The step responses of the first link and input disturbance output disturbances rejections for this filter are presented by simulations as below.

For the study of applying the general IMC low-pass filter in (5.1), the step reference input at 45 degree is applied to the first link while the second link is regulated at zero. The responses of both links are given in figure 5.3. It can be seen that the responses of the first link reach to the set point rapidly without overshoot and steady-state error for the parameter $\lambda < 0.05$. The speed of response is decreased when the parameter λ is increased. Meanwhile, the second link is also affected from the first link which is deviated according to the speed of the responses of the first link. The parameter of the second link is fixed at $\lambda = 0.15$.

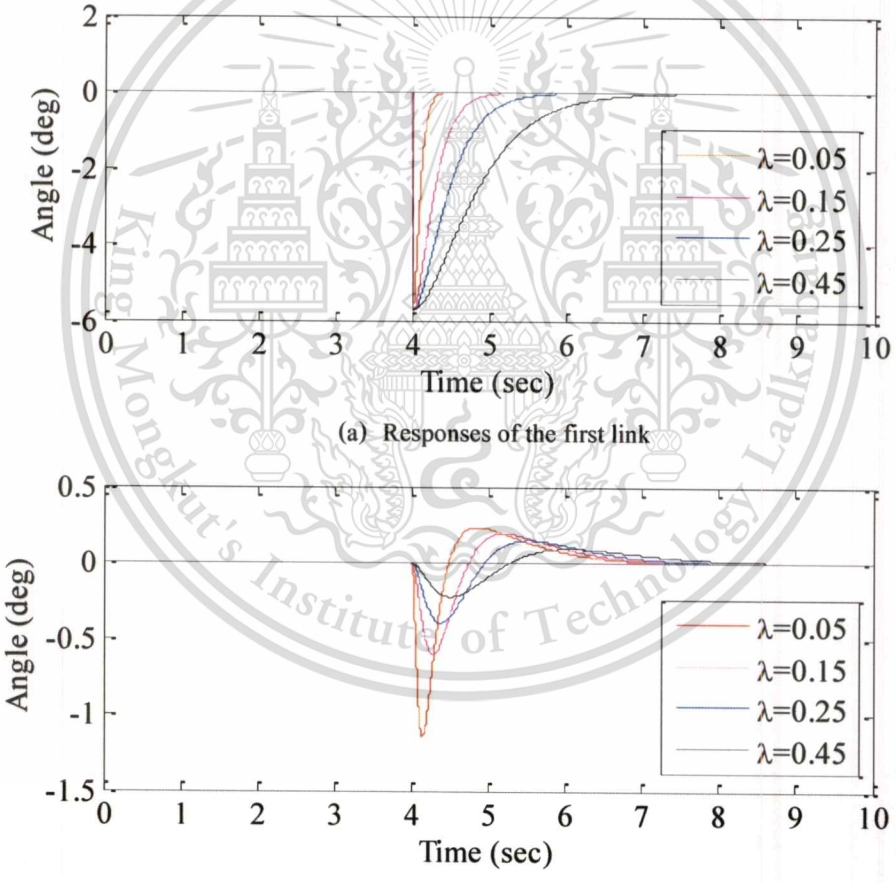

(a) Responses of the first link

(b) Responses of the second link

Figure 5.4 Responses due to output disturbance when applying the general IMC low-pass filter.

In order to study the effect of the output disturbance, the reference inputs at zero degree are applied to both links for 4 seconds. Then, an output disturbance of 0.1 radians is entered to the first link. It can be seen form figure 5.4 (a) that the angular positions of the first link are dropped about 5.7 degrees and returned to the set point which is the same characteristic as the step response. This means that the effect of output disturbance can be rejected. The effect of output disturbance in the second link is also rejected as shown in figure 5.4 (b).

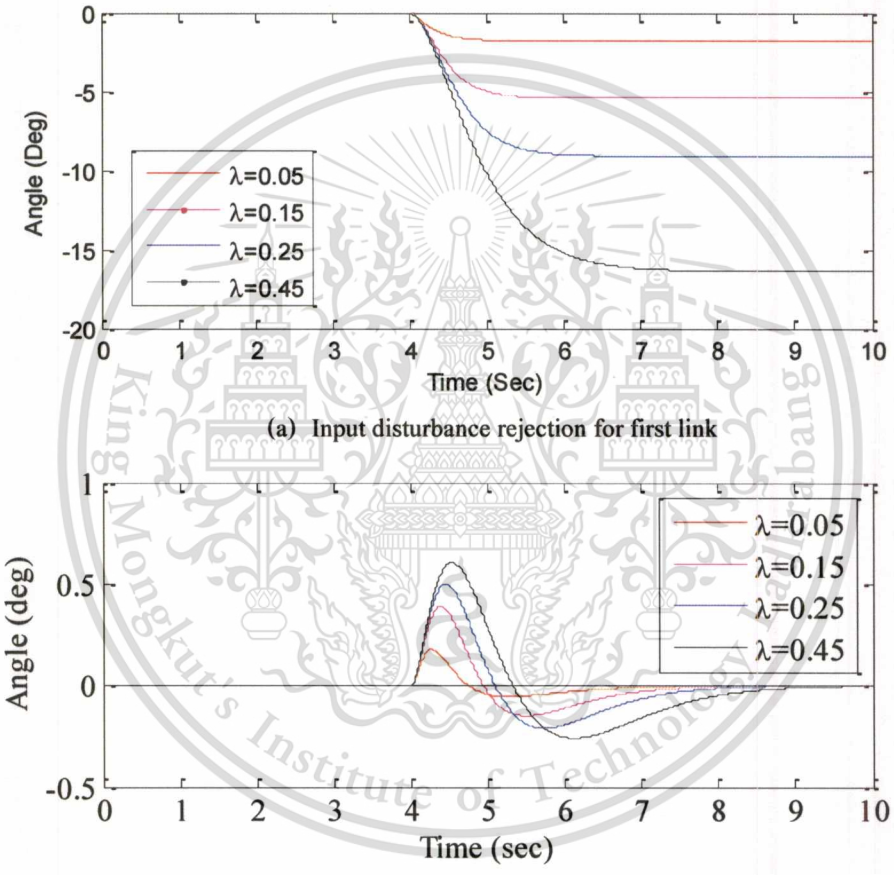

(a) Input disturbance rejection for first link

(b) Effects of the second link due to the first link

Figure 5.5 Responses due to input disturbance when applying the general IMC low-pass filter.

Next, the effect of input disturbance is studied. The reference inputs at zero degree are applied to both links for 4 seconds and then input disturbance at 0.1 radians is entered to the first link. The effects of input disturbances are shown in figure 5.5. It is seen from figure 5.5 (a) that angular positions of the first link are dropped and not able returned to the set point. This means that the effect of input

disturbance cannot be rejected. It is also seen from figure 5.5 (a) that when the parameter λ is increased the dropping angular of the first link is increased, and the deviation of the second link is also increasingly affected as shown in figure 5.5 (b).

From the study of general IMC low-pass filter shown above, it can be summarized that the link can be controlled accurately without overshoot and steady-state error and the effect of output disturbance can also be rejected when applying this filter. However, it cannot be able to eliminate the effect of input disturbance.

5.3 Proposed IMC Low-pass Filter

In this section, the characteristic of each parameter of the proposed IMC low-pass filter from (4.18) is studied in cases.

5.3.1 Characteristic of the Parameter y and z

The characteristics of parameter y and z while setting $x = 0$ are studied. Therefore, the proposed IMC low-pass filters is in the same form as the general IMC low-pass filter stated in previous section and the parameter y and z are indecently adjustable which is rewritten as

$$f(s) = \frac{zs+1}{ys^2 + zs+1}. \tag{5.1}$$

The characteristic of each parameter is studied case by case.

Case 1: The effect of Parameter y

In this case, the step response characteristic is first studied by setting step reference input at 45 degree for the first link and zero degree for the second link. The parameter z is fixed at 250 while the parameter y is adjusted from 1 to 200. The responses are shown in figure 5.6. From this figure, it can be seen that the step response speed of the first link still increase when the parameter y is decreased less than 1. In the contrast, when the parameter y is increased the response is slow down with increased undershoot.

In the same time, the second link is affected as well. For the fast response of the first link, the second link is deviated

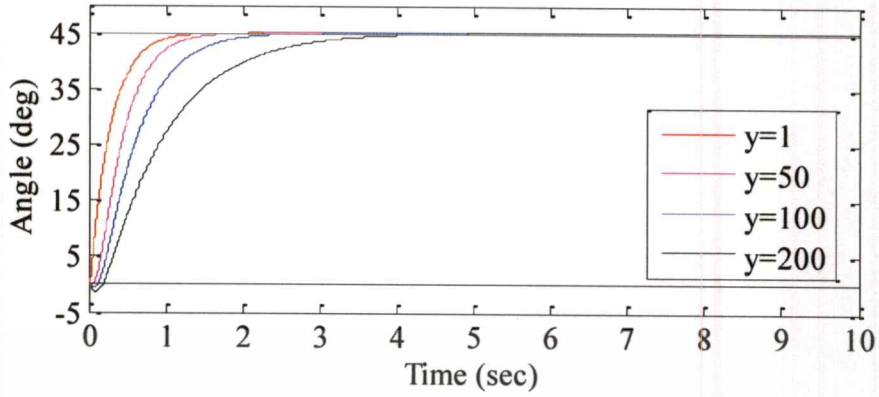

(a) Step response of the first link

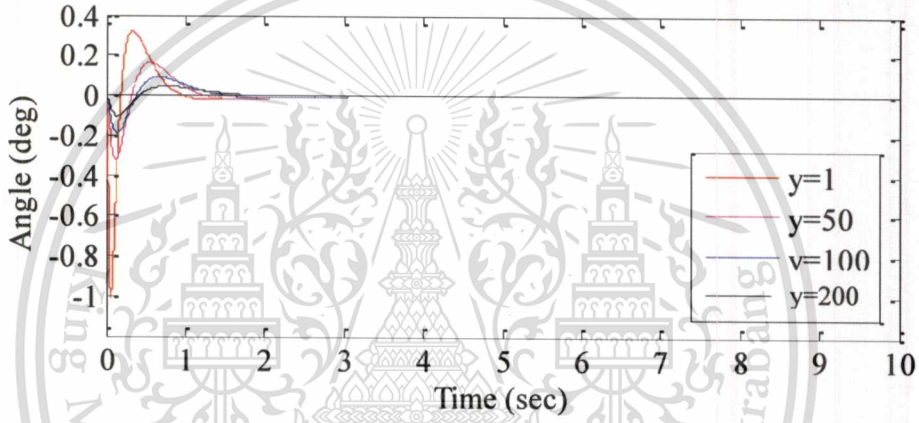

(b) Effect of the second link due to the first link

Figure 5.6 Step response of the parameter y for Case 1.

For the output disturbance rejection, the reference input and output disturbance are applied the same as output disturbance rejection in section 5.2 and its responses are shown in figure 5.7. It can be seen that the first link is dropped about 5.7 degree in every value of the parameter y and returned to the set point without overshoot and steady state error. Accordingly, for the fast response of the step response, the output disturbance response is also fast response and it is slightly slower when the parameter y is increased.

Meanwhile, the second link is deviated the same characteristic as the effect of the second link due to the first link in figure 5.6.

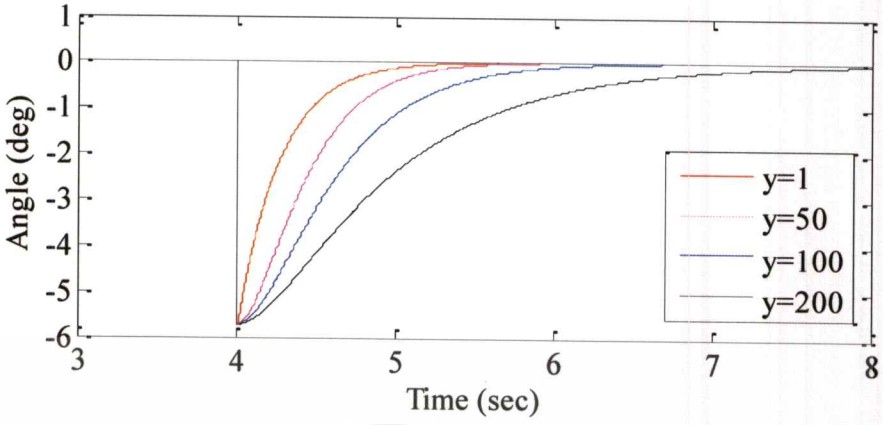

(a) Output disturbance rejection for the first link

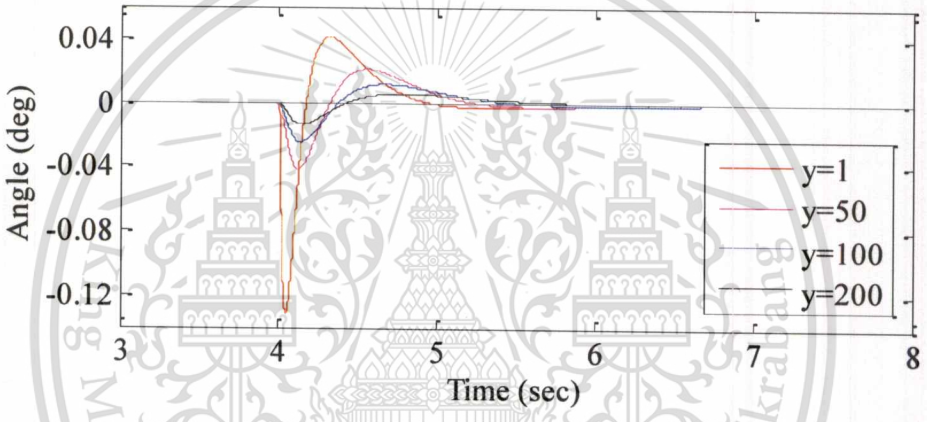

(b) Effect of the second link due to the first link

Figure 5.7 Output disturbance effect rejection of the parameter y for Case 1.

To study the effect of the parameter y, the reference input and input disturbance is entered to the first link the same as section 5.2. And its response is depicted in figure 5.8. It gives the result that when input disturbance at 0.1 radians is reduced the command voltage of the link; it is dropped accordingly with increasing of the parameter y without return to the set point.

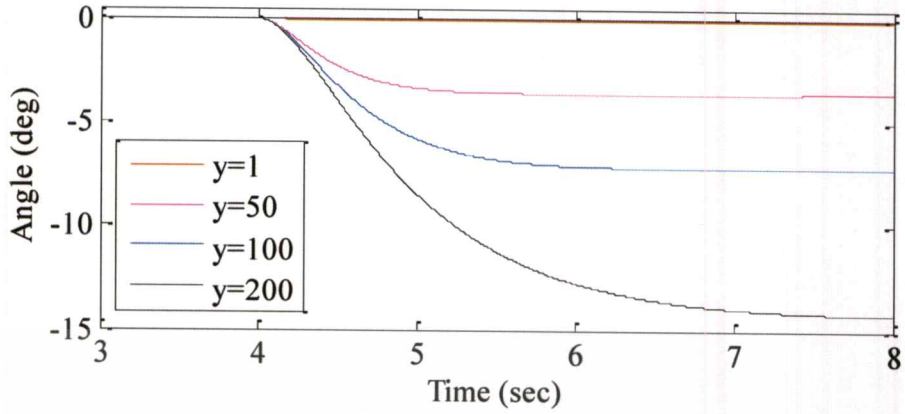

(a) Input disturbance rejection for the first link

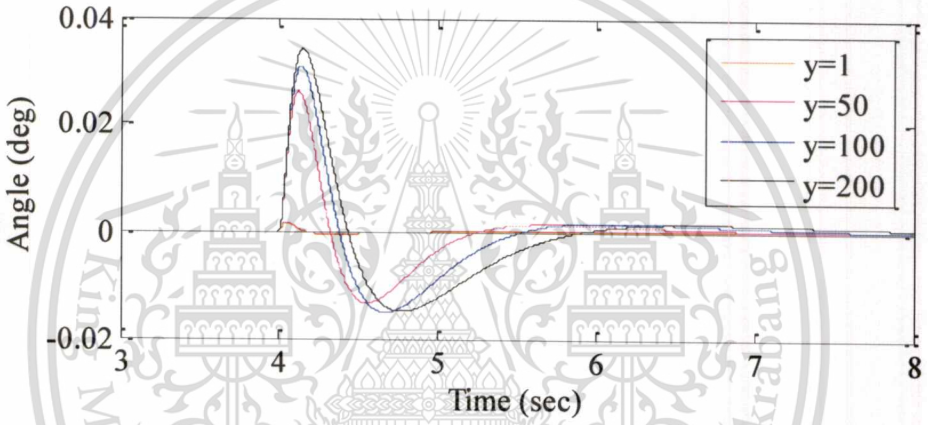

(b) Effect of the second link due to the first link

Figure 5.8 Input disturbance effect rejection of the parameter y for Case 1.

Case 2: The effect of parameter z

From the study of the parameter y above, suppose that y = 1 is satisfying response for case above. In this case, the characteristic of the parameter z is studied in Case 2.

Similarly, the step reference at 45 degree and zero degree are respectively applied to the first link and the second link while the parameter z is varied from z = 0 to z = 250. The responses of both links are given in figure 5.9. It shows that the response of the first link is slightly attained to the set point without overshoot and steady state error and finally it is saturated when the parameter z is increased higher than 50. On the contrast, if the parameter z is decreased the step response is slower with increased overshoot. Meanwhile, the second link is also affected. As the saturation of the first link at z > 50 the deviation of the second link is fixed as well. But decreasing of the parameter z causes the response speed of the first link decrease which is caused deviation of the second link decrease

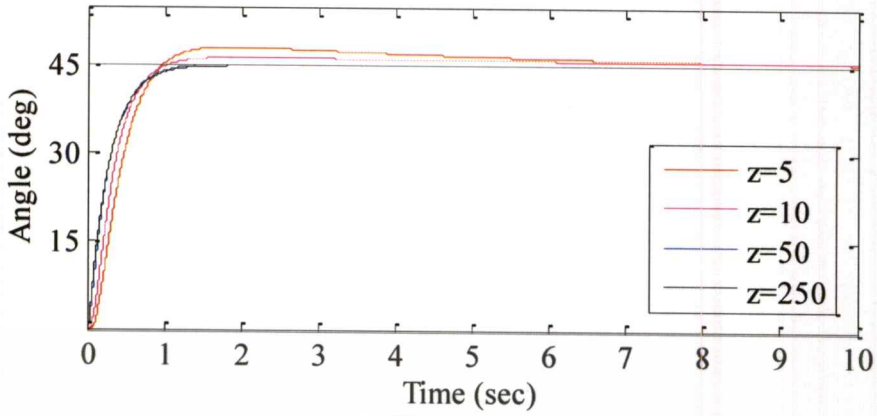

(a) Simulation results of output disturbances rejection

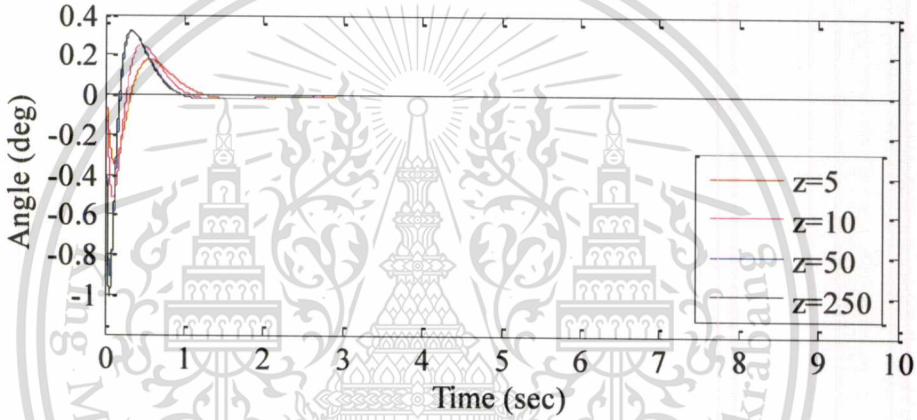

(b) Simulation results of input disturbances rejection

Figure 5.9 Step response of parameter z for Case 1.

The reference input and output disturbance the same as section 5.2 are assigned to both links. Figure 5.10 illustrates the responses of output disturbance rejection. It can be seen that the first link dropped about 5.7 degrees and forced back to the set point which is the same characteristic as step response in figure 5.9. Meantime, the second link is affected which is deviated maximally about 0.13 degree and eventually return to the set point.

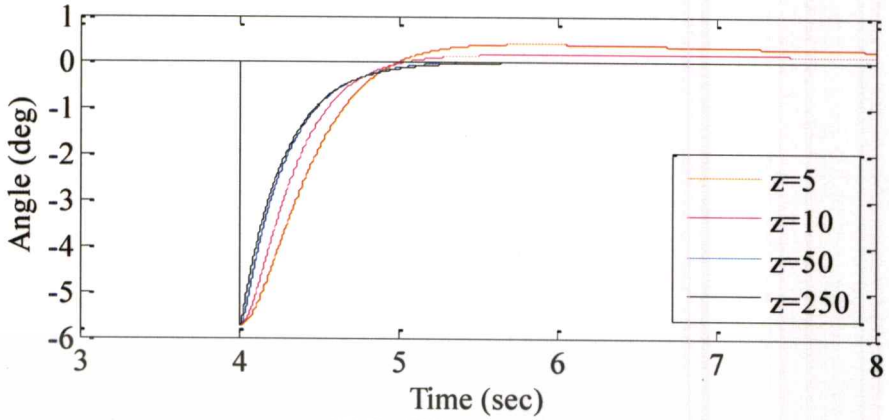

(a) Output disturbance rejection for the first link

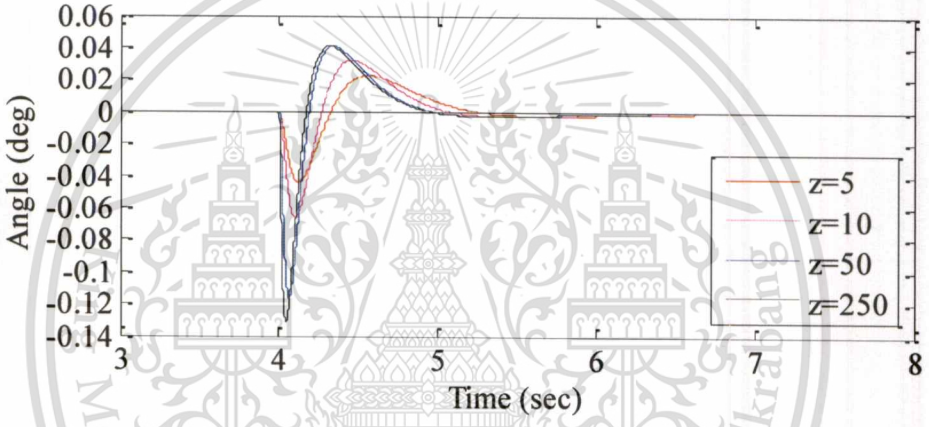

(b) Effect of the second link due to the first link

Figure 5.10 Output disturbance effect rejection of the parameter z for Case 2.

To study the input disturbance rejection characteristic of the parameter z, the reference input at zero degree is set for both links and then the input disturbance ay 0.1 radians is entered to the input of the first link to reduce the command voltage. The responses of the system are expressed in figure 5.11. It can be noticed that the first link is increasingly dropped when the parameter z is increased from z=5 and it tries to return to the set point but takes several second to attain to the set point. While the second link is also deviated maximally about 0.02 degrees and eventually returned to the set point.

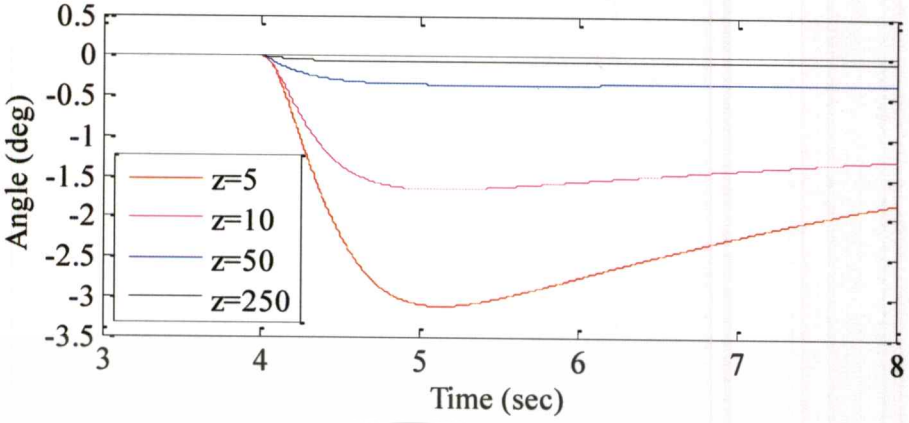

(a) Input disturbance rejection for the first link

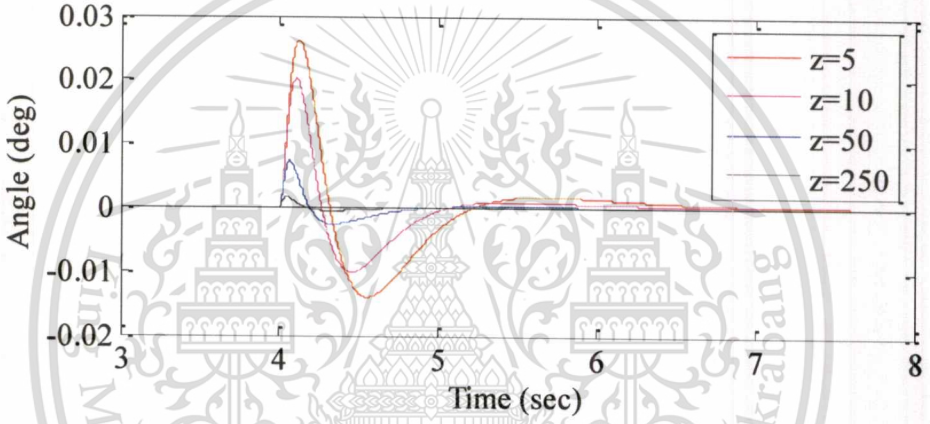

(b) Effect of the second link due to input disturbance of the first link

Figure 5.11 Input disturbance effect rejection of the parameter z for Case 2.

From study the characteristic both parameter y and z above, it can be summarized that the proposed filter without the parameter x which is more freedom for tuning the controller of the system, it is able to achieve the set point and is able to eliminate the input disturbance but last for several seconds to attain to the set point. Thus parameter x is needed to deal with this problem.

5.3.2 Characteristic of the Parameter x, y and z

In this section, the characteristic of the proposed filter x, y and z are studied by simulation. For experiments are mentioned after summarizing the suitable response's parameters. The step response, the effect of another link and elimination of input-output disturbance effects rejection are also demonstrated case by case.

Case 1 Effects of the Parameter x

Before defining the parameter of the filter, each parameter is trial in order to see the response of the parameter x. The acceptable response of the parameter is fixed while other parameters are adjusted to find optimal response. In this case, the parameter y=0.00057 and z=0.6 are fixed while the parameter x is adjust from 0.00015 to 0.00075. For this study, the step reference input at 45 degree is applied to the first link while the second link is regulated at zero degree. The responses of both links are depicted in figure 5.12. It can be seen that the first link move to the set point with acceptable overshoot and return to the set point within 2 seconds for the parameter x= 0.00015. When this parameter is increased the response is faster with the same overshoot. However, the increasing of the step response is more affected to the second link which the deviation of the second link is increased but it return to the set point within about 1.5 seconds.

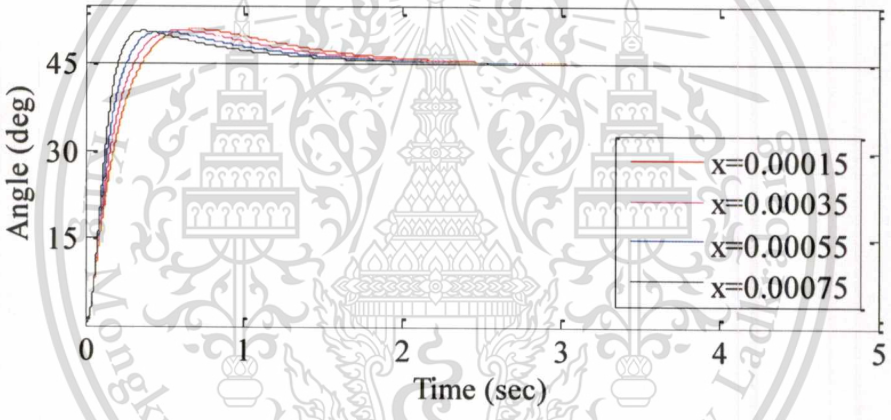

(a) Step response of the first link

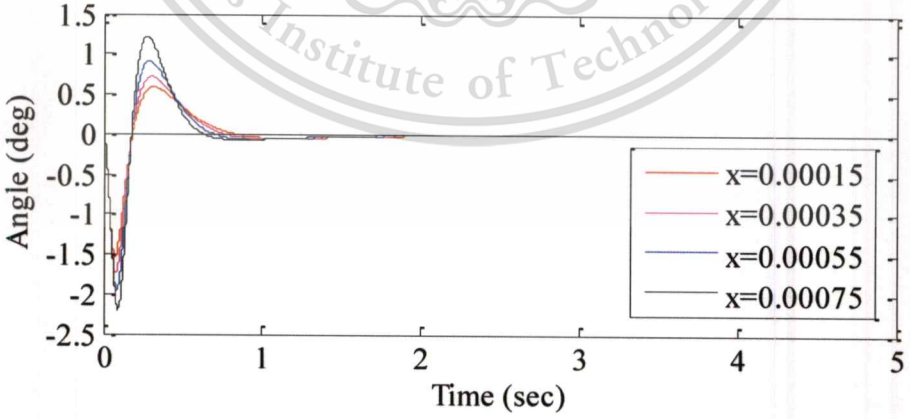

(b) Effect of the second link due to the first link

Figure 5.12 Step response of the parameter x for the proposed filter.

From varying the parameter x above, the output disturbance rejection of this parameter is also studied by regulating the reference input of both links at zero degree for 4 seconds and then the output disturbance at 0.1 radians is entered to the first link which is caused the first link drop about 5.7 degrees and return to the set point the same characteristic as step response in figure 5.12 both the first link and the second link.

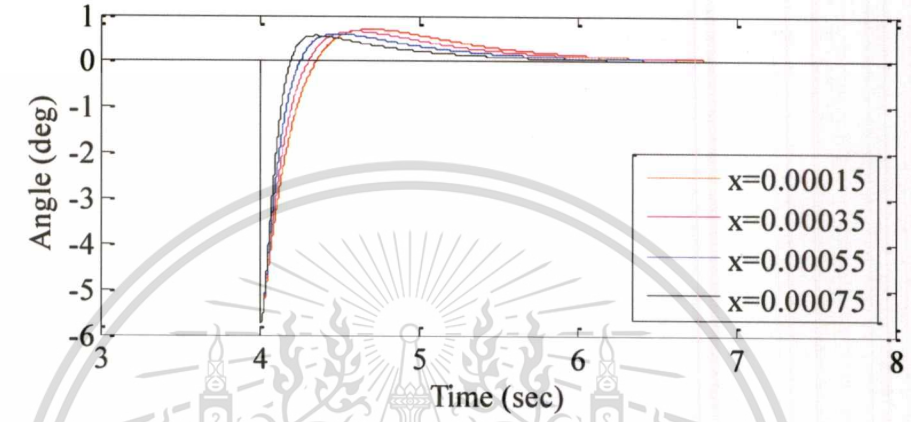

(a) Output disturbances rejection of the first link

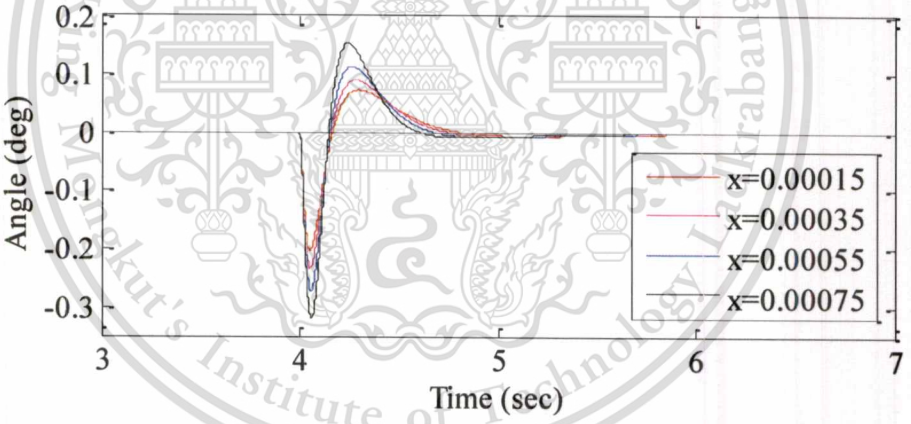

(b) Effect of the second link due to the first link

Figure 5.13 Output disturbance effect rejection of the parameter x for Case 1.

To demonstrate the input disturbance rejection, the reference input of both links and input disturbance the same as previous case are assigned to both links. The responses show similarly as the case of output disturbance rejection, figure 5.14.

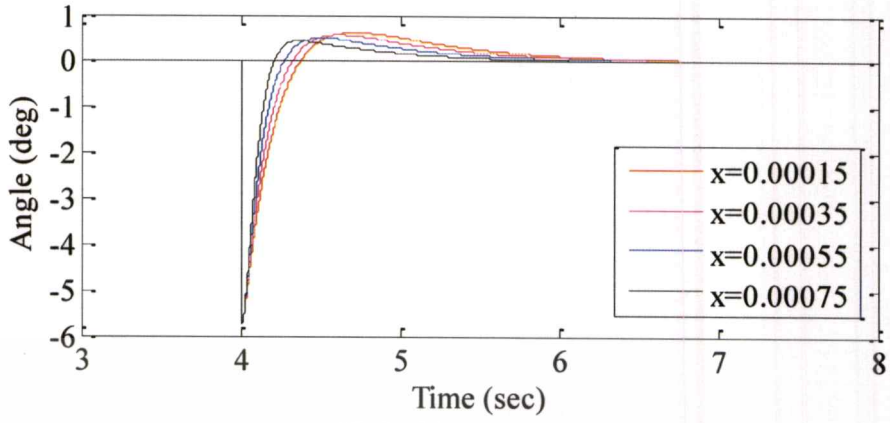

(a) Input disturbances rejection of the first link

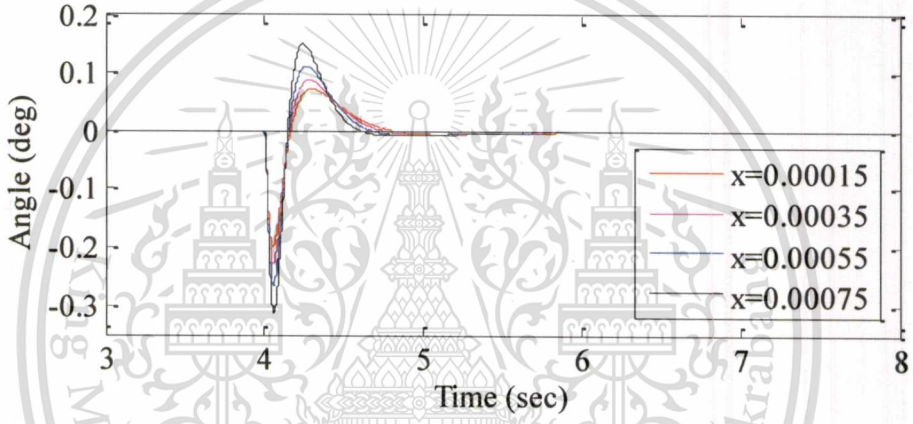

(b) Effect of second link due to the first link

Figure 5.14 Input disturbance effect rejection of the parameter x for Case 1.

Case 2 Effects of the Parameter y

From study the characteristic of the parameter x in Case 1, it is supposed that the parameter x=0.00055 and z=0.6 are acceptable result. Therefore, in this case the characteristic of y is studied. To see the characteristic response of the parameter y, the reference input at 45 degrees and zero degree are applied to the first link and the second link, respectively. The responses are shown in figure 5.15. From this figure it can be explained that when the parameter y is decreased from 0.0057 the response of the first link is slower and the overshoot is increased as well. On the contrast, when the parameter y is increased the response is faster. If this parameter continues to increase the overshoot is increasingly appeared until unstable while the second link is also accordingly oscillated.

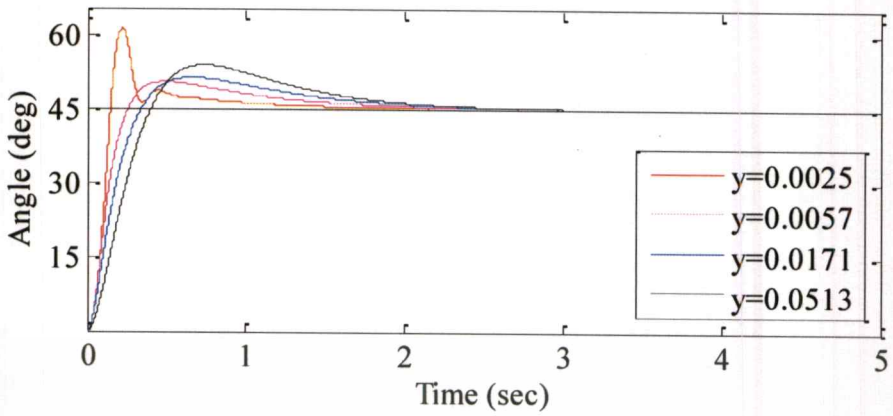

(a) Step response of the first link

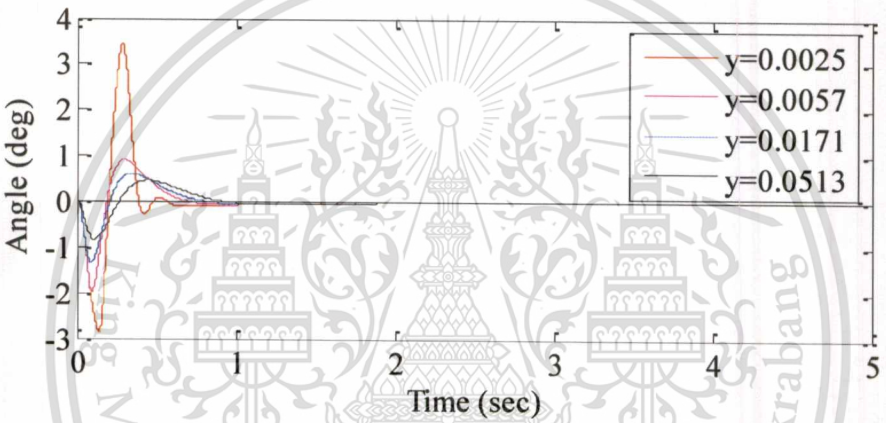

(b) Effect of second link due to the first link

Figure 5.15 Step response of the parameter y for the proposed filter.

To demonstrate the characteristic of the parameter y for the output disturbance rejection, the reference input for both links and output disturbance the same as previous case are assigned to the system. The responses are depicted in figure 5.16. The responses illustrate that the first link drops about 5.7 degree and is forced back to the set point and the second link is also oscillate the same characteristic as figure 5.15.

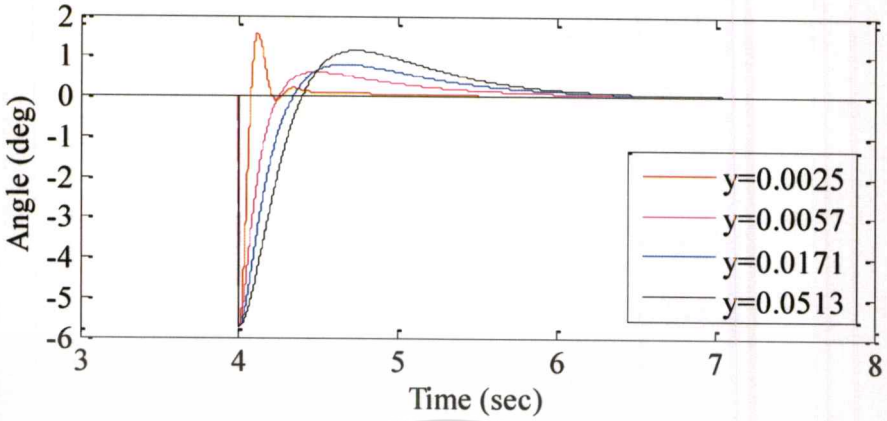

(a) Output disturbances rejection for the first link

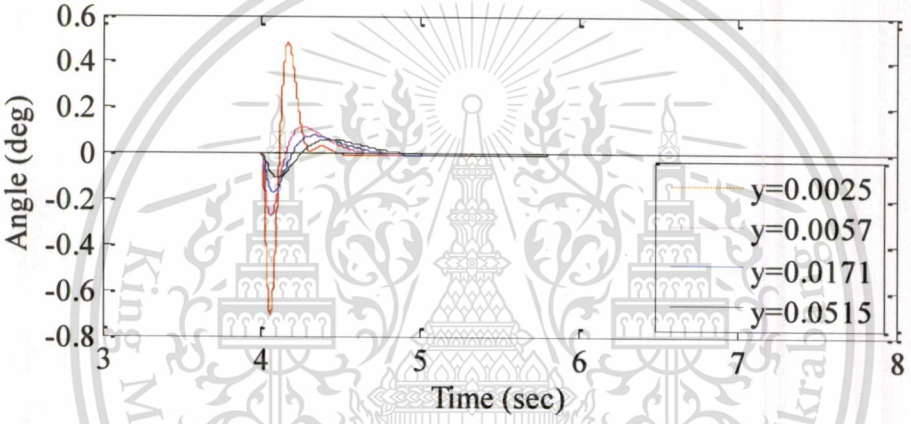

(b) Effect of second link due to the first link

Figure 5.16 Characteristic of the parameter y for the proposed filter.

Similarly, the reference input at zero degree is set for both links for 4 seconds and then the input disturbance at 0.1 radian is entered to the first link. The responses from the figure 5.17 can be explained that the first link drops about 0.1 degree at the parameter z=0.0025. The dropping of this link is increased at 0.2, 0.35 and 0.9 degrees when this parameter is increased at 0.0057, 0.0171 and 0.0513, respectively and return to the set point at nearly the same time about at 3 seconds without overshoot and steady state error. Meantime, the oscillation of the second link is increased as well when the parameter z is increased.

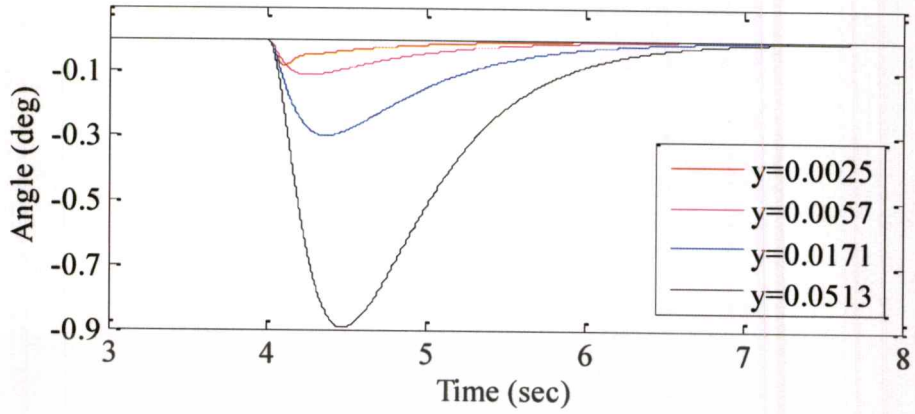

(a) Input disturbance rejection of the first link

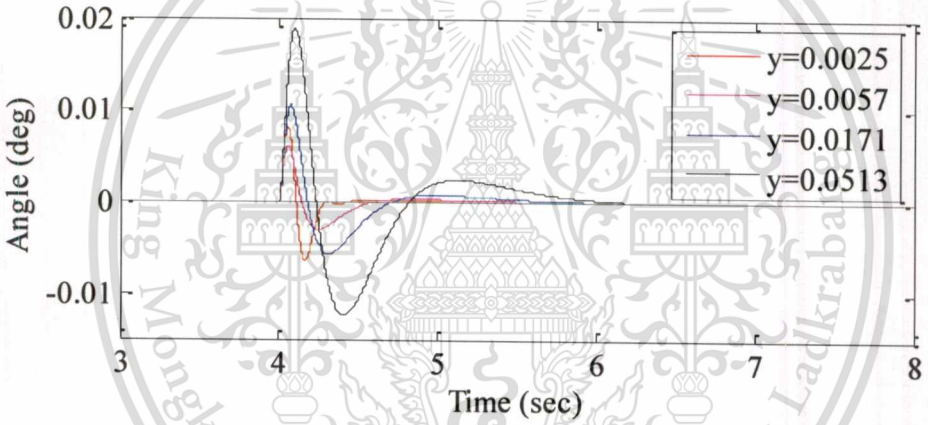

(b) Effect of the second link due to the first link

Figure 5.17 Effects of parameter y for Case 2.

Case 3 Effects of the Parameter z

By studying the characteristic of the parameter x and y above, suppose that the parameter x=0.00055 and y=0.0057 are satisfy performance. In this case the characteristic of the parameter z is studied. To see the see its characteristic the reference input at 45 and zero degree are assigned to the first link and the second link, respectively. The parameter z is study from 0.4 to 1.0. The responses are depicted in figure 5.18. From this figure it can be noticed that decreasing this parameter the response of the first link is faster but the overshoot is increased as well. On the contrast, when the parameter z is creased the overshoot is decreased but the response is slower.

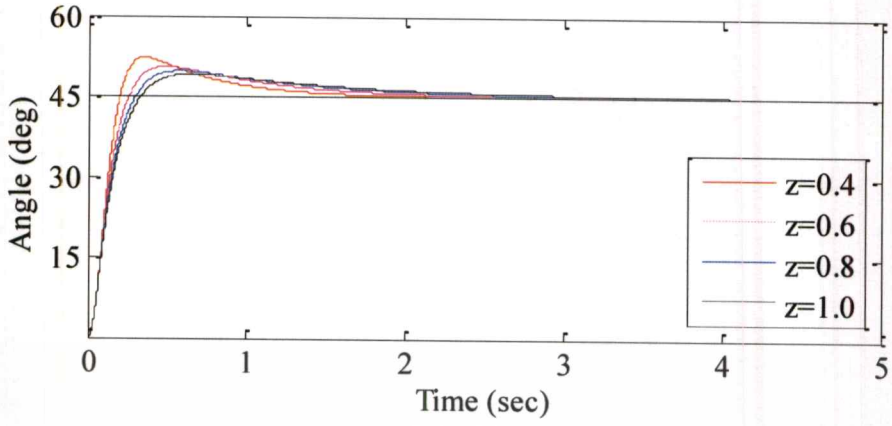

(a) Step response of the first link

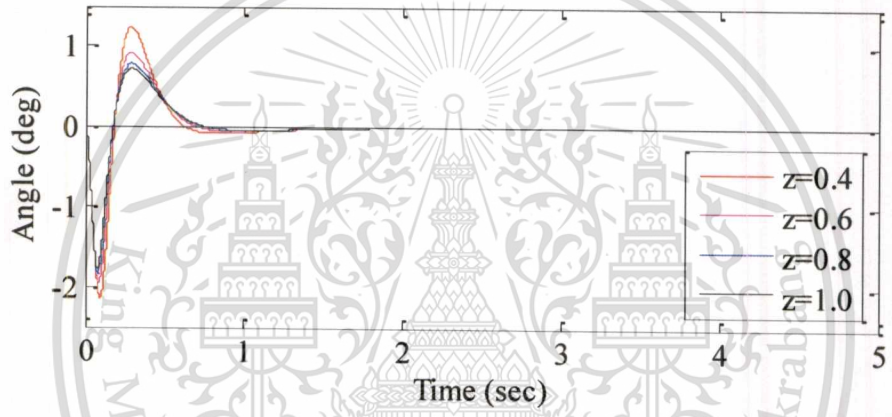

(b) Effect of the second link due to the first link

Figure 5.18 Step response of the parameter z for the proposed filter.

To study the characteristic of the output disturbance rejection, the reference input and input disturbance are similarly assigned to the system which its responses are shown in figure 5.19. From this figure it can be noticed that the first link drops and is forced back to the set point the same characteristic of step responses in figure 5.18.

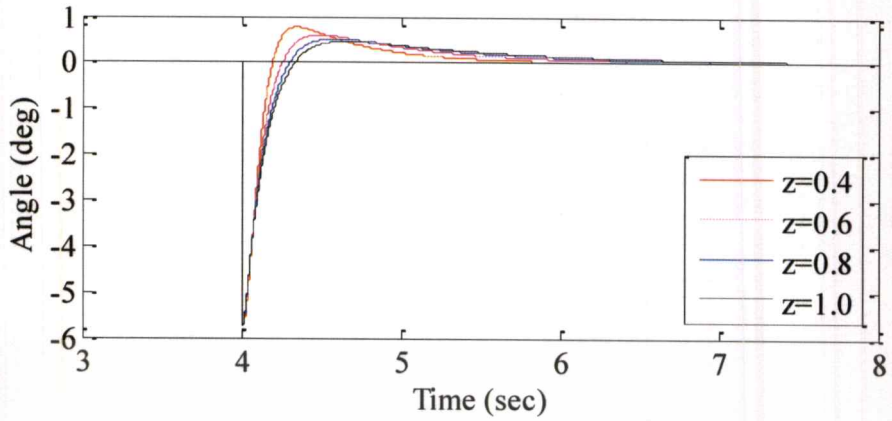

(a) Output disturbance for the first link

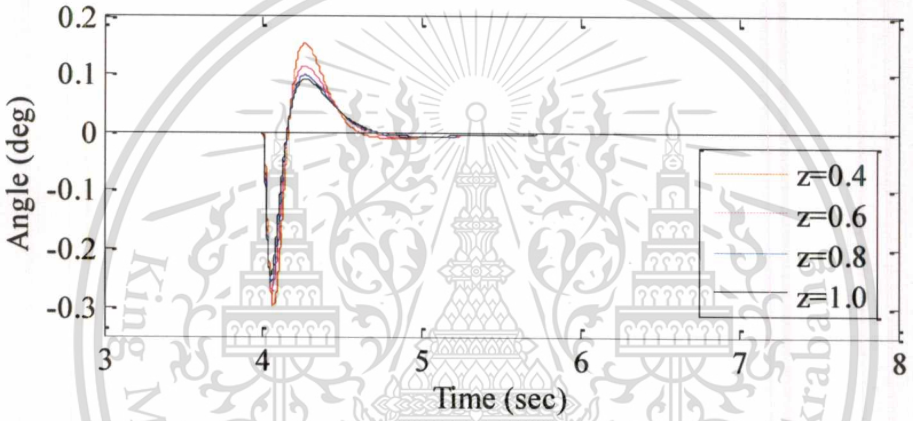

(b) Simulation results of input disturbances rejection

Figure 5.19 Effects of parameter z for Case 2.

The reference input at zero degree is regulated to both links for 4 seconds and input disturbance at 0.1 radians is entered to the first link to reduce the reference input. By entering this disturbance, the first link is increasingly dropped when the parameter z is increased from 0.4 to 1.0 and return to the set point

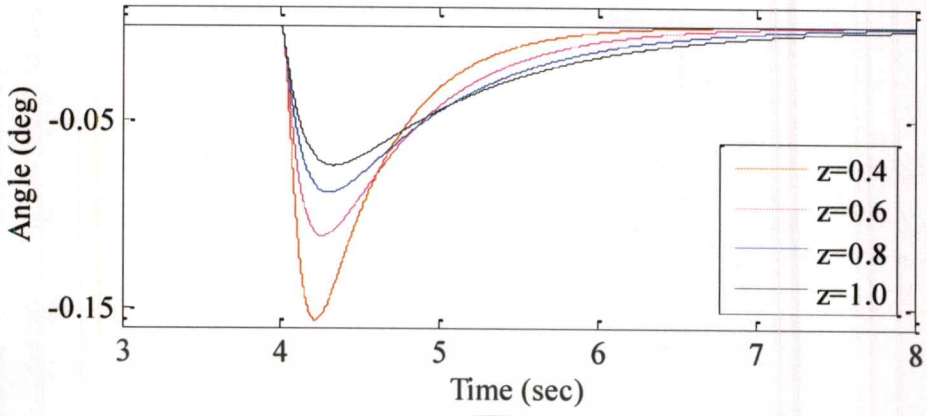

(a) Input disturbance rejection for the first link

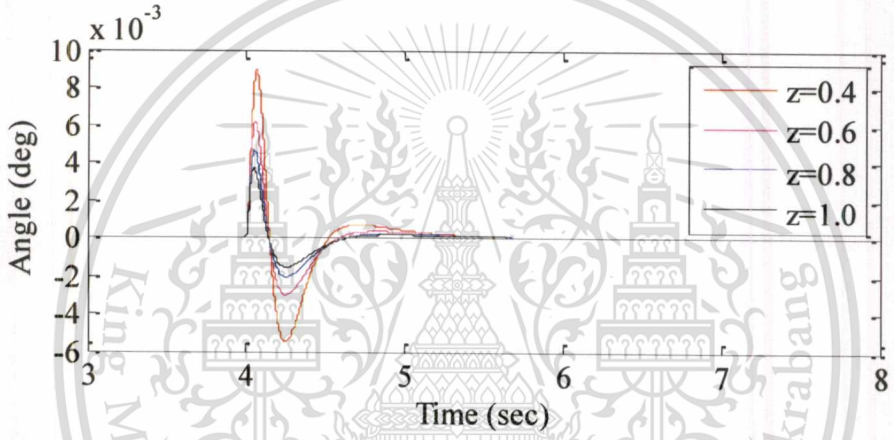

(b) Simulation results of input disturbances rejection

Figure 5.20 Effects of parameter z for Case 2.

From study three parameters characteristic above, the satisfied performance response of the proposed IMC low-pass filter are observed and its parameters are summarized in table 5.2. As the transfer function of the first link and the second link are in the same form. Thus, parameters of the second link are tuned base on the parameter of the first link which use the parameters of the first link first then try to tune the parameter x and y to obtain the compatible response to the first link.

Table 5.2 Parameter x, y and z for both links

	x	y	z	K_p	K_i	K_d
K_{pid1}	$55x10^{-5}$	$57x10^{-4}$	$6x10^{-1}$	42.5106	55.265	4.5949
K_{pid2}	$3x10^{-5}$	$12x10^{-3}$	$6x10^{-1}$	19.9497	27.2788	2.0038

The parameters in table 5.3 are also applied to experiments and then experimental results are compared to simulation results.

Firstly, the step responses are compared. To do this, the step reference input at 45 degrees is applied to simulations and experiments. The responses are shown in figure 5.21 and figure 5.22. It can be seen that the response of the experimental result is tracked closely with simulation result.

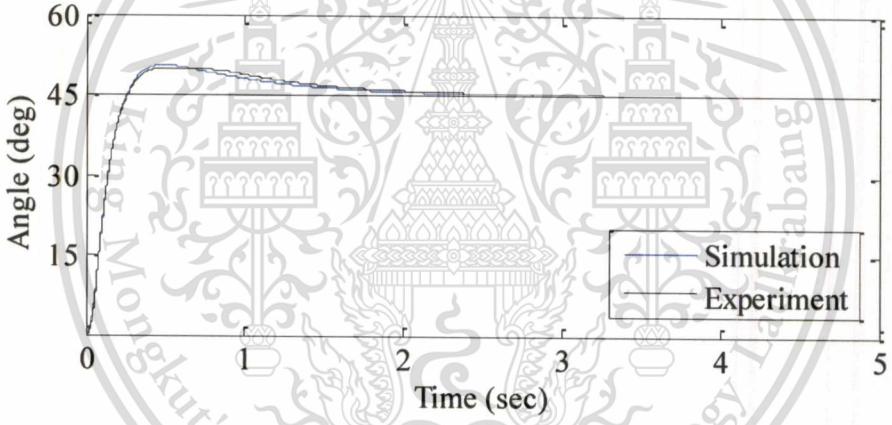

(a) Step response of the first link

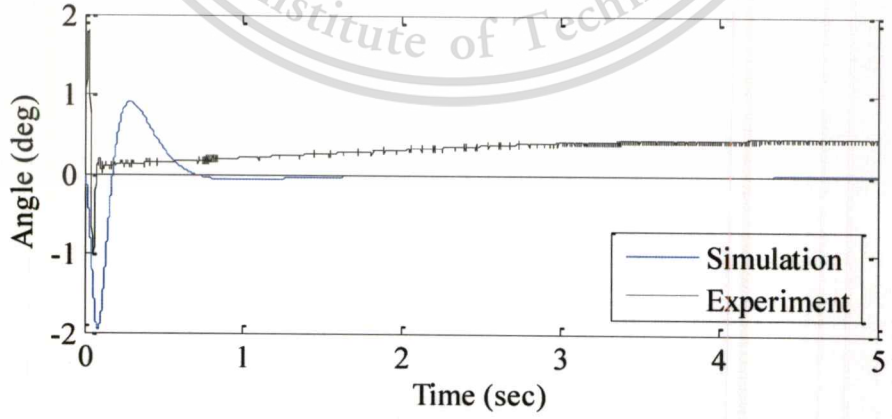

(b) Effect of the second link due to the first link

Figure 5.21 Step response for simulation and experimental results comparison of 1st link.

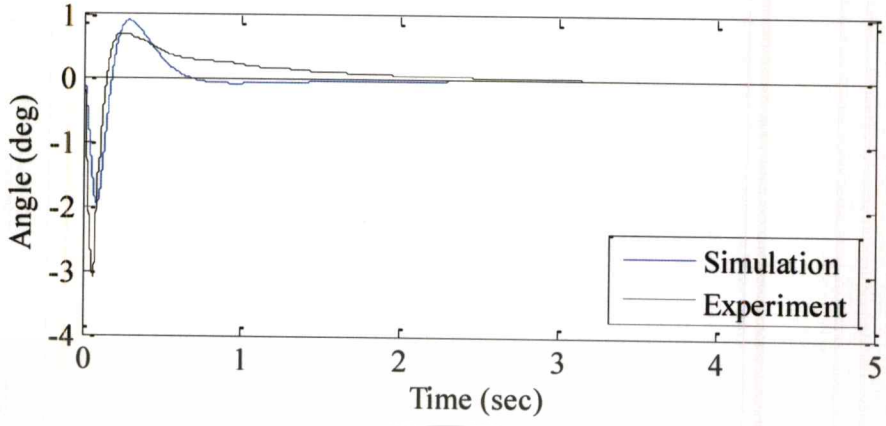

(a) Effect of the first link due to the second link

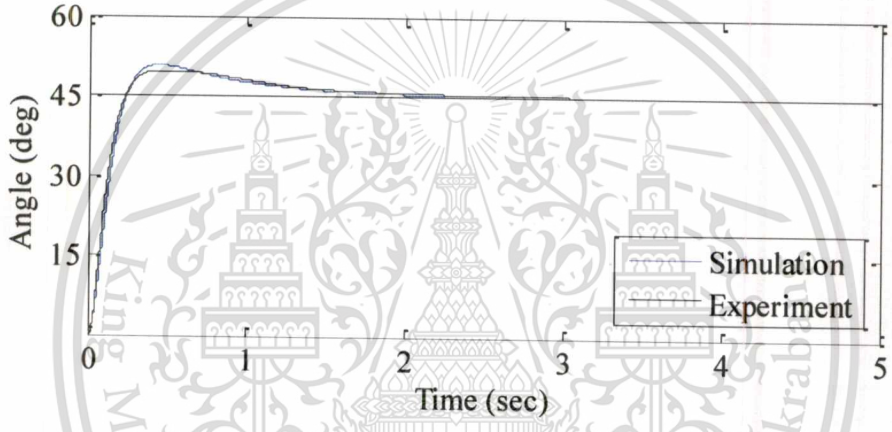

(b) Step response of the second link

Figure 5.22 Step response for simulation and experimental results comparison of 2nd link.

Secondly, the experimental result of output disturbance rejection is explained. As the output disturbance rejection cannot imitate the simulation. Therefore, the output disturbance is entered by pulling to the second link for a while and releases it. It can be seen that the link is oscillated and forced back to the set point. Meantime, the first link is also deviated in the same direction and return to the set point in the same time with the second link.

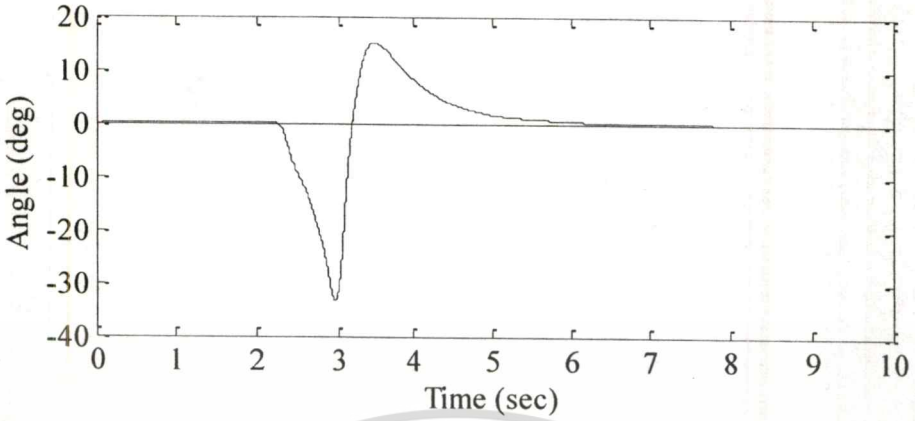

(a) Responses of the first link and the second link

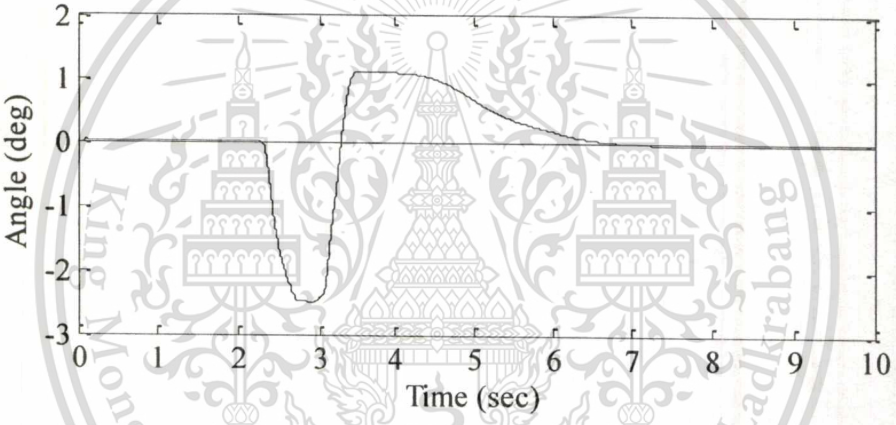

(b) Effect of the first link due to second link

Figure 5.23 Experimental results of the first link and the second link comparison.

Lastly, the input disturbance rejection is also compared with simulation. In this case, the reference input at 45 degrees and zero degree for the second link and the first link are applied, respectively. It can be seen that the second link drops about 4.5 degree both simulation and experimental result and are return to the set point closely within about 3 seconds but without overshoot and steady state error.

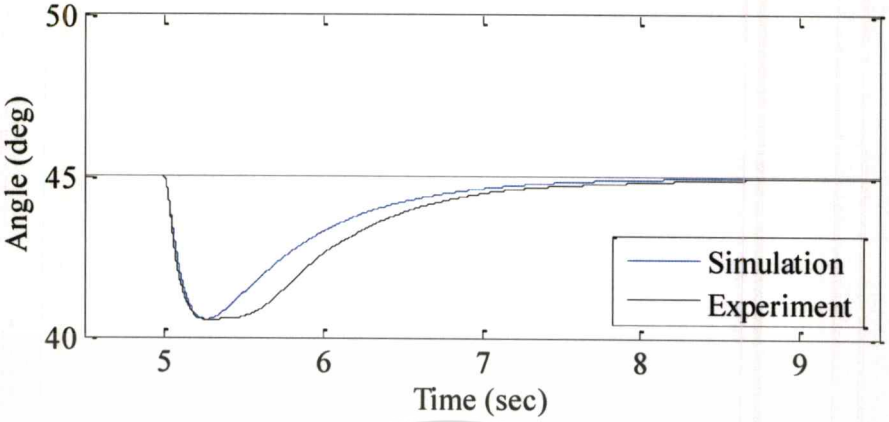

(a) Responses of the first link and the second link

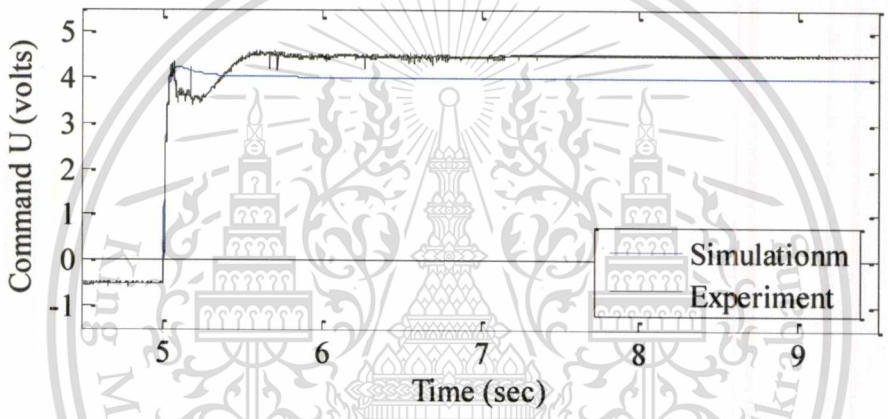

(b) Current command voltages for (a)

Figure 5.24 Experimental results of the first link and the second link comparison.

Chapter 6

Conclusion and Future Works

6.1 Conclusion

The IMC controller design and IMC-based PID controller transformation have been learned with several IMC low-pass filters for difference models. In this thesis, IMC-based PID controller design with a suitable IMC low-pass filter for the model of two-link SCARA robot has proposed in order to achieve fast response without steady-state error and able to deal with input disturbances and output disturbances rejection. The effectiveness of the IMC-Based PID controller design using the proposed low pass filter is verified by simulations and experiments. From the verification, it can be seen that the proposed control system has a good performance. The angular positions of the links can track the reference inputs with fast responses, with acceptable overshoot but without steady-state error. In addition, the effects of input and output disturbances can be rejected. Consequently, it can be conclude that the controller design technique with the proposed IMC low-pass filter for robot manipulator used in the laboratory is successful in tracking the set point and dealing with input and output disturbances rejection.

6.2 Future Works

In actual implementation, angular controls of two-link SCARA robot are effect into each other. To reduce with this problem, the coupling control is interesting work. By using IMC-based PID controller design method for this robot manipulator, the system gives a good performance. Therefore, the proposed control method is interesting for trajectory.

REFERENCES

[1] S. B. Niku, Introduction to Robotics: Analysis, Systems, Applications. Upper Saddle River, NJ: Pretice Hall, 2001.

[2] M. C. Popescu, I. Borosi, O. Olaru, L. Popescu, F. Grofu, The Simulation Hybrid Fuzzy Control of SCARA Robot, WSEAS Transactions on Systems and Control,vol3.pp.105-114, Feb.2008.

[3] F. Passold, M. R. Stemmer, Feedback Error Learning Neural Network Applied to a SCARA Robot, Poland proceeding poznan, Poland, pp.197-202, 2004.

[4] J. G. Ziegler, and N. B. Nichols, "Optimum Setting for Automatic Controllers," Trans. ASME, vol. 64, pp. 759-768, 1942.

[5] G. H. Cohen and G. A. Coon, "Theoretical Consideration of Retarded Control," Trans. ASME, vol. 76, pp. 827-834, 1953.

[6] P. M. Meshram, R. G. Kanojiya, Tuning of PID Controller Using Ziegler-Nichols Method for Speed Control of DC Motor, International Conference On Advances In Engineering, Science And Management (ICAESM -2012), Place, pp.117-122, 2012.

[7] A. Upadhyay, A. Agarwal, Controller Design and Analysis for Automation of Chemical Water Treatment System, 10th International Conference on Control, Automation, Robotics and Vision, Vietnam, pp.1625-1629, 2008.

[8] Y. Okada, Y. Yamakawa, T. Yamazaki, S. Kurosu Tuning Method of PID Controller for Desired Damping Coefficient, SICE Annual Conference 2007, Japan, pp.795-799, 2007.

[9] S. Akamatsu, M. Konishi and J. Imai, Position control of 2-link SCARA robot by Using Internal Model Control, Memoirs of the Faculty of Engineering, Japan, vol.43, pp.49-54, 2009.

[10] C. E. Garcia and M. Morari, Internal Model Control. 1. A Unifying Review and Some New Results, Industrial and Engineering Chemistry Process Design and Development, pp.308-323, 1982.

[11] D. E. Rivera, M. Morari, and S. Skogestad, Internal Model Control 4. PID Controller Design, Industrial and Engineering Chemistry Process Design and Development, vol. 25, pp. 252-265, 1986.

[12] J. Qibing, Q. Ling, W. Xuewei, and Q. Fei, Base on all-pole approximation a new internal model PID control method for the system with time delays, Proceeding of ICMA2009, Changchun China, pp.268-273, 2009.

[13] T. Benjanarasuth, SCARA robot locomotion control by two-degree-of-freedom simple servo adaptive controller, Proceeding of AISM 2010, Singapore, pp. 252-258, 2010.

[14] S. Suvilath, T. Benjanarasuth, U. Komine, K. Khongsomboun, IMC-Baesd PID controller design for a two-link SCARA robot, proceeding of TENCON2011, Indonesia, pp.1030-1034, 2011.

[15] D. Israkorn, "Position Control of Ultrasonic Linear Motor Using PDFF Controller Designed by CDM," *master thesis,* King Mongkut's Institute of Technology Ladkrabang (KMITL), Bangkok, 2003

[16] W. Charn, "Mamdani Fuzzy I-PD Controller for Angular Position Control for Two-link Robot Manipulator," *master thesis,* King Mongkut's Institute of Technology Ladkrabang (KMITL), Bangkok, 2007.

Appendix A

Specification of SCARA Robot

A.1 Dimension of the Two-link SCARA Robot

The dimension of the used robot for experiment in the laboratory is depicted in figure A.1

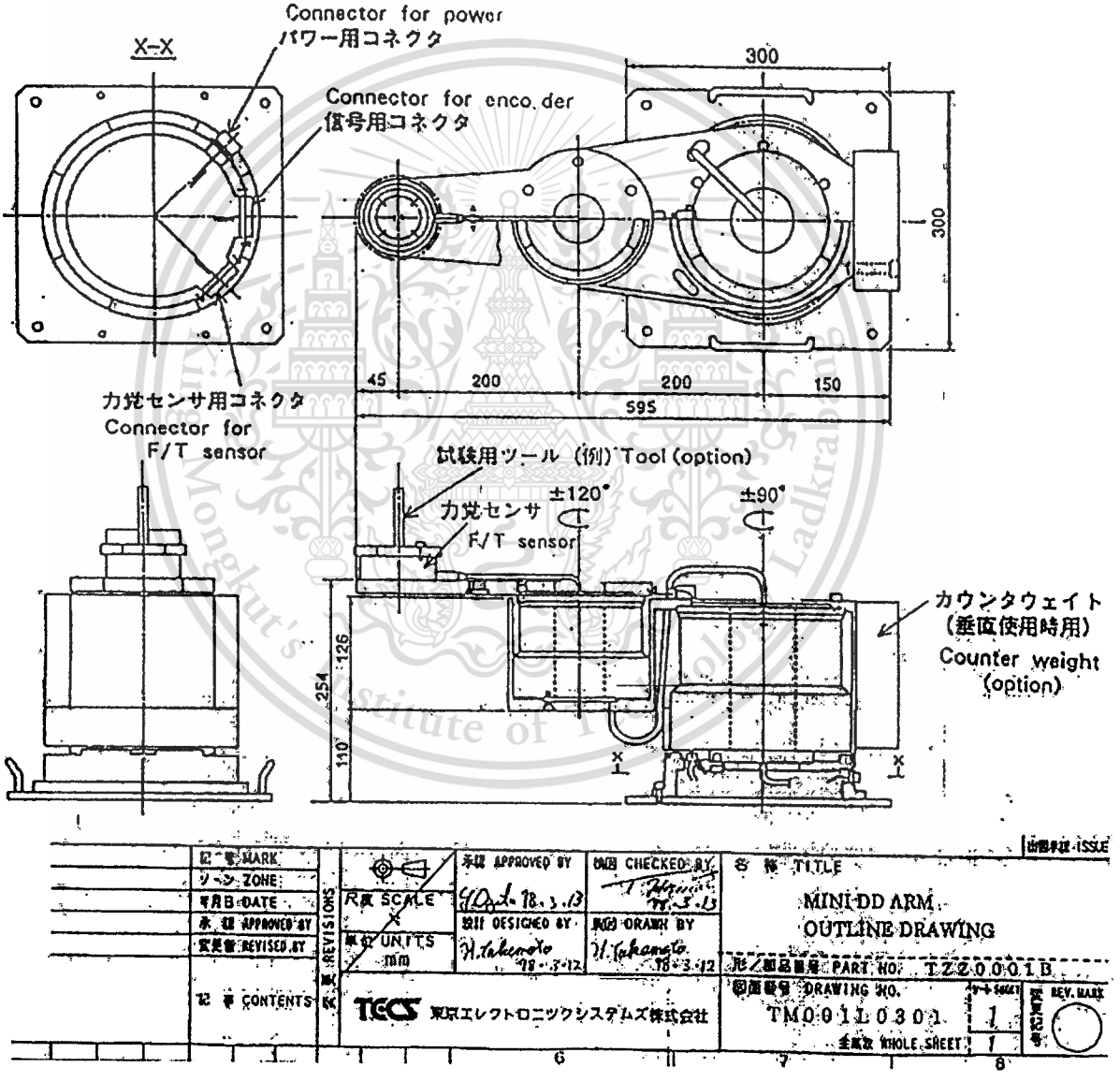

Figure A.1 Dimension of the two-link SCARA robot

A.2 Actuators

The actuator driven first link and second link of the SCARA robot are AC servo motors of YOKOKAWA Precision Corporation.

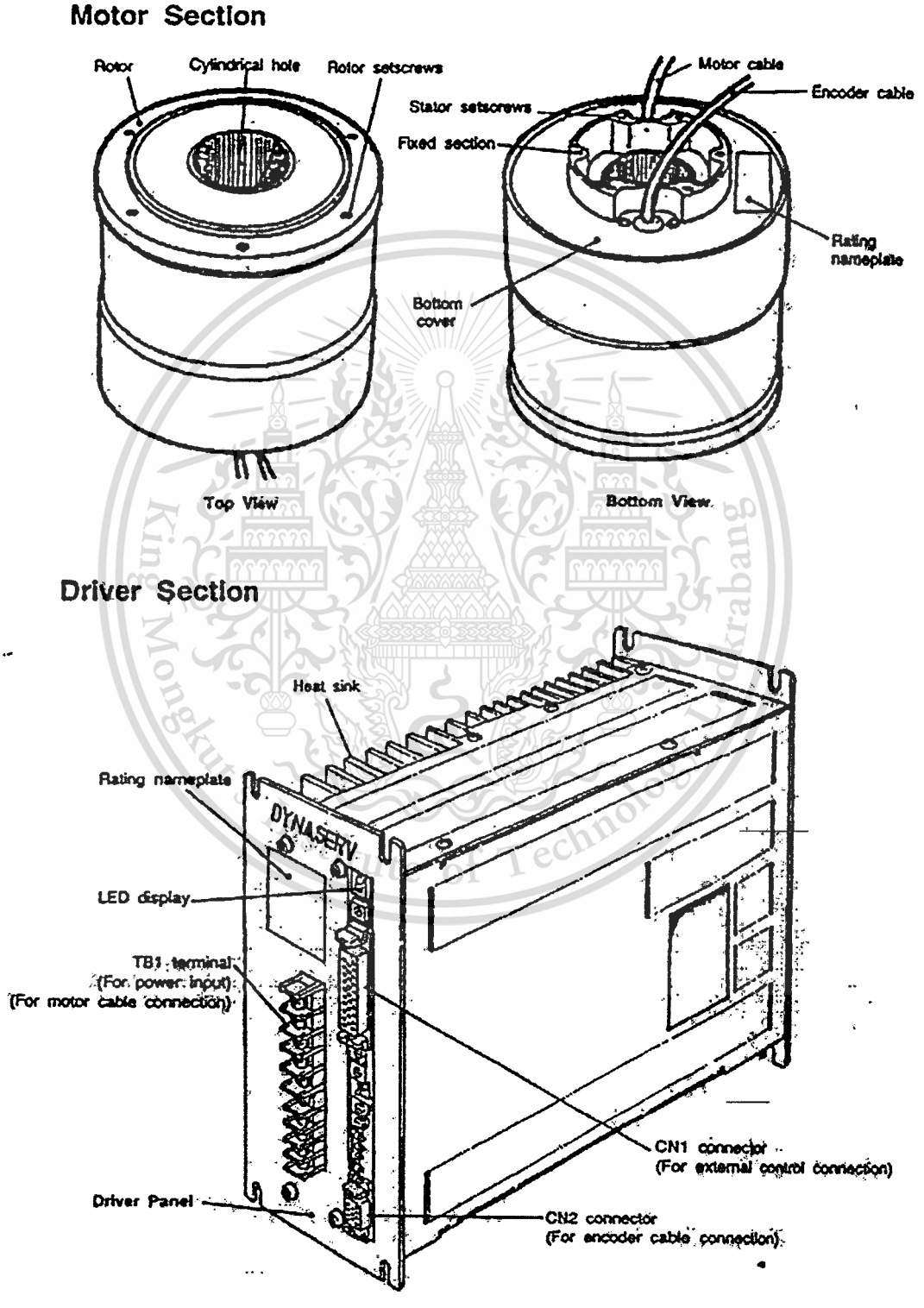

Figure A.2 Functional description

Their structures are identical as shown in figure A.2. The model for first link and second link are DR-1070E and DR-1015B. Their specification are shown in table A.1 and table A.2, respectively.

Series				DR-E Series						
Model				DR1250E□0	DR1220E□0	DR1160E□0	DR1130E□0	DR1100E□0	DR1070E□0	DR1030E□0
Motor & driver coupling	Max. torque		(N·m)	250	220	160	130	100	70	30
	Max. speed (rps)	100 to 115V AC Model		0.7	0.7	1.0	1.2	1.5	2.0	2.0
		200 to 230V AC Model		1.2	1.2	1.2	1.2	2.4	2.4	2.4
	Rated output (W)	100 to 115V AC Model		265	224	170	132	212	224	95
		200 to 230V AC Model		425	375	335	265	315	300	125
	Rated torque		(N·m)	83	73	53	43	33	23	10
	Rated speed (rps)	100 to 115V AC Model		0.5	0.5	0.5	0.5	1.0	1.5	1.5
		200 to 230V AC Model		0.8	0.8	1.0	1.0	1.5	2.0	2.0
	Encoder resolution		(p/rev)	614,400						
	Positioning accuracy		(arc-sec)	±45						
	Repeatability		(arc-sec)	±5						
	Max. power consumption		(kVA)	3.2	3.0	2.8	2.5	2.3	2.0	1.8
Motor section	Rotor inertia		($kg \cdot m^2$)	185×10^{-3}	170×10^{-3}	140×10^{-3}	125×10^{-3}	100×10^{-3}	85×10^{-3}	72×10^{-3}
	Static max. load	Axial load (N)	Compression	4.0×10^{4}						
			Tension	2.0×10^{4}						
		Overhung load	(N·m)	400						
	Torsional stiffness	Axial stiffness (mm/N)	Compression	2.0×10^{-6}						
			Tension	3.0×10^{-6}						
		Radial stiffness	(rad/N·m)	4.0×10^{-7}						
	Weight		(kg)	48	44	36	32	26	22	18
	Dimensions	(mm) Rotor dia. ×L		ϕ205×355	ϕ205×327	ϕ205×271	ϕ205×243	ϕ205×210	ϕ205×183	ϕ205×156
	Common item			Motor insulation: class F / Insulation resistance: 10MΩ Min.(500V DC) / Withstanding voltage: 1500V AC, 1 min. / Color: Black / Excitation: 3 Phase						
Driver section	Model	100 to 115V AC		SR1250E□2-100	SR1220E□2-100	SR1160E□2-100	SR1130E□2-100	SR1100E□2-100	SR1070E□2-100	SR1030E□2-100
		200 to 230V AC		SR1250E□2-200	SR1220E□2-200	SR1160E□2-200	SR1130E□2-200	SR1100E□2-200	SR1070E□2-200	SR1030E□2-200
	Input signal	Speed input	Domestic model	Analog voltage: ±6V DC						
			Export model	Analog voltage: ±10V DC						
		Positioning input		Serial pulse 1.6MHz Max.						
		Rotation direction command		+6V(CW) to -6V(CCW)						
	Output signal	Speed output		H: CW L: CCW						
		Encoder output		Track A/B(400kHz Max.) Zero position signal(1/rev)						
		Alarm output		Over current, Over voltage, Heat sink temperature rise, Voltage down, Encoder abnormal, CPU abnormal.						
		Monitor output		2.5Hz Step response output (test mode)						
	Power source			100 to 115V AC±10% / 200 to 230V AC±10% 50/60Hz						
	Power consumption driver (VA)	100 to 115V AC Model		1250	1120	900	750	1060	1120	710
		200 to 230V AC Model		1800	1600	1500	1250	1500	1400	900
	Weight		(kg)							

Table A.1 Specification of DYNASERV E Series.

Series			DR-A Series						DR-B Series				
Model			DR1400A□D	DR1300A□D	DR1200A□D	DR1150A□D	DR1100A□D	DR1050A□D	DR1060B□D	DR1045B□D	DR1030B□D	DR1015B□D	DR1008B□D
Motor & drive coupling	Max. torque (N·m)		400	300	200	150	100	50	60	45	30	15	8
	Max. speed (rps)	100 to 115V AC Model	0.4	0.5	0.8	1.0	1.2	1.8	1.4	1.8	2.4		
		200 to 230V AC Model	0.8	1.0	1.2	1.2	1.2	1.8	2.4				
	Rated output (W)	100 to 115V AC Model	212	160	212	160	212	160	125	95	95	63	33.5
		200 to 230V AC Model	425	315	425	315	212	160	125	140	125	63	33.5
	Rated torque (N·m)		133	100	67	50	33	17	20	15	10	5	3
	Rated speed (rps)	100 to 115V AC Model	0.25	0.25	0.5	0.5	1.0	1.5	1.0	1.0	1.5	2.0	2.0
		200 to 230V AC Model	0.5	0.5	1.0	1.0	1.0	1.5	1.0	1.5	2.0	2.0	2.0
	Encoder resolution (p/rev)		819,200						507,904				
	Positioning accuracy (arc-sec)		±30						±45				
	Repeatability (arc-sec)		±5						±5				
	Max. power consumption(kVA)		3.2	3.2	3.0	3.0	2.5	2.5	2.3	2.1	1.8	1.4	1.0
Motor section	Rotor inertia (kg·m²)		400×10^{-3}	320×10^{-3}	285×10^{-3}	230×10^{-3}	200×10^{-3}	180×10^{-3}	33×10^{-3}	26×10^{-3}	24×10^{-3}	21×10^{-3}	15×10^{-3}
	Static max. load	Axial load (N) Compression	4.0×10^{4}						3.0×10^{4}				
		Axial load (N) Tension	2.0×10^{4}						1.0×10^{4}				
		Overturning load (N·m)	400						200				
	Torsional stiffness	Axial stiffness (mm/N) Compression	2.0×10^{-6}						2.5×10^{-6}				
		Axial stiffness (mm/N) Tension	3.0×10^{-6}						3.0×10^{-6}				
		Radial stiffness (rad/N·m)	4.0×10^{-7}						2.0×10^{-6}				
	Weight (kg)		65	55	45	36	31	26	15.5	13	11	9.0	6.0
	Dimensions(mm) Roter dia.*d		φ268×358	φ264×304	φ264×250	φ264×212	φ264×185	φ264×158	φ150×97	φ150×179	φ150×151	φ150×123	φ145×85
	Common item		Motor insulation: class F / Insulation resistance: 10MΩ Min.(500V DC) / Withstanding voltage: 1500V AC, 1 min. / Color: Black / Excitation: 3 Phase										
Drive section	Model	100 to 115V AC	SR1400A□2-□□	SR1300A□2-□□	SR1200A□2-□□	SR1150A□2-□□	SR1100A□2-□□	SR1050A□2-□□	SR1060B□2-□□	SR1045B□2-□□	SR1030B□2-□□	SR1015B□2-□□	SR1008B□2-□□
		200 to 230V AC	SR1400A□2-2□□	SR1300A□2-2□□	SR1200A□2-2□□	SR1150A□2-2□□	SR1100A□2-2□□	SR1050A□2-2□□	SR1060B□2-2□□	SR1045B□2-2□□	SR1030B□2-2□□	SR1015B□2-2□□	SR1008B□2-2□□
	Input signal	Speed input Domestic model	Analog voltage ±6V DC						Analog voltage ±6V DC				
		Speed input Export model	Analog voltage ±10V DC						Analog voltage ±10V DC				
		Positioning input	Serial pulse 1.6MHz Max.						Serial pulse 1.6MHz Max.				
		Rotation direction command	+6V(CW) to +6V(CCW)						+6V(CW) to -6V(CCW)				
	Output signal	Speed output	H: CW L: CCW						H: CW L: CCW				
		Encoder output	Track A/B(400kHz Max.) Zero position signal(200p/rev)						Track A/B(400kHz Max.) Zero position signal(124p/rev)				
		Alarm output	Over current, Over voltage, Heat sink temperature rise, Voltage down, Encoder abnormal, CPU abnormal						Over current, Over voltage, Heat sink temperature rise, Voltage down, Encoder abnormal, CPU abnormal				
		Monitor output	2.5Hz Step response output (test mode)						2.5Hz Step response output (test mode)				
	Power source		100 to 115V AC$^{+10\%}_{-15\%}$ / 200 to 230V AC$^{+10\%}_{-15\%}$ 50/60Hz						100 to 115V AC$^{+10\%}_{-15\%}$ / 200 to 230V AC$^{+10\%}_{-15\%}$ 50/60Hz				
	Power consumption of driver(VA)	100 to 115V AC Model	1120	900	1060	850	1120	1000	710	670	670	500	400
		200 to 230V AC Model	1800	1400	1900	1500	1120	1000	710	800	750	500	400
	Weight (kg)		6						6				

* See drawings

Table A.2 Specification of DYNASERV A and B Series.

Appendix B

Related Conference

IEEE
INDONESIA SECTION

TENCON 2011

2011 IEEE REGION 10 CONFERENCE

Trends and Development in Converging Technology towards 2020

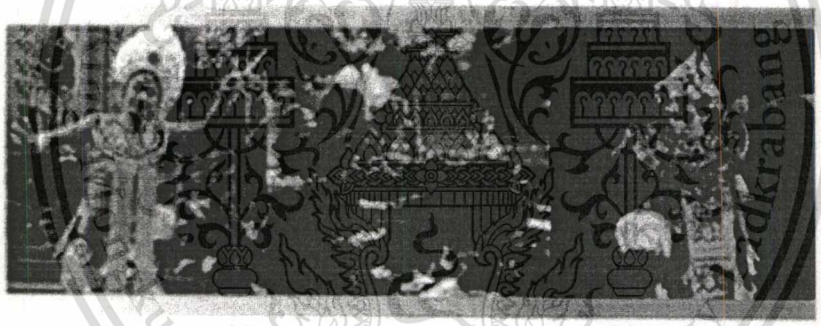

November 21-24, 2011
Bali, Indonesia

IMC-Based PID Controllers Design for a Two-Links SCARA Robot

Sipaseuth Suvilath
International College
King Mongkut's Institute of Technology Ladkrabang
Bangkok, Thailand
seuth484@yahoo.com

Taworn Benjanarasuth
Faculty of Engineering
King Mongkut's Institute of Technology Ladkrabang
Bangkok, Thailand
kbtaworn@kmitl.ac.th

Dr.Khamphong Khongsomboun
Faculty of Engineering
National University of Laos
Vientiane, Laos
khongsomboun@hotmail.com

Noriyuki Komine
School of Information and Telecommunication Engineering
Tokai University
Takanawa, Japan
komine@keyaki.cc.u-tokai.ac.jp

Abstract—**The paper presents the design of PID controllers for a two-link SCARA robot based on internal model control (IMC) technique. For the model of the two-link SCARA robot which includes an integrator, IMC filter must be selected properly so that the designed IMC controllers can be approximated as PID controllers by using Maclaurin approximation. The simulation results verify the applicability and satisfied performance of the proposed control system.**

Keywords- SCARA; IMC; internal model control; PID

I. INTRODUCTION

Nowadays, robots play an active role not only in research scenes but also in industrial scenes. A SCARA (Selective Compliance Assembly Robot Arm) robot is a type of them which is widely used in industries such as soldering robots of printed circuit boards, product assembly robots and so on. In order to perform accurately, the robot control system must be suitably implemented. Various methods for designing a controller such as fuzzy logic [1], neural network [2] and internal model control (IMC) [3] have been proposed and applied to the SCARA robot. However, these methods are quite complicated and/or difficult in the actual implementation. Among various control techniques, PID control scheme is the most employed in the industries due to its simplicity and many industrial PID controller products are readily available in the market. The PID controller parameters can be tuned by both analytical designs and experimental tuning rules. However in several practical cases, the design of PID controller gains is determined through trial and error process by a skilled expert.

In this paper, a simple IMC-based PID controller design method is studied. The design is composed of 2 steps which are IMC controller design and PID approximation. In the IMC controller design process, a low pass filter selection is very important because it affects the performance of the system. For several common plant models, the low pass filter selections are proposed in [4] but these filters cannot be used directly with the two-link SCARA robot. Consequently, a suitable low pass filter for this plant is proposed in this paper. After the IMC controller is designed, Maclaurin expansion [5] is utilized to find the corresponding approximated PID controller.

II. MATHEMATICAL MODELLING

The schematic diagram of the two-link robot manipulator considered in this paper is shown in Fig.1. θ_1 and θ_2 are angular positions, m_1 and m_2 are masses, l_1 and l_2 are lengths of each link, a_1 and a_2 are distances between the gravity center positions and rotational positions of both links, respectively.

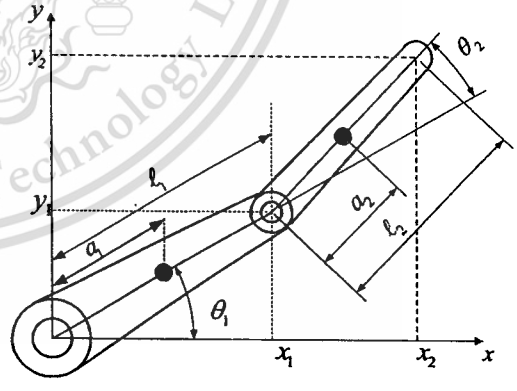

Figure 1. SCARA robot diagram.

The corresponding Cartesian coordinate at the end of each link can be computed directly from (1) and (2)

$$x_1 = a_1 C_1, \quad y_1 = a_1 S_1, \tag{1}$$

$$x_2 = l_1 C_1 + a_2 C_{12}, \quad y_2 = l_1 S_{12}, \tag{2}$$

where $S_1 = \sin\theta_1$, $C_1 = \cos\theta_1$, $C_{12} = \cos(\theta_1 + \theta_2)$ and $S_{12} = \sin(\theta_1 + \theta_2)$.

To obtain the dynamic model of the SCARA robot, the Lagrange's equation is applied to each join angular coordinate as in (3)

$$\frac{\partial}{\partial t}\left(\frac{\partial L}{\partial \dot{\theta}_i}\right) - \frac{\partial L}{\partial \theta_i} = T_i, \tag{3}$$

where T_i is the summation of all torques in a rotational motion of θ_i and L is the Lagrangian. The Lagrangian is defined by

$$L = K - P, \tag{4}$$

when K and P are the kinetic energy and potential energy of the systems respectively. As the two-link robot manipulator is designed to move in horizontal plane only, the potential energy is considered as zero or $P = 0$. The Lagrangian of this system can then be expressed as [6]

$$L = K = K_1 + K_2 = \frac{1}{2}\left[m_1 V_1^2 + m_2 V_2^2\right], \tag{5}$$

where $V_1^2 = \dot{x}_1^2 + \dot{y}_1^2 = a_1^2\dot{\theta}_1^2$, and $V_2^2 = \dot{x}_2^2 + \dot{y}_2^2$.

Substituting (5) into (3) yields the flowing two equations of motion.

$$T_1 = (J_1 + J_2 + 2rC_2)\ddot{\theta}_1 + (J_2 + 2rC_2)\ddot{\theta}_2 - rS_2(2\dot{\theta}_1\dot{\theta}_2 + \dot{\theta}_2^2), \tag{6}$$

$$T_2 = (J_2 + 2rC_2)\ddot{\theta}_1 + J_2\ddot{\theta}_2 + rS_2\dot{\theta}_1^2, \tag{7}$$

where $J_1 = m_1 a_1^2 + m_2 l_1^2$, $J_2 = m_2 a_2^2$ and $r = m_2 l_1 a_2$. The equations of motion in (6) and (7) may be written in a matrix-vector form of the link angles vector $\theta = [\theta_1 \quad \theta_2]^T$ as

$$T = M(\theta)\ddot{\theta} + V(\theta, \dot{\theta}) \tag{8}$$

where $M(\theta)$ and $V(\theta, \dot{\theta})$ are

$$M(\theta) = \begin{bmatrix} J_1 + J_2 + 2rC_2 & J_2 + 2rC_2 \\ J_2 + 2rC_2 & J_2 \end{bmatrix}, \tag{9}$$

$$V(\theta, \dot{\theta}) = \begin{bmatrix} 2rS_2\dot{\theta}_1\dot{\theta}_2 - rS_2\dot{\theta}_2^2 \\ rS_2\dot{\theta}_1^2 \end{bmatrix}. \tag{10}$$

For the two-links SCARA robot in this paper, the ideal servo motors with no gear are employed as its actuators and their dynamic behavior is governed by

$$J_M\ddot{\theta} + B_M\dot{\theta} + T = K_M E, \tag{11}$$

where $E = [E_1 \quad E_2]^T$ is the current command voltage vector while $J_M = diag(J_{Mi})$, $B_M = diag(B_{Mi})$ and $K_M = diag(K_{Mi})$ are respectively the moment of inertia matrix, rotor damping constant matrix and torque constant matrix of the motors.

Combining (8) and (11), the complete dynamic of the two-links SCARA robot is

$$(J_M + M(\theta))\ddot{\theta} + (B_M\dot{\theta} + V(\theta, \dot{\theta})) = K_M E. \tag{12}$$

Defining the state vector $x(t) = \left[\theta_1(t) \quad \theta_2(t) \quad \dot{\theta}_1(t) \quad \dot{\theta}_2(t)\right]^T$ and arranging (12), the nonlinear state equation can be derived. However, in order to design a controller by the IMC technique, the linear transfer functions are required. Therefore linearzing the nonlinear state equation around zeros is performed and the linear state equation and output equation are respectively obtained as (13) and (14)

$$\dot{x} = Ax + Bu, \tag{13}$$

$$y = Cx, \tag{14}$$

where $y = \theta$, $u = E$ and

$$A = \begin{bmatrix} 0 & I \\ 0 & N \end{bmatrix}, \quad B = \begin{bmatrix} 0 \\ Z \end{bmatrix} \text{ and } C = \begin{bmatrix} I & 0 \end{bmatrix},$$

when $I = \begin{bmatrix} 1 & 0 \\ 0 & 1 \end{bmatrix}$,

$$N = \frac{1}{\Delta}\begin{bmatrix} (J_{m2} + J_2)B_{m1} & -(J_2 + r)B_{m2} \\ -(J_2 + r)B_{m1} & J_{m1} + J_1 + 2r \end{bmatrix},$$

$$Z = \frac{1}{\Delta}\begin{bmatrix} (J_{m2} + J_2)K_{m1} & -(J_2 + r)K_{m2} \\ -(J_2 + r)K_{m1} & (J_{m1} + J_1 + J_2 + 2r)K_{m2} \end{bmatrix},$$

and $\Delta = -J_{m1}J_{m2} - J_{m1}J_2 - J_1J_{m2} - J_1J_2 - J_2J_{m2} - 2rJ_{m2} + r^2$.

From (13) and (14), the transfer matrix of the two-links SCARA robot can be directly computed and it appears in the form of (15)

$$G(s) = \frac{\theta(s)}{E(s)} = \frac{1}{s^3 + as^2 + bs}\begin{bmatrix} a_{11}s + b_{11} & -a_{12}s \\ -a_{21}s & a_{22}s + b_{22} \end{bmatrix}, \tag{15}$$

when $a, b, a_{11}, a_{12}, a_{21}, a_{22}, b_{11}$ and b_{22} are all positive real numbers for any realizable system.

III. IMC-Based PID Controller Design

The structure of IMC is shown in Fig. 2, in which G is a controlled object, $\hat{G}$ is the model of the controlled object, C is an IMC controller.

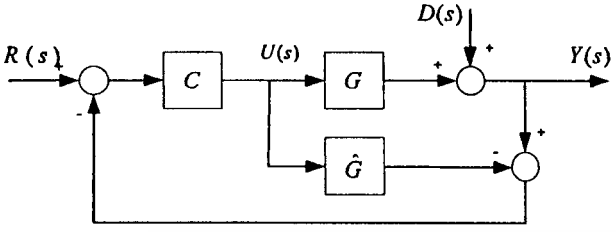

Figure 2. Structure of IMC system.

In general, the IMC controller can be designed by the following two steps.

Step1: Divide the model of the controlled object $\hat{G}(s)$ into two parts as $\hat{G}(s)=\hat{G}_+(s)\hat{G}_-(s)$, where $\hat{G}_+(s)$ contains all the time delays and right-half-plane zeros. While $\hat{G}_-(s)$ is the transfer function with minimum phase characteristic and contains no predictive item.

Step2: To design the internal model controller, a low-pass filter $f(s)$ must be added to $\hat{G}_-(s)$ to ensure the stability and robustness of the control system. The internal model controller is then chosen as (16)

$$C(s)=\hat{G}_-^{-1}(s)f(s). \tag{16}$$

In order to design a PID controller for a general feedback control system, the structure of IMC system in Fig. 2 is rearranged as Fig. 3 where

$$K(s)=\frac{C(s)}{1-\hat{G}(s)C(s)}, \tag{17}$$

and, reversely,

$$C(s)=\frac{K(s)}{1+\hat{G}(s)K(s)}. \tag{18}$$

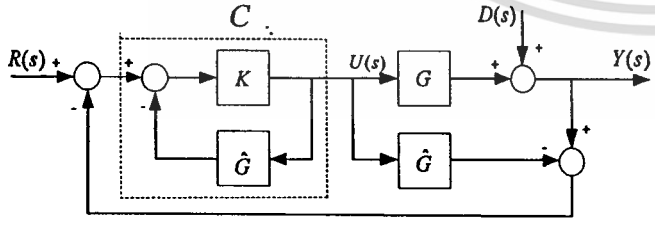

Figure 3. Equivalent structure of IMC system.

By analyzing the input/ output relation of the equivalent structure of IMC system in Fig. 3, the two models of the controlled object $\hat{G}(s)$ can be offset. The equivalent structure of IMC system in Fig. 3 is then equal to a general feedback control system in Fig. 4.

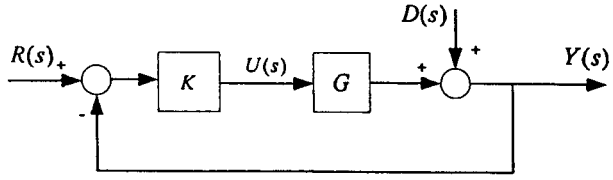

Figure 4. General feedback control.

From (16) and (17), the controller $K(s)$ for a general feedback control system can be obtained as (19)

$$K(s)=\frac{\hat{G}_-^{-1}(s)}{f^{-1}(s)-\hat{G}_+(s)}. \tag{19}$$

With a suitable choice of $f(s)$, the controller $K(s)$ can possess the integral action and appear in the following form

$$K(s)=\frac{1}{s}Q(s). \tag{20}$$

By performing the Maclaurin series expansion for $Q(s)$, the controller $K(s)$ can be expressed as

$$K(s)\approx\frac{1}{s}\left[Q(0)+\dot{Q}(0)s+\frac{\ddot{Q}(0)s^2}{2!}+\ldots\right]. \tag{21}$$

Comparing the structure of $K(s)$ in (21) to the general transfer function of the PID controller in (22)

$$K_{PID}(s)\approx K_p+\frac{K_i}{s}+K_d s, \tag{22}$$

the PID parameters can be obtained by ignoring the higher order terms in $K(s)$ and setting

$$K_p=\dot{Q}(0), K_i=Q(0) \text{ and } K_d=\frac{\ddot{Q}(0)}{2}. \tag{23}$$

Denote that the filter $f(s)$ must be selected properly so that $Q(s)$ has no zero at the origin to ensure non-zero integral gain and acceptable performance.

IV. Controller Design for SCARA Robot

For the model of SCARA robot in (15), two PID controllers will be designed for controlling each link separately. Denote that the transfer functions $\hat{G}_{11}(s)=\frac{\theta_1(s)}{E_1(s)}$ and $\hat{G}_{22}(s)=\frac{\theta_2(s)}{E_2(s)}$

are in the same format. Therefore, the controller design for both links can be conducted in the similar manner. Without loss of generality, the transfer functions $\hat{G}_{11}(s)=\frac{\theta_1(s)}{E_1(s)}$ of the first link will be used in the following design and the model of the controlled object $\hat{G}(s)$ in this case becomes

$$\hat{G}(s)=\hat{G}_{11}(s)=\frac{a_{11}s+b_{11}}{s^3+as^2+bs}, \tag{24}$$

and it can be decomposed as

$$\hat{G}_+(s)=1, \tag{25}$$

and

$$\hat{G}_-(s)=\frac{a_{11}s+b_{11}}{s^3+as^2+bs}. \tag{26}$$

In order to get the controller $K(s)$, many patterns of low-pass filter for integral plant were proposed in [4]. Those patterns, however, cannot be used as a filter in this paper due to mentioned patterns were particularly used for first and second order with integral plant. So that the suitable low-pass filter $f(s)$ for third order with integral plant, in the form of (27), is selected.

$$f(s)=\frac{zs+1}{xs^3+ys^2+zs+1}, \tag{27}$$

when x, y and z are positive real numbers and are the adjustable parameters of the IMC controller. Substitute (25), (26) and (27) to (19), the controller $K(s)$ becomes

$$K(s)=\frac{zs^3+(az+1)s^2+(bz+a)s+b}{s\left[a_{11}xs^2+(a_{11}y+b_{11}x)s+b_{11}y\right]}, \tag{28}$$

and $Q(s)$ becomes

$$Q(s)=\frac{zs^3+(az+1)s^2+(bz+a)s+b}{a_{11}xs^2+(a_{11}y+b_{11}x)s+b_{11}y}. \tag{29}$$

Then, the parameters K_p, K_i and K_d of a PID controller can be directly computed from (23).

V. SIMULATION RESULTS

In this section, the simulations of the proposed control system are conducted by Matlab/Simulink. The values of the parameters of the two-links SCARA robot in the laboratory are as follows [7]:

$m_1=4.37\ kg$, $m_2=1.24\ kg$, $l_1=l_2=200\ mm$, $a_1=63\ mm$, $a_2=80\ mm$, $J_{m1}=0.085\ kg\cdot m$, $J_{m2}=0.060\ kg\cdot m$, $K_{m1}=2.7590\ N\cdot m/V$, $K_{m2}=1.3281\ N\cdot m/V$, $B_{m1}=0.8691\ N\cdot m/(rad/s)$ and $B_{m2}=0.4347\ N\cdot m/(rad/s)$.

The following simulations are conducted by using two independent PID control loops for each links as shown in Fig. 5 to control the original nonlinear model of the SCARA robot in (12). The parameters x, y and z of the low-pass filter in (27) are tuned to obtain PID controllers' gains. For the first link, the parameters $x=0.4$, $y=2.2$ and $z=550$ are chosen and the corresponding parameters of the PID controller (PID1) are $K_p=78.764$, $K_i=0.143$ and K_d=6.603. For the second link, $x=0.1$, $y=15$ and $z=600$ are appointed and the resulting PID controller (PID2) with $K_p=13.097$, $K_i=0.021$ and K_d=1.956 is obtained. An investigation is done in the following 3 cases.

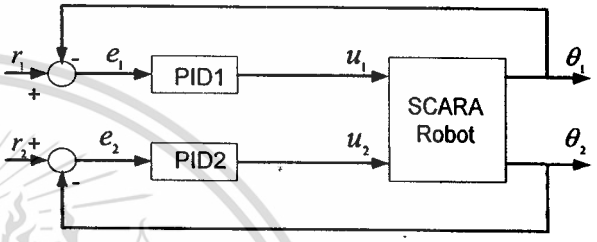

Figure 5. Proposed control system structure.

Case 1: Applying step reference inputs to the first link only.

In this case, the step reference inputs at 30°, 45° and 60° are applied to the first link while the second link is regulated at 0°. In addition, the 10° output step disturbance is applied to the first link of the system at 1.1 seconds. The $\theta_1(t)$ and $\theta_2(t)$ responses are illustrated in Fig. 6 and Fig. 7 respectively. From Fig. 6, the first link can be attained to all set points with the settling time 0.8 second without over shoot and steady-state error . Meanwhile, it can be observed from Fig. 7 that the second link is affected to deviate maximally around 3.5% of each applied step reference and eventually return to 0°. Moreover, the control system can reject the effects of the disturbances so that the angles of both links can be forced back to the desired positions.

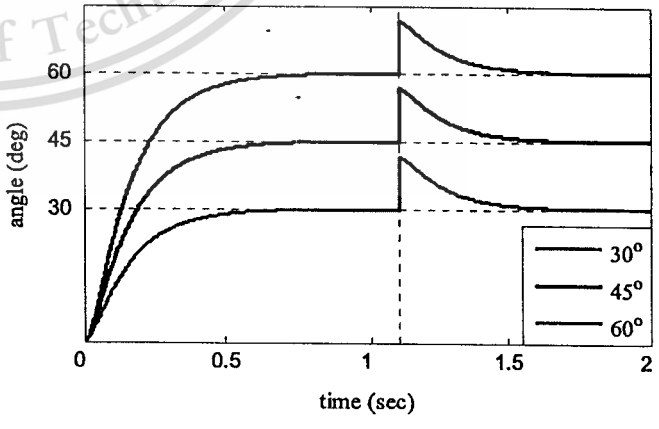

Figure 6. The response of first link for Case 1.

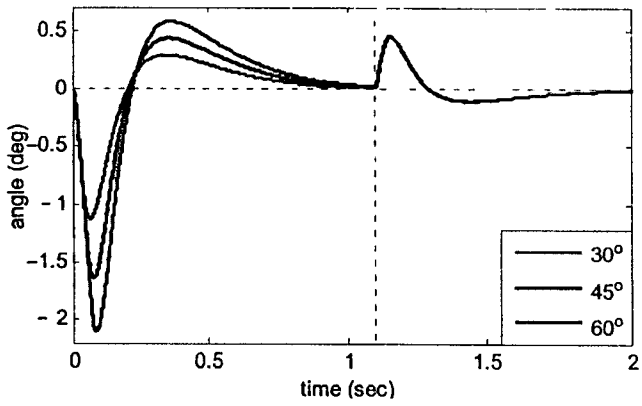

Figure 7. The response of second link for Case 1.

Case 2: Applying step reference inputs to the second link only.

Similar to Case 1, the same step reference inputs and disturbances are applied but to the second link instead while trying to keep the first link at 0°. The corresponding results for the second and first links are shown in Fig. 8 and Fig. 9 respectively. The responses of the second link in Fig. 9 exhibit the same characteristics as those of the first link in Case 1 and vice versa for the first link in Fig 8. However, the first link can maintain around 0° more closely than the second link in Case 1. It maximally deviates just less than 0.5% of the applied step reference inputs.

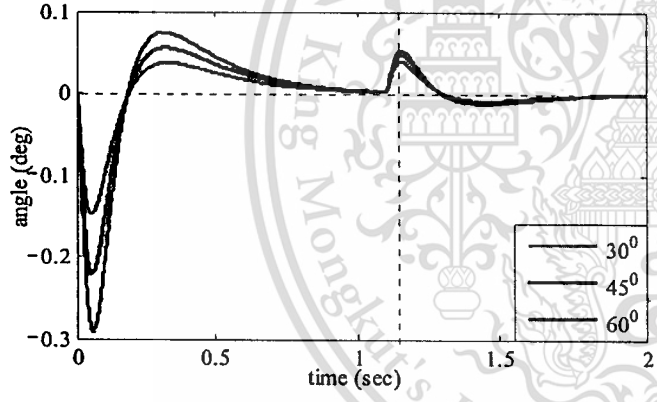

Figure 8. The response of first link for Case 2.

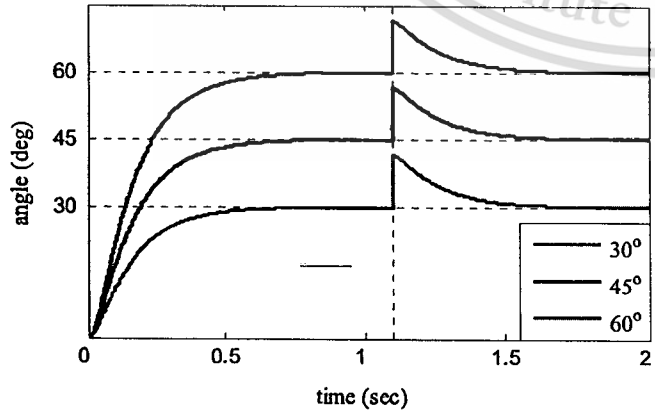

Figure 9. The response of second link for Case 2.

Case 3: Applying step reference inputs to both links.

In this case, the step reference inputs at 60° and 30° are specified for the first link and the second link respectively. The $\theta_1(t)$ and $\theta_2(t)$ responses are illustrated in Fig. 10. It can be clearly seen that the responses of both links are nearly identical to the case of a single link movement. Both links reach the desired angles without overshoot and steady state error within 0.55 seconds for first link and 0.35 seconds for second link of settling time.

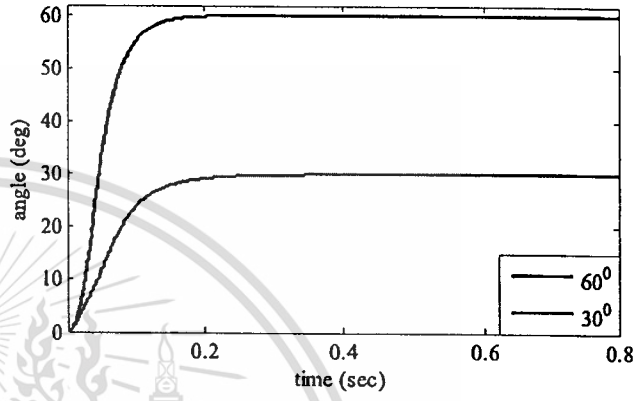

Figure 10. The response of two links movement.

VI. CONCLUSION

In this paper, PID controllers design based on IMC for a two-link SCARA robot is presented. The suitable IMC low-pass filter is proposed so that the PID controller can be derived by applying Maclaurin series expansion to the IMC controller in a general feedback control loop. The simulation results verify that the PID controllers designed by the proposed method can control the angular positions of the SCARA robot precisely without steady state-state error. The responses can track the reference inputs quickly without overshoot and the effects of output disturbances can be rejected.

REFERENCES

[1] M. J. Er, M. T. Lim and H. S. Lim, "Real-time hybrid adaptive fuzzy control of a SCARA robot," Microprocessors and Microsystems, vol. 25, 2001, pp. 369-378.

[2] M.J. Erand K.C. Liew, "Control of adept one SCARA robot using neural networks,"IEEE Transaction on Industrial Eletronic, vol. 44, no. 6, Dec. 2007, pp. 762-768.

[3] S. Akamatsu, M. Konishi and J. Imai, "Position control of 2-link SCARA robot by using internal model control", Memoirs of the Faculty of Engineering, Okayama University, vol. 43, Jan. 2009, pp. 49-54.

[4] Rivera, D.E, M. Morari, and S. Skogestad, "Internal model control . PID controller design ," Industrial and Engineering Chemistry Process Design and Development, vol. 25, 1986, pp. 252-265.

[5] J. Qibing, Q. Ling, W. Xuewei, and Q. Fei, "Base on all-pole approximation a new internal model PID control method for the system with time delays," Proceeding of ICMA2009, pp.268-273.

[6] S. B. Niku, Introduction to Robotics: Analysis, Systems, Applications. Upper Saddle River, NJ: Pretice Hall, 2001.

T. Benjanarasuth, "SCARA robot locomotion control by two-degree-of-freedom simple servo adaptive controller," Proceeding of AISM 2010, pp. 252-258.

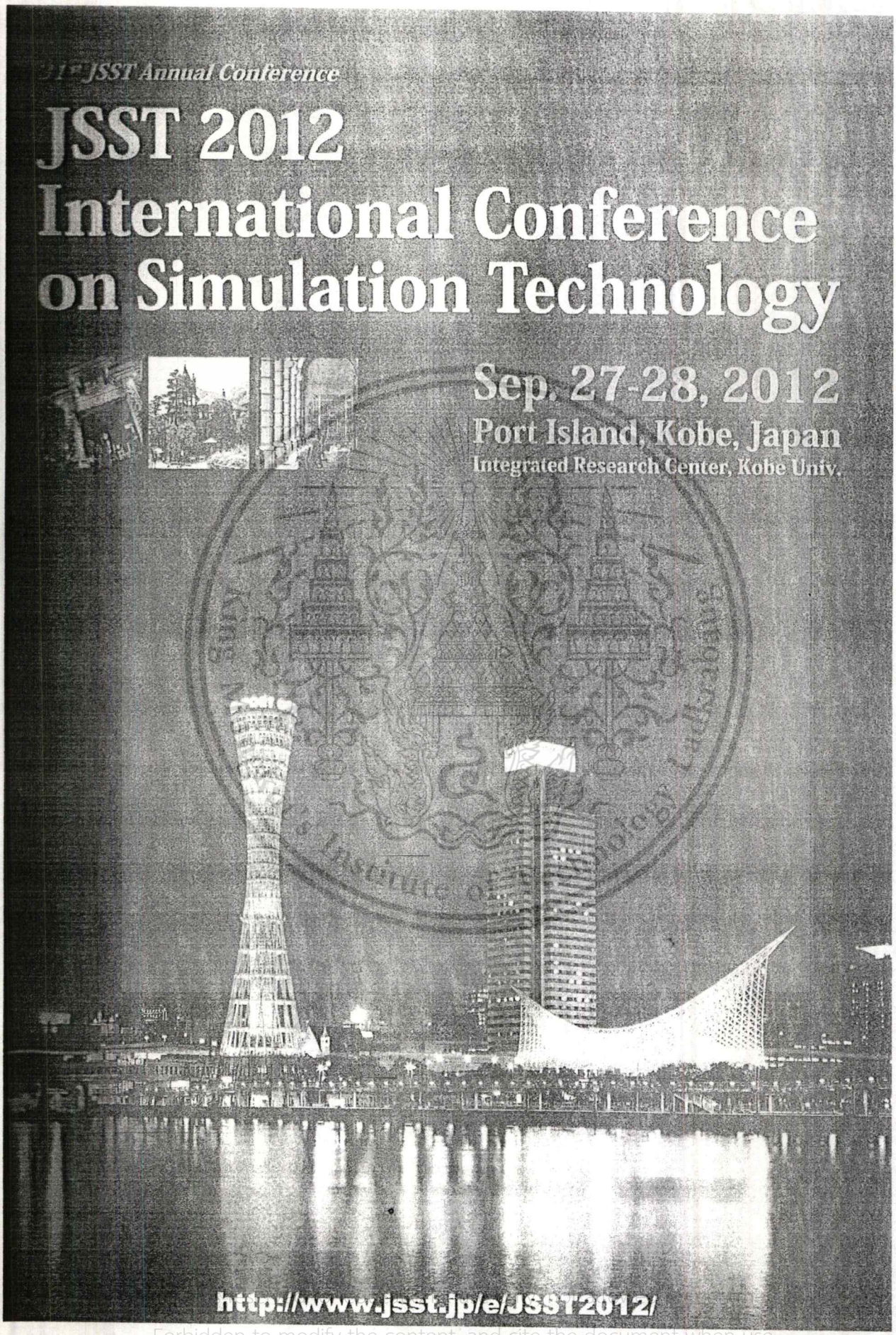

Experiments on IMC-Based PID Controller Design for a Two-link SCARA Robot

Sipaseuth SUVILATH [1], Tawom BENJANARASUTH [2], Noriyuki KOMINE [3] and Khamphong KHONGSOMBOUN [4]

[1] International College, King Mongkut's Institute of Technology Ladkrabang, Thailand
[2] Faculty of Engineering, King Mongkut's Institute of Technology Ladkrabang, Thailand
[3] Schools of Information and Telecommunication Engineering, Tokai University, Japan
[4] Faculty of Engineering, National University of Laos, Laos

Abstract

In this paper, Internal Model Control (IMC) technique is applied to design a PID controller for a two-link SCARA robot, of which the model contains an integral term. In IMC controller design, a filter structure must be selected suitably because it directly affects the performance of the system. In order to derive the PID controller, the IMC controller using a proposed low-pass filter is approximated by Maclaurin series expansion. With the proposed low-pass filter, the angular positions of the two-link SCARA robot can track the reference input and the effect of step type input disturbance can be rejected. The effectiveness of the IMC-based PID controller is verified by both simulations and experiments.

Keywords – Internal Model Control, IMC, Maclaurin, PID

1 Introduction

A SCARA robot (Selective Compliance Assembly Robot Arm) is a type of robots. It is widely used in factory automation, for examples, automotive assembly line robots and soldering robots. As the manipulators are usually used to perform high-precision tasks, robot controllers are required in order to control the motion of a robot effectively and accurately.

Fuzzy Logic and Neural Network methods have been presented to design controllers for SCARA robots [1, 2]. By using these methods, the angular position can track the reference input satisfactorily; however, the controller design procedures and implementation are quite complicated.

Among various controllers, the PID controller is the most popular controller that has been adopted in the industrial process control due to its simplicity, successfully practical applicability and availability in the market. Therefore many researchers have proposed several tuning rules for the PID controller with common process structures such as Ziegler-Nichols and Cohen-Coon [3, 4]. However in actual implementation, the PID controller parameters are mostly tuned by trial-and-error method. For instance, the PID controller tuned by trial-and-error method is employed to control the SCARA robot [5].

In addition, IMC method has been applied to design a controller for the SCARA robot [6]. In this method, the performance of the system depends on IMC low-pass filter's structure and its parameters. The introduced IMC filter is equivalent to specifying a reference trajectory for the output [7]. In IMC controller design, the transfer function structure of the controller is in a rational form.

Because of the popularity of the PID controller and the advantage of the IMC controller design technique, the IMC-based PID controller design has been introduced [8]. To do so, the designed IMC controller with its transfer function in a rational form is approximated by Maclaurin series expansion. By ignoring the higher order terms of the approximated IMC controller, the remaining terms are matched to the PID controller structure so that the PID controller can be obtained. In IMC-based PID controller design, difference structures of the low-pass filters have been proposed [8, 9]. However, these structures are not appropriate for the SCARA robot model since the effect of the input disturbance cannot be rejected in the corresponding control system.

In this paper, a suitable low-pass filter is proposed for the model of the SCARA robot in order to deal with the input disturbance rejection problem. The effectiveness of the IMC-Based PID controller design using the proposed low-pass filter is verified by simulations and experiments.

2 Mathematical Model

The schematic diagram of the two-link SCARA robot is shown in Fig.1, where θ_1 and θ_2 are the angular positions of each link, m_1 and m_2 are the masses of each link, l_1 and l_2 are the lengths of each link, and a_1 and a_2 are the distance between the gravity centre positions and rotational positions of the first link and the second link.

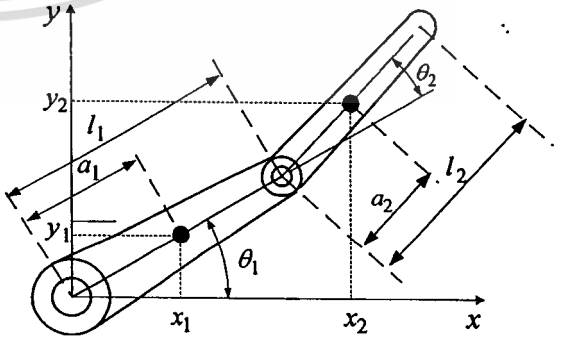

Fig. 1. SCARA robot schematic diagram.

The positional equations of the first link and the second link are described in (1) and (2), respectively.

$$x_1 = a_1 c_1, \quad y_1 = a_1 s_1, \tag{1}$$

$$x_2 = l_1 c_1 + a_2 c_{12}, \quad y_2 = l_1 s_1 + a_2 s_{12}, \tag{2}$$

where $c_1 = \cos\theta_1$, $s_1 = \sin\theta_1$, $s_{12} = \sin(\theta_1 + \theta_2)$ and $c_{12} = \cos(\theta_1 + \theta_2)$.

From (1) and (2), the Lagrangian equations [10] are employed in order to obtain the dynamical model of the two-link SCARA robot. Then, the following non-linear state space equation of the robot can be found [11],

$$\dot{x}_1 = x_3 \tag{3a}$$

$$\dot{x}_2 = x_4 \tag{3b}$$

$$\dot{x}_3 = \frac{(J_2 + J_{M2})\left[rs_2(2x_3x_4 + x_4^2) - B_{M1}x_3 + K_{M1}E_{a1}\right]}{\Delta} + \frac{(J_2 + rc_2)(rs_2x_3^2 + B_{M2}x_4 - K_{M2}E_{a2})}{\Delta} \tag{3c}$$

$$\dot{x}_4 = \frac{(J_1 + J_2 + J_{M1} + 2rc_2)(K_{M2}E_{a2} - rs_2x_1^2 - B_{M2}x_4)}{\Delta} + \frac{(J_2 + rc_2)(rs_2x_3^2 + B_{M2}x_4 - K_{M2}E_{a2})}{\Delta}, \tag{3d}$$

where

$\Delta = J_1J_2 + J_1J_{M2} + J_2J_{M2} + J_{M1}J_2 + J_{M1}J_{M2} + 2J_{M2}rc_2 - r^2c_2^2$,

when J_1 and J_2 are the moment inertia of each link $r = m_2l_1a_2$, J_{M1} and J_{M2} are the moment inertia of the motor of each link, B_{M1} and B_{M2} are the rotor damping constants of each link, K_{M1} and K_{M2} are the torque constants of each link and E_{a1} and E_{a2} are the current command voltage of each link. The state variables are $x_1 = \theta_1$, $x_2 = \theta_2$, $x_3 = \dot{\theta}_1$ and $x_4 = \dot{\theta}_2$.

The non-linear state space equations in (3) are linearized [9, 10] and the linear transfer matrix can then be derived as a form of (4),

$$G(s) = \frac{Y(s)}{U(s)} = \begin{bmatrix} G_{11}(s) & G_{12}(s) \\ G_{21}(s) & G_{22}(s) \end{bmatrix} = \begin{bmatrix} \dfrac{a_{11}s + b_{11}}{s^3 + as^2 + bs} & \dfrac{-a_{12}s}{s^3 + as^2 + bs} \\ \dfrac{-a_{21}s}{s^3 + as^2 + bs} & \dfrac{a_{22}s + b_{22}}{s^3 + as^2 + bs} \end{bmatrix}, \tag{4}$$

where $Y(s) = \begin{bmatrix} Y_1(s) \\ Y_2(s) \end{bmatrix} = \begin{bmatrix} \theta_1(s) \\ \theta_2(s) \end{bmatrix}$ and $U(s) = \begin{bmatrix} U_1(s) \\ U_2(s) \end{bmatrix} = \begin{bmatrix} E_{a1}(s) \\ E_{a2}(s) \end{bmatrix}$.

The transfer matrix in (4) will be used in the controller design.

3 IMC-Based PID Controller Design

3.1 IMC Controller Design Algorithm

The structure of IMC control system is shown in Fig. 2, $G(s)$ is a controlled object, $\hat{G}(s)$ is the model of the controlled object and $C(s)$ is the IMC controller, $R(s)$ is a reference input, $E(s)$ is an error, $U(s)$ is a command signal, $U_d(s)$ is a command signal with an input disturbance, $D_i(s)$ is an input disturbance, $D_o(s)$ is an output disturbance and $Y(s)$ is an output.

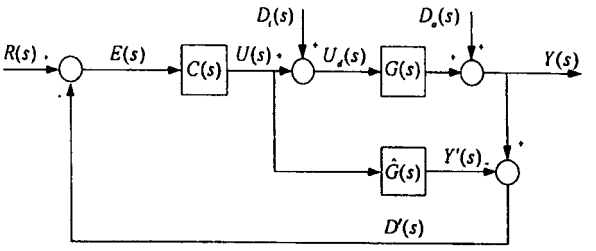

Fig. 2. IMC control scheme.

The closed loop transfer functions from Fig. 2 can be written as

$$Y(s) = \frac{\Psi_1(s) + \Psi_2(s) + \Psi_3(s)}{1 + \left[G(s) - \hat{G}(s)\right]C(s)}, \tag{5}$$

where

$\Psi_1(s) = C(s)G(s)R(s)$,

$\Psi_2(s) = G(s)\left[1 - C(s)\hat{G}(s)\right]D_i(s)$,

$\Psi_3(s) = \left[1 - C(s)\hat{G}(s)\right]D_o(s)$.

From the closed-loop transfer function in (5), it can be observed that if $G(s) = \hat{G}(s)$ and using $C(s) = \hat{G}(s)^{-1}$ then reference input tracking and disturbances rejection are achieved. However, the controller might be improper and unstable; consequently, the IMC controller design is conducted by two following steps.

Step 1: Divide the model of the controlled object $\hat{G}(s)$ into two parts as $\hat{G}(s) = \hat{G}_+(s)\hat{G}_-(s)$. $\hat{G}_+(s)$ is the transfer function contains all the time delays and right-half-plane zeros of $\hat{G}(s)$. $\hat{G}_-(s)$ is the transfer function with minimum phase characteristic and contains no predictive item of $\hat{G}(s)$.

Step 2: Derive the IMC controller $C(s)$ by multiplying the IMC low-pass filter $f(s)$ with $\hat{G}_-(s)^{-1}$ as in (6), to ensure the stability and robustness of the control system.

$$C(s) = \hat{G}_-(s)^{-1}f(s). \tag{6}$$

3.2 Rearrangement of IMC Control System

The IMC structure in Fig. 2 can be transformed into a general feedback control structure. The transformation relation is depicted in Fig. 3.

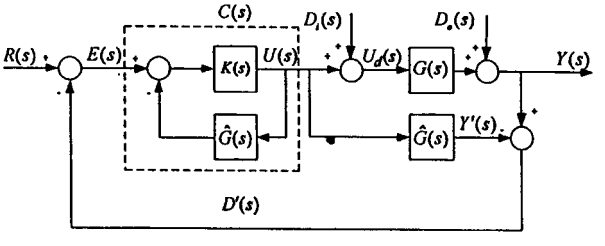

Fig. 3. Equivalent IMC structure.

The controller $C(s)$ in Fig. 3 is the IMC controller and can be written as

$$C(s)=\frac{K(s)}{1+\hat{G}(s)K(s)}. \tag{7}$$

From Fig. 3, it is obvious that $\hat{G}(s)$ can be cancelled each other so that the general feedback control structure in Fig. 4 is then derived.

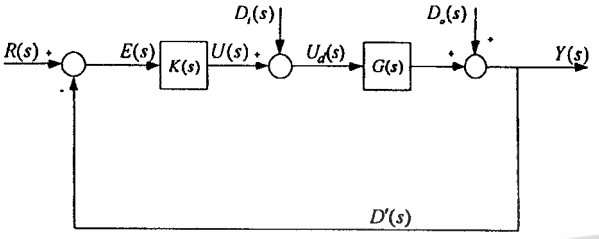

Fig. 4. General feedback control structure.

From (6) and (7), the controller $K(s)$ in Fig. 4 can be expressed as

$$K(s)=\frac{\hat{G}_{-}^{-1}(s)}{f^{-1}(s)-\hat{G}_{+}(s)}. \tag{8}$$

3.3 PID Controller Parameters Approximation

To obtain the PID controller, $K(s)$ must contain an integral term. To meet this requirement, the IMC low-pass filter $f(s)$ with a suitable structure must be selected so that the controller $K(s)$ can be rewritten in the form of (9) where $Q(s)$ is a non-integral term. This controller structure will also guarantee the step input disturbance effect rejection.

$$K(s)=\frac{1}{s}Q(s). \tag{9}$$

Performing the Maclaurin series expansion for $Q(s)$, the controller $K(s)$ can be expressed as

$$K(s)\cong\frac{1}{s}\left[Q(0)+\dot{Q}(0)s+\frac{\ddot{Q}(0)s^2}{2!}+\ldots\right]. \tag{10}$$

By maintaining the first three terms and ignoring the other higher order terms, the remaining terms match to the PID controller. So the controller $K(s)$ can be approximated as

$$K(s)\cong K_p+\frac{K_i}{s}+K_d s, \tag{11}$$

where

$$K_p=\dot{Q}(0), \tag{12a}$$

$$K_i=Q(0), \tag{12b}$$

$$K_d=\ddot{Q}(0)/2. \tag{12c}$$

3.4 IMC-Based PID Controller Design for the SCARA Robot

From the nature of SCARA robot, the command signal of the first link mainly influences the angular position of the first link and the command signal of the second link mainly influences the angular position of the second link. Therefore, in this paper, the two closed-loop PID controllers are designed independently for $\frac{Y_1(s)}{U_1(s)}=G_{11}(s)$ and $\frac{Y_2(s)}{U_2(s)}=G_{22}(s)$ as depicted in Fig. 5.

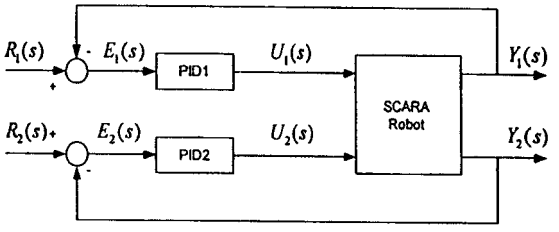

Fig. 5. Proposed control system structure.

Since the transfer function of the first link $G_{11}(s)$ and the transfer function of the second link $G_{22}(s)$ obtained in (4) are in the same format, the controller design for both links can be conducted in the same manner where the transfer function of the first link will be considered as the controlled object model for designing the controller. From Step 1 of the IMC controller design, the transfer function of the first link

$$G_{11}(s)=\hat{G}(s)=\frac{a_{11}s+b_{11}}{s^3+as^2+bs} \tag{13}$$

can be divided into two parts as

$$\hat{G}_{-}(s)=\frac{a_{11}s+b_{11}}{s^3+as^2+bs}, \tag{14}$$

and

$$\hat{G}_{+}(s)=1. \tag{15}$$

In Step 2, the suitable low-pass filter for designing the IMC controller $K(s)$ is proposed as

$$f(s)=\frac{zs+1}{xs^3+ys^2+zs+1}. \tag{16}$$

With this proposed low-pass filter, it is obvious that the controller is in the form of (9). By substituting (14), (15) and (16) to (8), the IMC controller $K(s)$ is obtained as

$$K(s)=\frac{1}{s}\cdot\frac{zs^3+(az+1)s^2+(bz+a)s+b}{a_{11}xs^2+(a_{11}y+b_{11}x)s+b_{11}y}. \tag{17}$$

To approximate the controller $K(s)$ in (17), non-integral term is assigned as $Q(s)$ in (18)

$$Q(s)=\frac{zs^3+(az+1)s^2+(bz+a)s+b}{a_{11}xs^2+(a_{11}y+b_{11}x)s+b_{11}y}. \tag{18}$$

Finally, the PID controller parameters can be computed by (12).

Numerically, the constant parameters for the two-link SCARA robot in the laboratory are used as listed in Table 1.

Table 1. Constant parameters for the two-link SCARA robot

Parameters	Values	Unit
m_1	4.37	kg
m_2	1.24	kg
$l_1 = l_2$	200	mm
a_1	63	mm
a_2	80	mm
J_{M1}	0.085	$kg \cdot m$
J_{M2}	0.060	$kg \cdot m$
K_{M1}	2.7590	$N \cdot m/V$
K_{M2}	1.3281	$N \cdot m/V$
B_{M1}	0.8691	$N \cdot m/(rad/s)$
B_{M2}	0.4347	$N \cdot m/(rad/s)$

With the properly tuned parameters x, y and z of the low-pass filter, the parameters of the PID controller of each link can be derived as shown in Table 2 .

Table 2. Parameters of the designed PID controllers

	x	y	z	K_p	K_i	K_d
PID1	15×10^{-5}	5×10^{-3}	5×10^{-1}	41	65	4
PID2	20×10^{-5}	4×10^{-3}	5×10^{-1}	46	73	4

4 Simulation and Experimental Results

In this section, the simulation and experimental results for controlling the two-link SCARA robot by using the proposed controller are demonstrated. In the simulations, the non-linear model of the two-link SCARA robot in (3) is used as a controlled object. In the experiments, the actual SCARA robot shown in Fig. 6 is employed. The PID controllers with the parameters in Table 2 are used in both simulations and experiments. The simulations and experiments are studied in cases as follows.

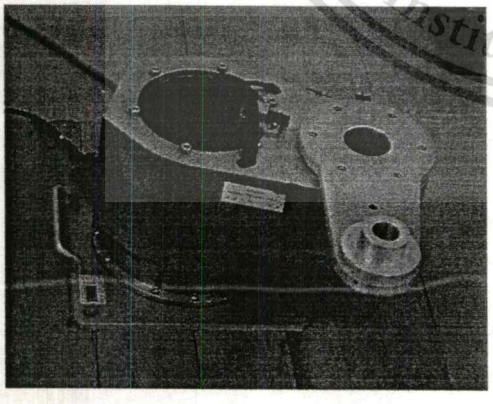

Fig. 6. Actual SCARA robot used in laboratory.

Case 1: The reference inputs or set-points (SP) at 45° and at 0° are respectively applied to the first link and second link. The responses are depicted in Fig. 7. The experimental result is similar to the simulation result. From Fig. 7(a), the response of the first link can track the reference input at 45° with the rise time $t_r = 0.45s$, maximum overshoot $M_P = 22\%$ and settling time $t_s = 2.7s$ and without steady-state error. Meanwhile the second link is maximally deviated around 1.3° and returned to 0° within the same settling time as can be seen in Fig. 7(b).

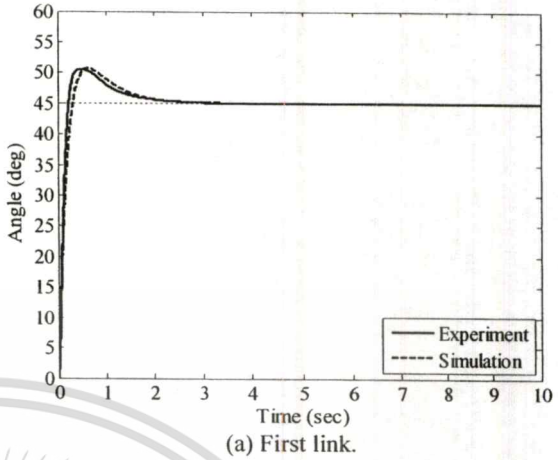

(a) First link.

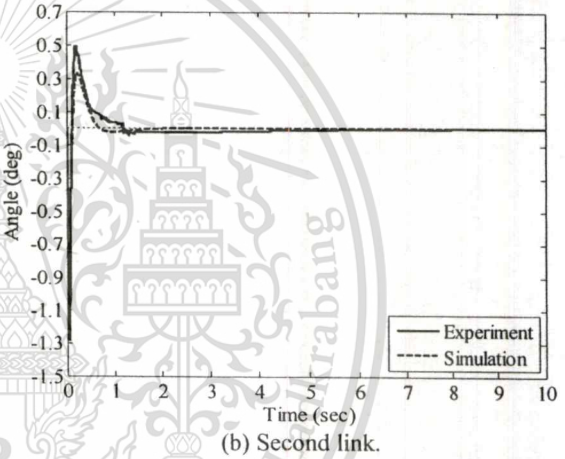

(b) Second link.

Fig. 7. Simulation and experimental results for Case 1.

Case 2: The reference inputs at 0° and at 45° are respectively applied to the first link and second link. In this case, the responses are shown in Fig. 8. The results exhibit similar characteristics to Case 1. From Fig. 8(b), the second link can track the reference input at 45° with the rise time $t_r = 0.45s$, overshoot $M_P = 20\%$ and settling time $t_s = 2.7s$ and without steady-state error. From Fig. 8(a), the deviation of the first link in this case is less than 0.6°, which is much smaller than the deviation of the second link in Case 1. However, in the experimental result, the angular position of the first link exhibits a temporary offset once it is driven back near 0°. This is due to the static friction of the actual robot but the angular position is eventually forced back to 0° once the command signal is sufficiently accumulated to drive the link.

Case 3: In this case, the reference inputs at 45° are applied to both links. The responses are shown in Fig. 9. It can be seen that the response of first link is similar to the response of the first link in Case 1 and that of the second link is similar to the response of the second link in Case 2. The step type input disturbances at 4 volts are programmed to enter the system at 4.5 seconds for both links. The angular positions of both links drop at maximum about 5° and they can be eventually forced

back to the set-points at 45° without steady-state errors within the same settling time of each link

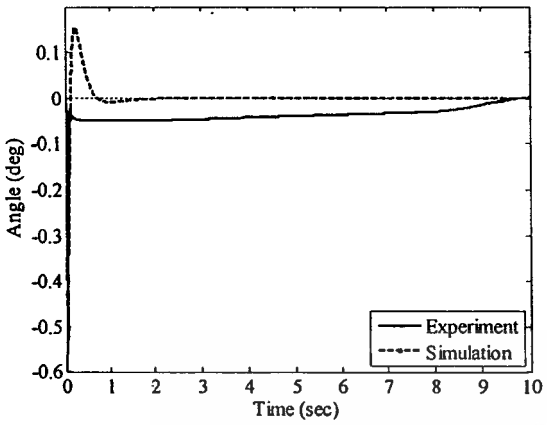

(a) First link.

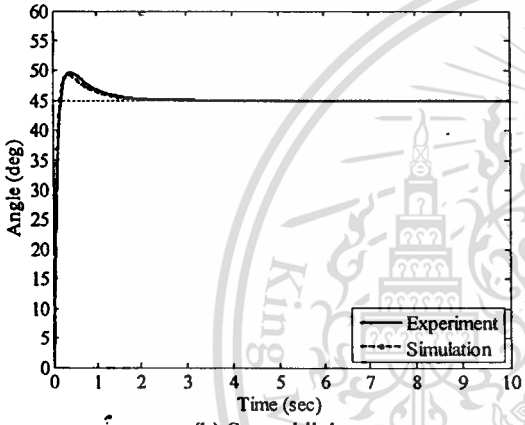

(b) Second link.

Fig. 8. Simulation and experimental results for Case 2.

The performances of the system in the above three cases can be summarized in Table 3 from the experimental results. It can be noticed from these results that since the parameters of the proposed IMC low-pass filter are selected nearly equal in designing the controllers of both links, the performance of both links are then nearly identical.

Table 3. System performances

		SP	t_r	t_s	M_P
Case 1	1st link	45°	0.45*s*	2.7*s*	22%
	2nd link	0°	–	–	–
Case 2	1st link	0°	–	–	–
	2nd link	45°	0.45*s*	2.4*s*	20%
Case 3	1st link	45°	0.45*s*	2.7*s*	22%
	2nd link	45°	0.45*s*	2.4*s*	20%

5 Conclusion

In this paper, the suitable low-pass filter for designing the IMC-based PID controller for the two-link SCARA robot has been presented. From the simulations and experiments, it can be seen that the proposed control system has a good performance. The angular positions of the links can track the reference inputs without steady-state error and the transient responses are fast with acceptable overshoot. In addition, the effects of input disturbances can be rejected.

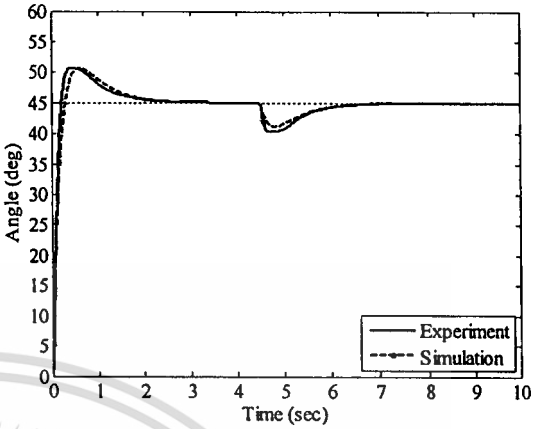

(a) First link.

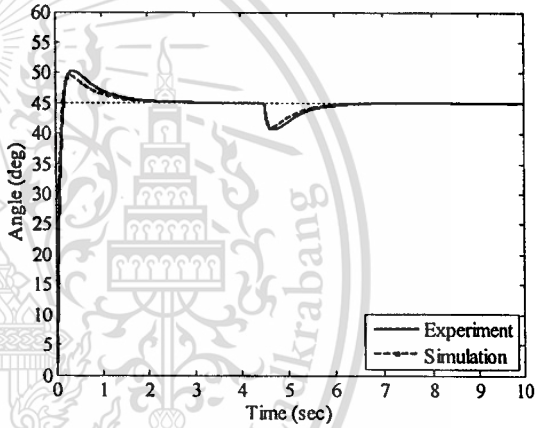

(b) Second link.

Fig. 9. Simulation and experimental results for Case 3.

Acknowledgements

Authors would like to thank AUN-SEED/Net for the financial support to this research work.

References

[1] M. C. Popescu, I. Borosi, O. Olaru, L. Popescu, F. Grofu, The Simulation Hybrid Fuzzy Control of SCARA Robot, WSEAS Transactions on Systems and Control, vol. 3, pp. 105-114, 2008.

[2] F. Passold, M. R. Stemmer, Feedback Error Learning Neural Network Applied to a SCARA Robot, Poland proceeding poznan, Poland, pp. 197-202, 2004.

[3] J. G. Zieggler, N. B Nichols, Optimal Setting for Automatic Controllers, ASEM Transactions , vol. 64, pp. 759-768, 1942.

[4] G. H. Cohen, G. A. Coon, Theoritical Consideration of Retarded Control, ASEM Transactions , vol. 75, pp. 827-834, 1953.

[5] Y. Okada, Y. Yamakawa, T. Yamazaki, S. Kurosu Tuning Method of PID Controller for Desired Damping Coefficient, Proceedings of SICE Annual Conference, Japan, pp. 795-799, 2007.

[6] S. Akamatsu, M. Konishi, J. Imai, Position Control of Two-link SCARA Robot by Using Internal Model Control, Memoirs of the Faculty of Engineering, Okayama University, vol. 43, pp. 49-54, 2009.

[7] C. E. Garcia, M. Morari, Internal Model Control. 1. A Unifying Review and Some New Results, Industrial and Engineering

Chemistry Process Design and Development, vol. 21, pp. 308-323, 1982.

[8] D. E. Rivera, M. Morari, S. Skogestad, Internal Model Control 4. PID Controller Design , Industrial and Engineering Chemistry Process Design and Development, vol. 25, pp. 252-265, 1986.

[9] J. Qibing, Q. Ling, W. Xuewei, Q. Fei, Base on All-pole Approximation a New Internal Model PID Control Method for the System with Time Delays, Proceedings of ICMA2009, Changchun China, pp. 268-273, 2009.

[10] S. B. Niku, Introduction to Robotics: Analysis, Systems, Applications, Upper Saddle River, NJ: Pretice Hall, 2001.

[11] T. Benjanarasuth, SCARA Robot Locomotion Control by Two-degree-of-freedom Simple Servo Adaptive Controller, Proceedings of AISM2010, Singapore, pp. 252-258, 2010.

[12] S. Suvilath, T. Benjanarasuth, U. Komine, K. Khongsomboun, IMC-Baesd PID Controller Design for a Two-link SCARA Robot, Proceedings of IEEE TENCON2011, Indonesia, pp. 1030-1034, 2011.

Author Biography

The author, Sipaseuth Suvilath was born in Phongsaly, Laos, on January 17, 1985. He received his B. Eng. degree in Electronic Engineering in 2009 from National University of Laos (NUOL). After that he had worked at Lao Brewery Company as Technician for 6 months. In the same year, he resigned from that company and became a teaching assistant for 6 months which in charge of Microcontroller and Programmable Logic Control (PLC). In 2010, he became a member of Control Laboratory under the AUN/SEED-Net program to pursue his M. Eng. degree. Mathematical modeling and IMC-based PID controller design for the two-link SCARA manipulator are his main research.